THE NATURE AND DYNAMICS OF THE ROTORUA ERUPTIVE EPISODE, OKATAINA VOLCANIC CENTRE, TAUPO VOLCANIC ZONE

A thesis
submitted in partial fulfillment
for the Degree
of
Master of Science
in Earth Sciences
by

GEOFFREY N. KILGOUR

KO TE TANGATA

The University of Waikato
Te Whare Wananga o Waikato

University of Waikato
2002

Abstract

The 15.7 cal yrs B.P. Rotorua eruptive episode is the latest expression of western Okataina volcanism. Okataina is one of the world's most active rhyolitic volcanoes and this eruptive episode provides an ideal opportunity to examine the nature, dynamics and impacts of a large magnitude explosive eruption from this volcanic centre.

This re-investigation of the Rotorua eruptive episode has lead to the grouping of the deposits into two distinct phases of eruption. The Rotorua Tephra and Eastern Dome (previously thought to be Te Rere-related) are termed 'Rotorua A' phase. Trig 7693 and Middle domes (previously linked to the source of the Rotorua Tephra) have been grouped with the Upper Rotorua Tephra into the 'Rotorua B' phase. These groupings are predominantly based on mineralogy and geochemistry on samples of pyroclastic and dome deposits.

The eruptive sequence began with a small initial ash without a basalt trigger, followed soon after by a plinian fall deposit (1.62 km^3) directed to the NW. Dome growth ensued (Eastern dome), creating an extensive rhyolite dome (0.72 km^3) in the Okareka Embayment. Soon after Eastern dome growth (based on the absence of paleosol development) the Rotorua B phase was initiated. This phase of predominant effusive dome growth lead to the construction of the coalesced Trig 7693 and Middle domes. Periodic vulcanian explosions and dome collapses lead to the localised dispersal to the S and E, of pyroclastic density currents and fall.

A new age of 12941 ± 75 ^{14}C years BP was obtained from charcoal in a surge deposit at a proximal site. This results in a revised age for the Rotorua eruption of 15 700 cal yrs BP. The eruption duration is estimated to exceed 15 yrs, based on a total dome volume of 1.37 km^3, assuming a growth rate of 3 m^3/s.

To the NW, the Rotorua A plinian deposit (A_p-1 to A_p-10 sub units) is overall normally graded, however cm-scale bedding is evident throughout the deposit. The grain size ranges from a block-sized, basal sub unit to a medium ash, upper. The plinian tephra is biotite-poor compared to the distinct Rotorua B deposits (previously 'Upper Rotorua Tephra'), which is biotite-rich.

Whole rock geochemistry on the Rotorua A pyroclastics, forms an apparent trend, suggesting the magma supplying the explosive phase was compositional zoned prior to eruption and was subsequently disrupted immediately prior to or during eruption. The Rotorua A and B phases plot as distinct clusters in all binary element plots. Intensive parameters calculated on Fe-Ti oxides highlights the distinction between Rotorua A (Rotorua Tephra and Eastern Dome) and Trig 7693 and Middle domes. Isotopic evidence indicates the Trig 7693 and Middle domes were supplied by a separate magma batch to the Rotorua A phase, suggesting small (<1 km^3) magma batches were residing in close proximity.

An eruption of this size today would cause the total destruction of Rotorua City (home to >50,000 people) due to ~1.5 m of volcanic ejecta accumulating in this region. This would cripple the central North Island for weeks to months. Due to the length of the eruption, mitigation would be required for an extended period after the initial phase of the eruptive episode. Livestock would be severely affected from blanketing tephra, along with the complete collapse of intensive forestry operations in the Rotorua District. National and international flights from Hamilton and Auckland airports would be heavily disrupted causing major economic losses. Respiratory problems and contaminated water intake would continue for a long period after the cessation of volcanic activity.

Acknowledgements

Firstly I would like to thank my chief supervisor Dr Richard Smith. Your boundless enthusiasm for all things volcanological provided for some well-needed inspiration during the thorough laboratory experiments undertaken in this study. Also I am thankful for giving of your limited time to see me when I required feedback.

Associate Professor Roger Briggs is whole-heartedly appreciated for advice on geochemistry and taking time out from administration duties to discuss my originally perplexing data. Associate Professor David Lowe provided significant support to this project both in a personal capacity and in discussions on tephrostratigraphy and ^{14}C dating. Thank you to Ian Nairn for discussions in the initial stages of fieldwork and for late-stage information on the stratigraphy of the Okareka Embayment, this was invaluable.

Thanks to fellow staff and students of the Earth Sciences Department for a thoroughly memorable experience. Technical (especially Annette and Renat) and administrative staff (Sydney and Elaine) are thanked for there ability to accommodate my requests at short notice without fail. The entire Volcano Research Group, even Tom and Stu, provided for good times during the VGM and (who could forget) Hawai'i. Jess Rae, my fellow volcanophile was always around for a chat or simply to distract me while I was busily involved in serious research. I thoroughly appreciate your help.

Special thanks goes to Deborah Bowyer for thoughtful discussions and for supplying unpublished PhD data on the domes of the Okareka Embayment. Without your data, I would not have been able to piece together the story I have modelled.

George, Marion, Gareth and Jenny Andrews (superb cousins) provided a great base for fieldwork on the margins of the OVC. George and Gareth took me golfing on numerous occasions to further my knowledge of the regional geology and provide extensive practice of recovery shots from the deep rough.

Fletcher Forests are thanked for allowing access to key localities in the Whakarewarewa and Highlands forestry blocks.

Funding assistance from the Broad Memorial Fund as well as the GSNZ Masters award aided with field costs and general living on a very limited income.

To my mates, who have always been there to bring me back to Earth. Also for motivation, when at one point (1997) I was advised to go to Polytech to study flower arranging. This ‘advice’ was due to my previously poor University form. Thanks Hamish. A special “thank you” to Kathryne for always being there and for reference assistance.

Last but definitely not least, my parents and family who have always been interested in what I have been up to, even though they may not fully understand why. To Craig and Janet, my loving parents who have always believed in me. Your support throughout University (especially financial!!) was magnificent. I will pay you back someday.

Table of Contents

Chapter 3 – Textural and Component Analysis

Chapter Four – Mineralogy and Geochemistry

Chapter 5 – Eruptive History

List of Figures

List of Tables

Chapter One
Introduction

1.1 Introduction

Volcanic eruptions involving silicic magma can be the most long-lived and catastrophic of all natural phenomenons. Okataina volcano has produced numerous moderate to large-volume silicic eruptions over at least the last 250 ka, most recently 650 years ago from Tarawera (Nairn, 1981, Froggatt & Lowe, 1990, Nairn *et al.*, 2001 and references therein).

The most recent silicic eruption from the western side of Okataina caldera was the Rotorua eruptive episode (Nairn, 1980) at 15,700 cal yrs BP. This eruption is notable for a number of reasons that make it worthy of detailed study.

1) Dispersal was atypically to the NW, providing a rare opportunity to trace the products of a plinian eruption to its distal margins.
2) This dispersal pattern is across the now built-up areas of Rotorua city and extends to New Zealand's largest population centre of Auckland. The Rotorua eruptive episode therefore provides an excellent scenario for modelling the impacts of an eruption on New Zealand, at a range of spatial and temporal scales.
3) The deposits are generally well exposed in proximal and medial areas and exhibit highly variable grain size over narrow vertical intervals. These deposits provide an opportunity to study a plinian-style eruption of apparently widely fluctuating intensity.

4) The Rotorua eruptive episode involved a transition from explosive to effusive behaviour.

1.2 Aims of Study

The main objectives of this study are:

1) Examine in detail the products of the Rotorua eruptive episode to determine the nature and dynamics of the eruption processes.
2) Re-evaluate the eruption history of the Okareka Embayment of Okataina volcano.
3) Assess the impacts of the eruption/s on today's society using a scenario-based approach.

1.3 Geological Setting

1.3.1 Taupo Volcanic Zone (TVZ)

Active rhyolitic volcanism is entirely concentrated in the Taupo Volcanic Zone (TVZ). The TVZ is the most frequently active and productive rhyolitic system on Earth (Wilson *et al.*, 1995). Development of the TVZ is the result of westward subduction of the Pacific Plate beneath the North Island (Figure 1.1). Extending from Ohakune to White Island (Whakaari), the TVZ is aligned in a NNE to SSW-trending zone of late Pliocene to Quaternary arc volcanism (Wilson *et al.*, 1995). Wilson *et al.* (1995) define the TVZ as an area enclosed around all caldera structural margins and individual vent sites, and on land extends up to ca. 200 km in length and ca. 60 km maximum width. Rhyolitic volcanism occurs in the middle of three distinct segments between two andesitic-dacitic provinces (Figure 1.2), and rhyolite makes up ca. 95 % of the total of TVZ eruptives (Graham *et al.*, 1995; Houghton *et al.*, 1995). Eight rhyolitic centres have been identified to date, based primarily on the evidence of structural depressions, namely: Taupo, Whakamaru, Maroa, Reporoa, Mangakino, Kapenga, Rotorua and Okataina. Of these, Taupo and Okataina are considered to be active.

1.3.2 Okataina Volcanic Centre (OVC)

The Okataina Volcanic Centre is the most recently active rhyolitic centre in TVZ. Okataina may have become active ca. 500 ka with eruptives presently only partially exposed (Manning, 1996). Okataina Volcano consists of three segments (Figure 1.3) 1) Haroharo caldera – the central and predominant feature containing the Haroharo and Tarawera Vent Zones, 2) Puhipuhi basin to the east and 3) Okareka Embayment – the south-western sector containing the Northern Dome (Te Rere related) and the Trig 7693 rhyolite complex (Rotorua A and B related – see section 1.4)

The history of Okataina can be conveniently divided into two phases, 'caldera forming' (ca. 500 – 65 ka) and 'caldera filling' (ca. 65 ka – present) (Table 1.1). Caldera forming events involved large ignimbrite eruptions, causing repeated subsidence. These events formed multiple overlapping collapse structures of the Haroharo caldera and Puhipuhi basin (Nairn, 1989).

Caldera filling events occurred after the voluminous Rotoiti eruption (ca. 65 ka), consisting of the Mangaone (ca. 45 – 22.8 ka) and Rotorua (ca. 21 ka to the present) subgroups (Froggatt & Lowe, 1990). The Mangaone subgroup consists of at least 12 pyroclastic units, as suggested by Jurado-Chichay & Walker (2000). The Rotorua subgroup consists of 11 previously known eruptions (Froggatt & Lowe, 1990). Of these, only the Te Rere and Rotorua Eruptive Episodes have been derived from the Okareka Embayment.

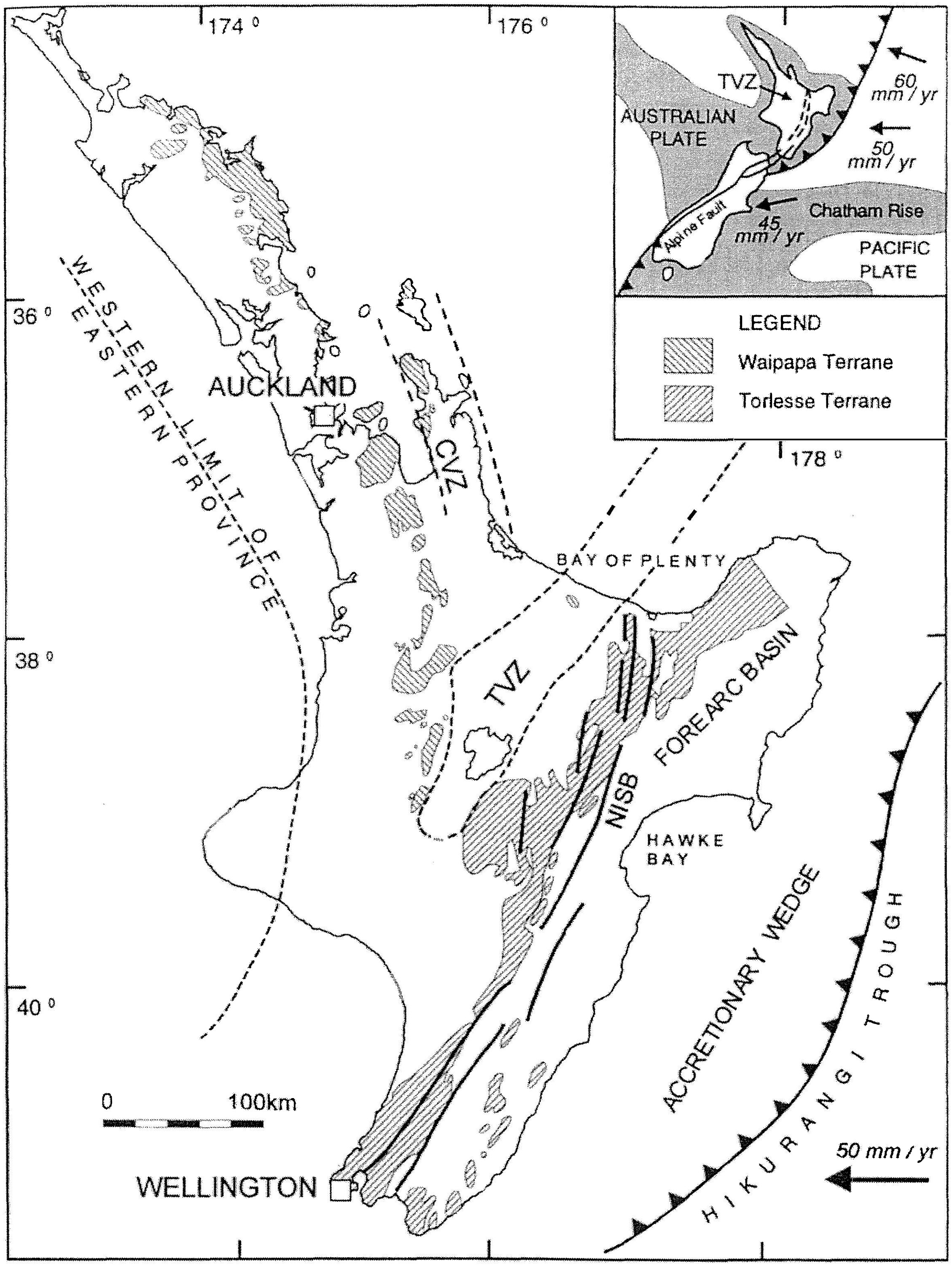

Fig 1.1 The tectonic regime acting to create the active Taupo Volcanic Zone. Westward subduction of the Pacific Plate beneath the North Island of New Zealand has lead to conditions for intensive activity in the zone of the central North Island. TVZ = Taupo Volcanic Zone; CVZ = Coromandel Volcanic Zone; NISB = North Island Shear Belt. Arrows indicate the direction of subduction (modified from Graham *et al.* 1995).

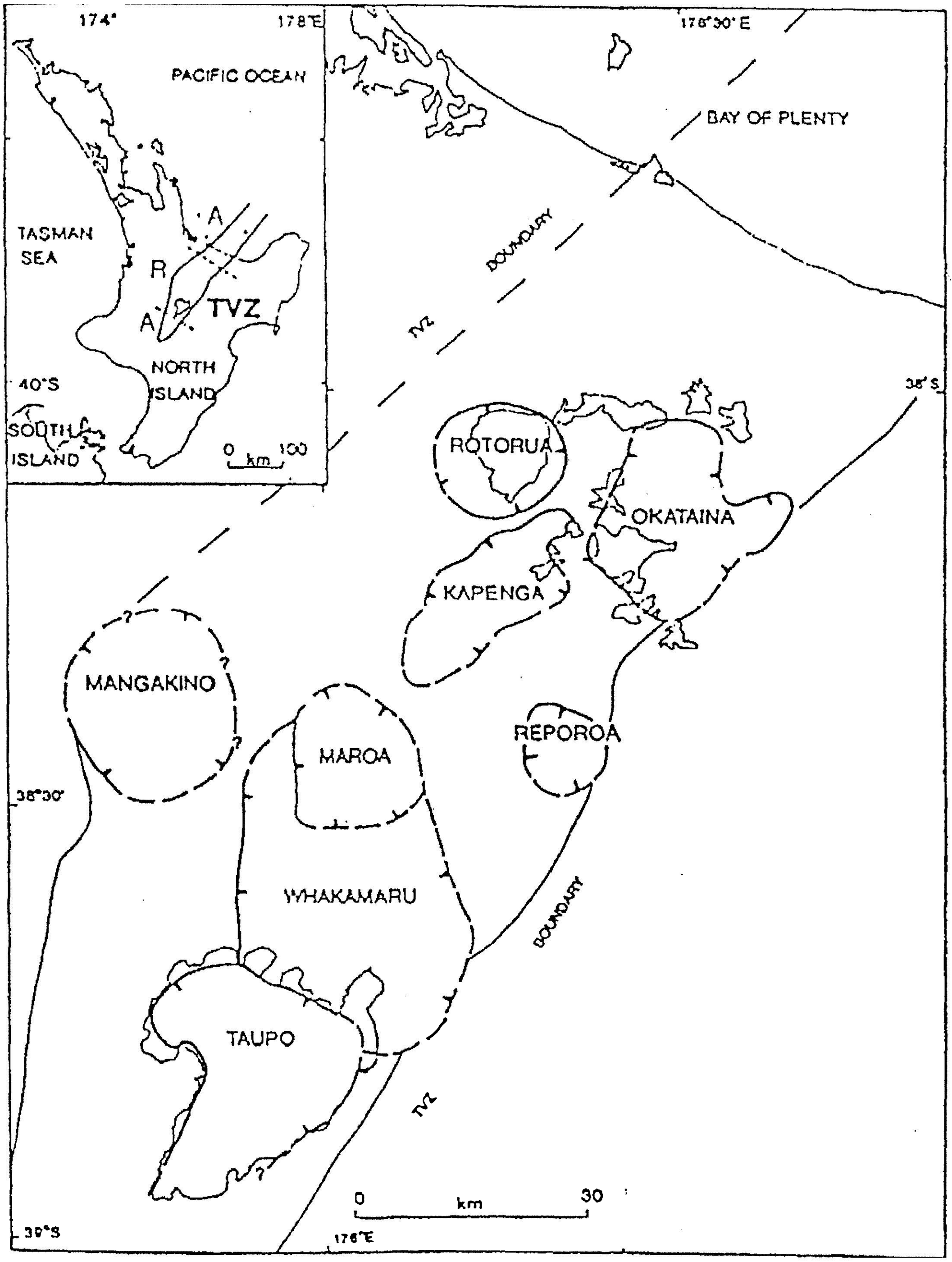

Fig 1.2 The Taupo Volcanic Zone (TVZ), with the boundaries of the calderas assigned. Inset indicates the location of the three distinct compositional segments (Andesitic (A) and Rhyolitic (R) dominated) (after Houghton *et al.*, 1995).

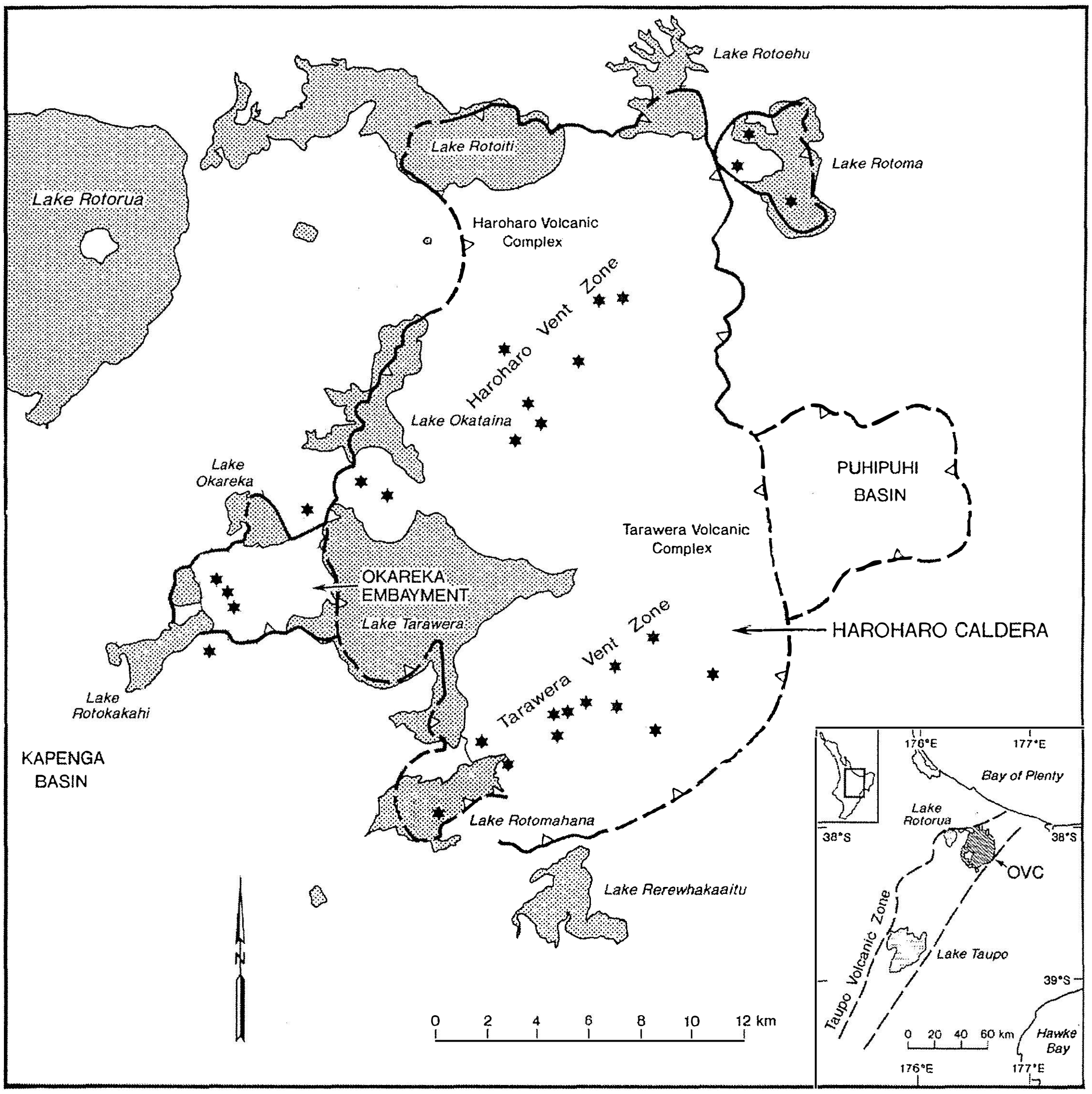

Fig 1.3 Regional map of the Okataina Volcanic Centre (OVC) showing the location of the Haroharo Caldera, Puhipuhi Basin and Okareka Embayment (source of the Rotorua Tephra and location of the associated lava domes). Stars mark post 21 ka vent locations. Inset shows position of OVZ in the Taupo Volcanic Zone (modified from Nairn, 1992).

Table 1.1 The post Rotoiti tephrostratigraphy of the Taupo Volcanic Zone. Ages taken from (‡) Froggatt and Lowe (1990), (#) Wilson *et al.* (1988), (†) Calibrated ages based on Stuiver *et al.* (1998) and Lowe *et al.* (1999), (§) Jurado-Chichay and Walker (2000), (#) Hogg *et al.* (in press), ($) New age calculated in this study.

Subgroup	Formation	Age (^{14}C yr BP)	Age (Cal. yr BP)	Volcanic Centre
Rotorua	Kaharoa Tephra	770+/- 20 ‡	1314 +/- 11 *	Okataina
Taupo	Taupo Tephra	1850 +/- 10 ‡	c. 200 AD	Taupo
Rotorua	Rotokawau Tephra	3440 +/- 70 ‡		Okataina
	Whakatane Tephra	4830 +/- 20 ‡	5550 †	
	Mamaku Tephra	7250 +/- 20 ‡	8050 †	
	Rotoma Tephra	8530 +/- 10 ‡	9500 †	
	Waiohau Tephra	11 850 +/- 10 ‡	13800 †	
	Rotorua Tephra	**13 020 +/- 80 $**	**15700 $**	
	Rerewhakaaitu Tephra	14 700 +/- 110 ‡	17600 †	
	Okareka Tephra	18 000 ‡	22500 †	
	Te Rere Tephra	21 100 +/- 320 ‡	25000 †	
	Kawakawa Tephra >Aokautere Ash	22 600 #	26500 #	Taupo
Mangaone	L (post Omataroa)	28 220 +/- 630 ‡		Okataina
	K Omataroa (Om)	c. 29 000 ‡		
	J Awakeri (Aw)	27 730 +/- 350 ‡		
	I Mangaone (Mn)	31 600 +/- 250 ‡	31400 §	
	H			
	G		33000 §	
	F Hauparu (Hu)	c. 39 000 ‡		
	E Te Mahoe (Tm)	c. 41 000 ‡		
	D Maketu (Mk)			
	Pongakawa (Pg)		36700 §	
	Pupuwharau (Pp)	c. 43 000 ‡		
	Tahuna (Ta)			(Taupo)
	C	c. 45 000 ‡		Okataina
	B Ngamotu (Nt)			
	A Basal Ngamotu		43000 §	
Rotoiti	Rotoiti Tephra > Rotoehu ash > Rotoiti Ignimbrite > Matahi Scoria	c. 50 000 ‡	55 000 #	

1.4 The Rotorua eruptive episode and nomenclature

The Rotorua Tephra was first described by Thomas (1888) and later by numerous authors (Grange, 1929; Vucetich & Pullar, 1964; Ewart & Healy, 1965) in a tephrostratigraphic and soil development context. Nairn (1980) was the first to apply a volcanological interpretation of the nature and dynamics of the eruption.

The deposits of the Rotorua eruptive episode lie stratigraphically between the Rerewhakaaitu and Waiohau eruptive episodes. The Rotorua event has been divided in this study into two distinct stages, 1) an explosive plinian phase producing a widespread plinian fall deposit to the NW with associated dome growth (Eastern dome see later chapters) and 2) a subsequent and distinct dome-building phase leading to the growth of the coalesced Trig 7693 and Middle domes and pyroclastics previously known as the 'Upper Rotorua Tephra' (Nairn, 1980). 'Rotorua Tephra' and 'Upper Rotorua Tephra' will be used synonymously with Rotorua A and B eruptive phases respectively. The proposed nomenclature for the eruption that produced the 'upper Rr' pyroclastics and the Trig 7693 and Middle domes is here termed 'Rotorua B'. Rotorua B is used to distinguish products that are geochemically distinct from the plinian pumice fall deposits of Rotorua A. The general term used to describe Rotorua A and B phases are collectively termed the 'Rotorua eruptive episode' and will be used herein.

1.5 Age of the Rotorua episode

Using previously obtained dates on the Rotorua Tephra at distal sites (Froggatt & Lowe, 1990 and references therein) and from charcoal samples within proximal density currents (one obtained in this study), a revised age of 13,020 ± 80 (15,700 cal yrs BP) has been determined based on 8 analyses. The age of the Rotorua eruptive episode has been re-examined due to the interpretation of the stratigraphy and geochemistry (see section 2.10)

1.6 Outline of Thesis

The thesis is presented in seven chapters.

Chapter 2 describes the stratigraphy and dispersal of the Rotorua A and B pyroclastic deposits. Calculations of the pyroclastic and dome volumes are given, along with models of eruption dynamics. Chapter 3 examines the textural and component characteristics of the Rotorua A and B pyroclastic deposits to quantify the state of the magma and vent conditions immediately prior to and during the eruption. In chapter 4, whole rock geochemistry on pyroclastic rocks from this study is presented, in conjunction with recent unpublished data. This is used to quantify the state of the distinct batches of Rotorua magma. Data quoted in literature is included to validate the derived magmatic models within the Okareka Embayment of the Okataina Volcanic Centre. A revised model for the eruptive history of the Rotorua A and B phases is presented in chapter 5, and the implications of the new findings are discussed. Chapter 6 assesses the hazard posed by the Rotorua eruptive episode today using volcanological interpretations to examine the quantitative effects locally and regionally. Chapter 7 concludes the thesis with the key findings of this study and provides recommendations for future research.

Chapter Two

Stratigraphy and Dispersal

2.1 Introduction

Thomas (1888) was the first to describe the Rotorua Tephra. Subsequent authors (eg. Grange, 1937; Vucetich & Pullar, 1964) established the tephrostratigraphy of the deposits from the Okataina Volcanic Centre (OVC). These studies were conducted largely in order to understand the soil forming processes rather than to determine the volcanological implications of the tephras. Nairn (1980) was the first to describe the deposit in a volcanological context, by providing a general account of the unit stratigraphy and the nature of the associated eruptions. However, a detailed analysis of the eruption was not attempted due to the limited scope of that study.

This chapter provides a detailed account of the internal stratigraphy of the Rotorua Tephra and gives the dispersal of the assigned sub-units, from a large number of site localities (Figure 2.2). Using the isopach data collected in this study in conjunction with results from Waikato (Lowe, 1988) and Auckland lake cores (Sandiford *et al.,* 2001) (Figure 2.1), a revised estimated volume is calculated using the method of Pyle (1989). Isopleth maps have been produced in order to model column heights and plume dynamics using the method of Carey & Sparks (1986).

2.2 Field Methods

The collection of field data involved a number of descriptive characteristics to be noted at the > 80 sites (Figure 2.2) described, primarily by drawing detailed stratigraphic columns and providing descriptions at each locality. Characteristics such as: total thickness, subunit stratigraphy and thickness, and the maximum 5 pumice and lithic clasts at each sub-unit, were needed for creating the isopach and isopleth maps.

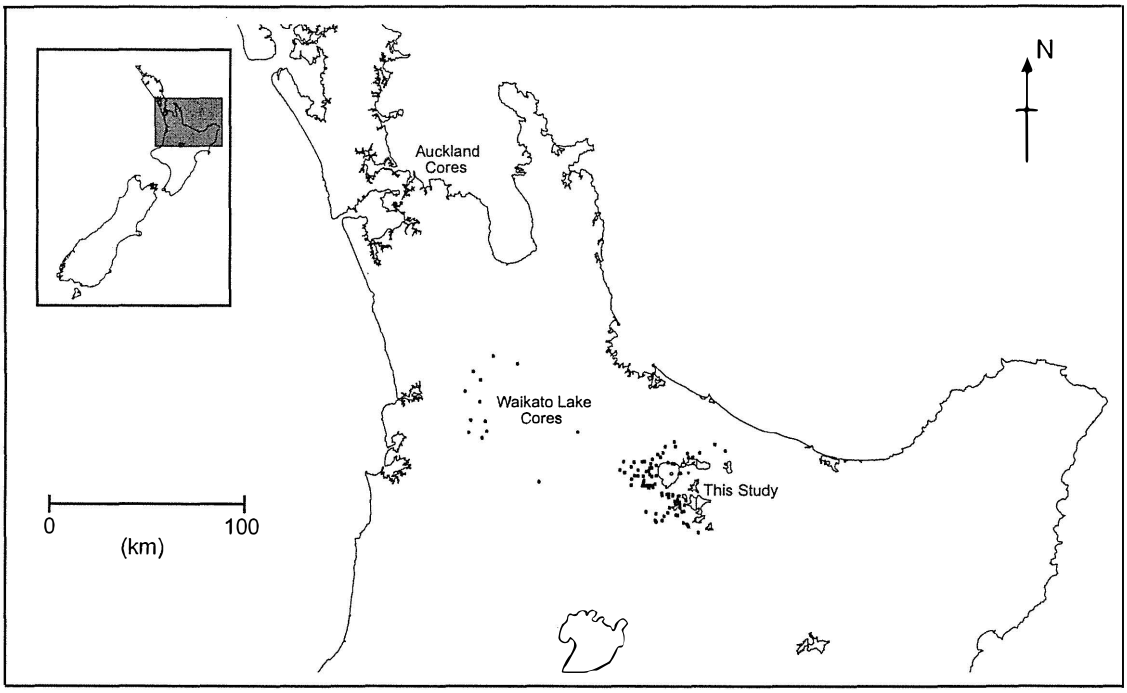

Fig 2.1 Locations of site localities used in the dispersal and volume calculations of the Rotorua Tephra. Waikato lake core data from Lowe (1988), and Auckland core data from Sandiford *et al,* (2001). Inset indicates area sampled of North Island, New Zealand.

2.3 General Description

In this study, two distinct phases of the Rotorua eruptive episode have been identified based on mineralogy, geochemistry and stratigraphy. These phases are termed Rotorua A and Rotorua B phases of the Rotorua eruptive episode. The Rotorua A phase consists of the 'Rotorua Tephra' (of previous studies) and Eastern dome of the Okareka Embayment (previously considered part of the Te Rere eruption). The Rotorua B phase consists of the 'Upper Rotorua Tephra' (as defined by Nairn, 1980)) and the coalesced Trig 7693 and Middle domes.

2.3.1 Rotorua A

The Rotorua Tephra is a conspicuous, crystal-poor pyroclastic deposit in the western Bay of Plenty. The highly permeable fine to coarse lapilli is characteristically Fe-stained in many sections. Along State Highway 5, the red-brown tephra overlays the Mamaku Ignimbrite and in parts, rest directly on it. At more proximal locations, the deposit is characterised by coarse lapilli and block-sized pumice in the basal coarse unit (proximal subunit A_p-2; see section 2.5), with a medium and fine lapilli upper (subunit A_p-10). Due to this change in the grain size of the deposit from proximal to distal locations, a description of the deposit in the proximal, medial and distal sites is given.

Eastern dome in the Okareka Embayment is a relatively low-lying dome compared to the Trig 7693 and Middle domes. Eastern dome has an irregular topography with low angle flow margins. It is bounded by Lakes Tikitapu and Rotokakahi to the west, Lake Okareka to the north, and Lake Tarawera in the east (see Figure 2.13). Previously this lava dome was considered part of the older Te Rere eruptives (22.0 cal ka BP). New data from this study are presented here and in chapter 4 on which Eastern dome is assigned to the Rotorua eruptive episode.

2.3.2 Rotorua B

The Upper Rotorua Tephra is a locally dispersed (to the south and east), crystal-rich pyroclastic deposit. In very proximal locations (1-2 km) the Upper Rotorua Tephra contains a range of grainsizes, from medium ash to coarse lapilli.

The coalesced Trig 7693 and Middle domes have the typically steep-sided morphology of a rhyolite dome (see Figure 2.13). The surface of the domes has been heavily incised, leading to an irregular topography. Situated towards Lakes Tikitapu and Rotokakahi, these domes are located on the westernmost limb of the Okareka Embayment.

2.4 Stratigraphic History of the Okareka Embayment

Previous investigations by Nairn (1980; 1992) have established the volcanic history of the Okareka Embayment of Okataina Volcanic Centre. Two major eruptive episodes have been sourced from the Okareka Embayment: 1) portions of the Te Rere eruptive episode (21.1 ^{14}C ka) and 2) the Rotorua eruptive episode. The Eastern dome was inferred by Nairn (1992) to be of Te Rere origin, due to the presence (at one locality) of Okareka tephra (18 ^{14}C ka) immediately overlying the dome (I.A. Nairn, 2002 pers comm.). However, the locality (U16/ 063305) used to determine the age of the dome is problematic as it is situated at the confluence of two lava flows (Eastern and Crater Farm). A re-investigation of this site indicates the dome lava at the base of the section represents the flow front of Crater Farm dome. A geochemical investigation (see Ch. 4) indicates the Eastern dome is more probably related to the Rotorua Tephra (Rotorua A). Trig 7693 and Middle domes are geochemically related to the Upper Rotorua Tephra (Rotorua B), with a distinction between the two phase being significant (see chapter 4).

2.5 Stratigraphic Determinations of the Rotorua Tephra

The climactic phase of the Rotorua eruptive episode (Rotorua Tephra) is a uniquely well exposed plinian fall deposit. The excellent exposure has enabled the tephra to be traced over a large area, which allows the nature of the deposit to be examined in detail.

By logging in detail the deposit at over 80 sites throughout the region, it has been possible to identify a proximal and medial subunit stratigraphy. These subunits have provided the framework for mapping the dispersal of individual phases of the eruption. The proximal stratigraphy (within 5 km of the vent) has been divided into 10 subunits (A_p-1 to A_p-10) (#1 in Figure 2.4), based on grain size and componentry. However, as distance increases from the vent, the number of recognisable and mappable subunits decreases. The medial stratigraphy (10-20 km) (#4 - #34a in Figure 2.4) exhibits 6 subunits (A_m-1 to A_m-6), depending on location. At distal locations (>20 km) (#43 in Figure 2.4), such as on the Mamaku plateau, 3 sub-units are visible and can be traced into the Waikato lakes.

2.6 PROXIMAL PYROCLASTIC STRATIGRAPHY

The proximal Rotorua eruptive episode deposits are of two main types: 1) proximal equivalents of the widespread plinian fall – 'Rotorua Tephra', and Rotorua A of this study 2) pyroclastic density current deposits and associated fall – 'Upper Rotorua Tephra' and Rotorua B of this study. The proximal fall stratigraphy is based on 5 locations within 5 km of the vent. Limited exposure is available very close to source (1-2 km) due to dense vegetation and burial during subsequent dome growth. Proximal sites give the best indication of vent and plume dynamics; therefore the type section was used for quantifying the eruption dynamics. The type section of the Rotorua Tephra is located in the Okareka Quarry (Figure 2.3) as assigned by Nairn (1980). Although the quarry is situated 3.7 km NW of the vent, the site is retained as the type locality due to the quality of exposure and proximity to the vent. As the quarry lies along the dispersal axis, the location provides an excellent location to determine the internal stratigraphy of the Rotorua Tephra.

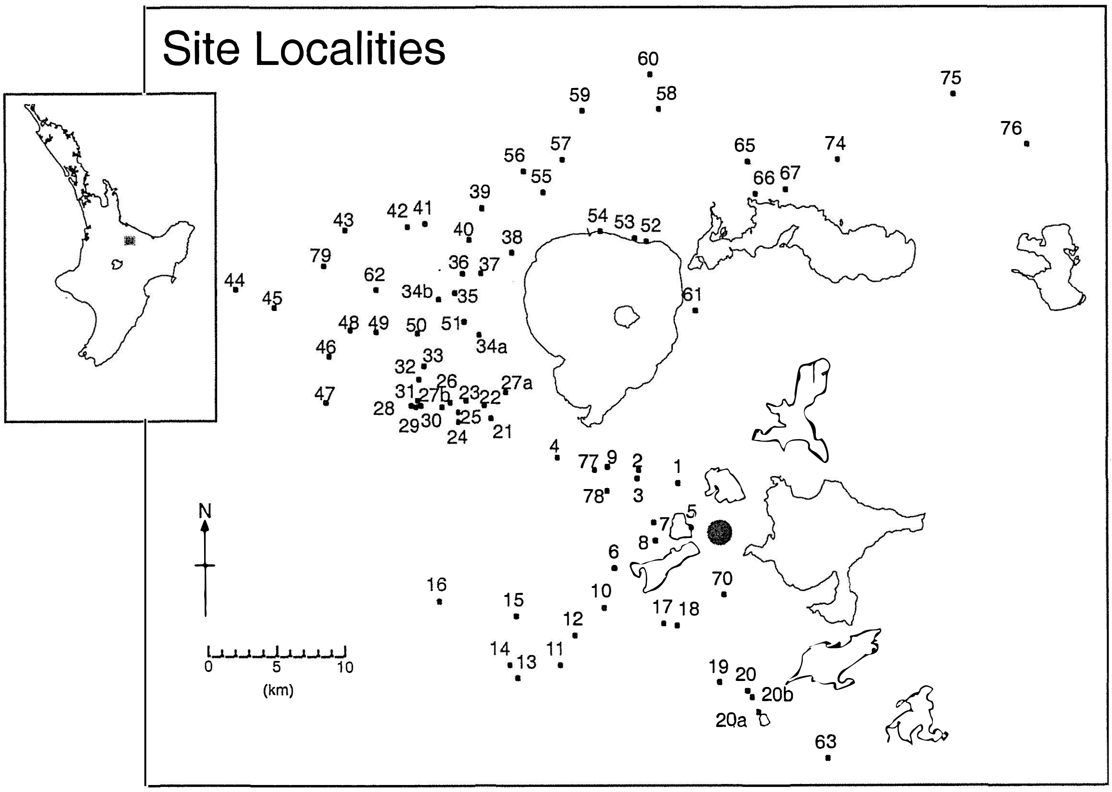

Fig. 2.2 Map showing numbered site localities referred to in the text. Grey dot indicates vent location. Inset indicates the location of the field sites in the Rotorua District Grid references are given in Appendix I.

The stratigraphy in the quarry exhibits conformable bedding. The deposit is generally normally graded, which is unusual (Sparks *et al.*, 1997) however fine-scale (cm) pulses throughout the unit are evident suggesting rapidly varying eruption intensities (Figure 2.3). While the quarry provides the type location for the Rotorua Tephra (Rotorua A), the Upper Rotorua Tephra (Rotorua B) is not represented in the quarry due to the very localised dispersal to the south and east of the vent. The Te Mu Road section (U16/ 048273) provides a limited exposure of the proximal Rotorua B deposits (see 2.5.2). This site exhibits pyroclastic density currents with intermittent fall (Figure 2.4). Nairn (1980) describes deposits that are inaccessible due to lack of outcrop such as block and ash flows and fall deposits.

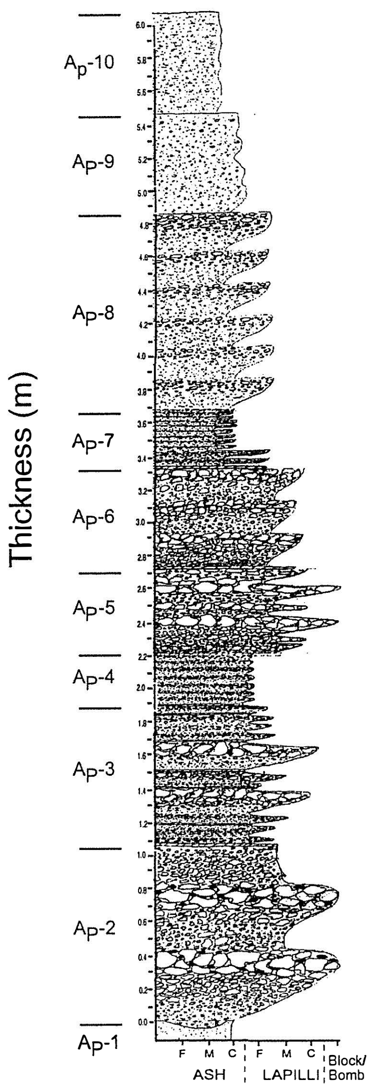

Fig. 2.3 Proximal stratigraphy of the Rotorua Tephra at the Okareka Quarry type locality (U16/ 018316). Note the overall normal grading with fine scale bedding throughout the deposit.

2.6.1 Rotorua A - Proximal Fall Stratigraphy (A_p)

A_p - 1

The base of this subunit lies on a paleosol overlying the Rerewhakaaitu tephra. This basal subunit is a fine-medium ash and has a patchy distribution, is moderately sorted and is up to 10 cm thick. Componentry of this medium ash consists of vesicular pumice (75 %), lithics (20 %) and dense pumice (5 %). Bedding is massive.

A_p - 2

Due to the discontinuous nature of A_p-1, this subunit is often found in contact with the basal paleosol. The grain size of A_p-2 ranges from fine lapilli to block-sized (>100 mm) pumice clasts. The unit is reverse to normally graded and contains 2 reversely graded block beds. The pumice has a sub-angular to sub-rounded morphology, is vesicular, crystal poor and contains hypersthene, hornblende +/- augite (crystals found throughout the sequence). Pumice makes up 75-80% of the subunit. The lithics are solely rhyolite lava, and comprise 15-20% of the deposit. The lithic clasts are angular to sub-angular. Maximum lithic sizes are approximately 35-40mm in diameter. A fine ash layer of 10 mm thickness marks the top of subunit A_p-2.

A_p - 3

Subunit A_p-3 is finer grained than A_p-2, containing coarse ash to medium lapilli + rare block–sized pumice. This subunit exhibits fine scale bedding, involving 19-20 packages of coarse and fine beds within ~80 vertical cm. The subunit consists of 80-85% pumice, 10-15% lithics and ~5% obsidian. The pumice is slightly more vesicular (75-78 %) in hand specimen than A_p-2 (72-74 %) and has a sub-angular morphology. Numerous fine ash units (6) are present at the base of the bedded units. 2 block beds occur within this predominantly coarse ash and medium lapilli subunit. A 15 mm fine ash layer caps the top of A_p-3.

A_p - 4

Subunit A_p-4 is a finer-grained unit than A_p-3. The deposit ranges from coarse ash to fine lapilli and is well sorted. Seven graded units are evident with no fine ash layers over the 30 cm thickness. The distinguishing feature of A_p-4 is the slightly higher proportion of lithics (15-20%) with rare (5%) black-green obsidian. Grain morphology is more angular (sub angular) than C, for both the pumice and lithic clasts.

A_p - 5

A 25 mm fine ash bed marks the base of A_p-5. This subunit is a 50 cm thick subunit and predominantly consists of medium to coarse lapilli. Six reversely graded beds are identified, of these, two are block sized. The overall grain size ranges from fine lapilli (5-10 mm) to blocks (90-100 mm). Lithics are highly concentrated at the base (15-20 %) while in the block beds the lithic concentration is lower (5-10 %). Dense pumice is rare (<5 %), therefore the proportion of vesicular pumice ranges from 80-85 % for the base, to 90-95 % elsewhere. The pumice clasts are sub rounded to sub angular, while the lithics are sub angular. A_p-5 is a moderately sorted subunit. A 25 mm fine ash bed marks the top.

A_p - 6

Overlying the fine ash bed, a concentration of coarse ash sized rhyolite lithics (15-20%) forms the base of the first reversely graded bed. 3 such beds, ranging from coarse ash to coarse lapilli are identified. Each bed is well sorted and contains sub rounded pumice (85-90%) and sub angular rhyolite lithics (10-15 %). Rare dense pumice and streaky pumice make up <5 % of this subunit.

A_p - 7

A thick (30 mm) fine ash unit marks the base of A_p-7. This 35 cm thick subunit is poorly sorted and lithic rich. Its appearance is much greyer than the other units due to the ~20 % lithics and 10 % dense pumice. A series of fine scale bedding occurs at a 25-30 mm frequency. The subunit is normally graded, with 2 medium lapilli beds underlying nine coarse ash beds. The pumice is sub rounded and the lithics and dense pumice are sub angular.

A_p - 8

Coarser than A_p-7, A_p-8 is a coarse ash to medium lapilli bedded subunit. The six reversely graded beds are vesicular, pumice rich (80-85 %) compared with A_p-7. Rhyolite lithics make up 10-15 % of the subunit, with rare dense pumice (<5 %). Moderately dense pumice is evident within this subunit. The pumice clasts are sub rounded with sub angular lithics. The beds are moderately to well sorted and are regularly spaced (15-20 cm).

A_p - 9

This subunit is light brown and is massive, showing no signs of bedding. The grainsize is coarse ash to fine lapilli and is well sorted. The clasts are predominantly sub-rounded pumice (85-90 %) with sparse amounts of sub angular lithics (10 %) and dense pumice (<5 %). 60 cm thick, A_p-9 is defined at the top by a rapid decrease in grain size (A_p-10).

A_p - 10

Subunit A_p-10 represents the uppermost unit of the quarry in the NW direction. The grain size ranges from medium to coarse ash and grades into a soil, below the Waiohau tephra. No bedding is visible in this well sorted, 60 cm thick subunit. The proportion of components is: pumice – 90 %, lithics – 5 %, dense pumice – 5 %. The pumice and lithic clasts are sub angular.

2.6.2 Rotorua B - Proximal Fall and Flow Stratigraphy (B_p)

B_p - 1

Nairn (1980) described a block and ash flow deposit at the base of the Te Mu Rd section. The deposit consists of angular lithic blocks up to 1 m diameter in a lapilli matrix. The deposit is approximately 2 m thick to the base of the exposure.

B_p - 2

Subunit B_p-2 is a fall unit of bedded coarse ash to lapilli. The subunit consists of multiple beds reverse to normally graded. This subunit is presently not exposed and is described in Nairn (1980).

B_p - 3

This ignimbrite unit consists of coarse lapilli, moderately rounded, crystal-rich pumice in a peach-grey matrix. The base is not exposed. The coarse pumice clasts in the ignimbrite are denser compared to the fall deposits above and contain a higher crystal content compared with the Rotorua tephra. Rare lithics and dense pumice are evident.

B_p - 4

A sharp contact exists between the ignimbrite and the overlying fall deposit. This fall deposit consists of four packets of tephra. The 30 cm thick unit has a coarse lapilli, reversely graded unit overlain by a finely bedded sequence of medium ash to fine lapilli. Pumice clasts are crystal-rich and are dominant in the deposit. Fine scale bedding (cm) exists in this fall deposit.

B_p - 5

A sharp contact at the top of subunit B_p-4 marks the transition from a fall deposit to a series of light grey pyroclastic surges. The 10 cm thick unit contains four superposed events. The composite surge bed is continuous over a short area exhibiting limited pinch and swell bed morphology. The deposit has a fine ash base reversely grading into a fine lapilli overlain by a coarse ash upper.

B_p - 6

A fall deposit overlies subunit B_p-5 and contains a coarse ash to coarse lapilli (reversely graded) base and medium ash/fine lapilli upper. The coarse ash base contains approximately 50-60 % dense pumice overlain by coarse lapilli of predominantly crystal-rich pumice. Clast morphology is sub-angular. The medium ash/fine lapilli unit is moderately well sorted and exhibits fine scale bedding over the 25 cm thickness of the subunit

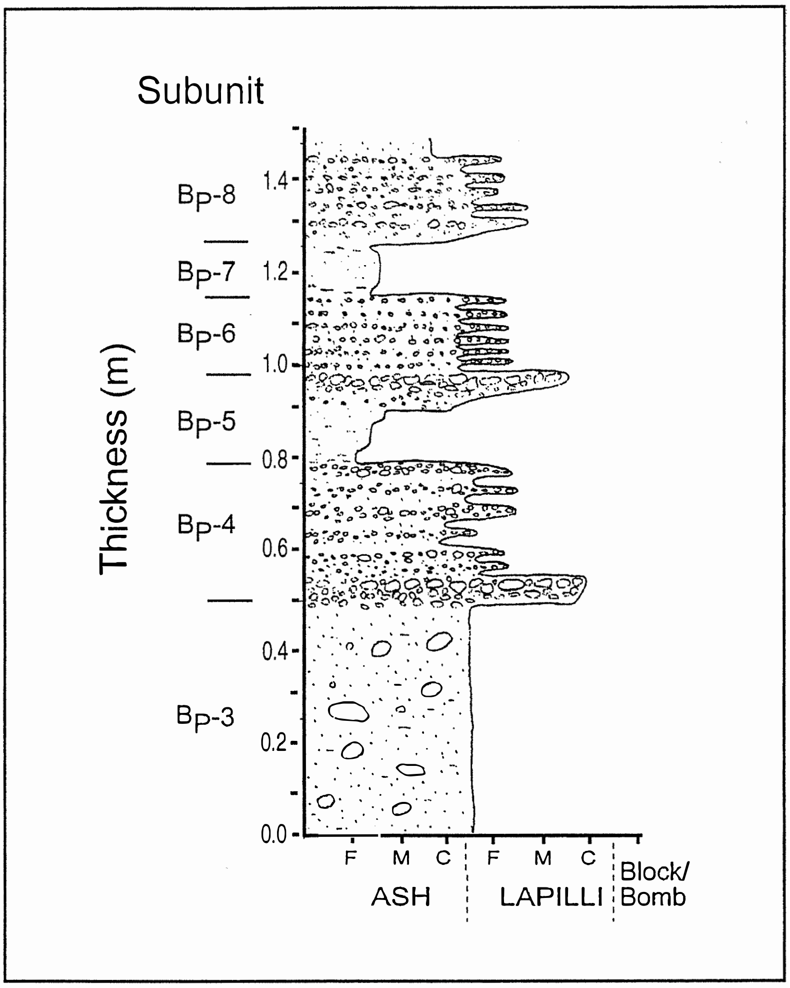

Fig. 2.4 The Te Mu Rd section (U16 048273) showing the Rotorua B pyroclastic deposits. Pyroclastic fall units (B_p-4, 6 and 8) are intercalated with pyroclastic density currents (B_p-3, 5 and 7).

B_p - 7

Subunit B_p - 7 contains a series of five fine surge beds. The deposit is a 10 cm thick unit consisting of an overall normally graded coarse to fine ash. The surge beds are laterally continuous over short distances but exhibit fine pinch and swell over greater lengths. Brown vitric ash separates the five grey surges.

B_p - 8

A normally graded fall deposit overlies the surge below. The fall deposit is finely bedded over the 23 cm thickness from a coarse lapilli base to a medium ash upper. Pumice clasts are crystal-rich with the deposit containing rare lithics (<2 %). Clast morphology is sub-angular and the deposit is moderately sorted. A gradation of the medium ash upper into the paleosol above marks the latest stage of the sequence.

2.7 Rotorua Tephra Medial Stratigraphy (A_m)

2.7.1 General Description

The stratigraphy in the medial sections is based on a large number (> 40) of site localities. Small variations in both syn- and post - eruptive atmospheric effects, lead to variability in the number of medial subunits present at a given location. The medial deposits (all associated with the Rotorua A phase) often can be traced to their proximal equivalents, however local turbulence and near-vent effects will be decreased leading to a more composite stratigraphy further from the vent.

A_m – 1

Subunit A_m-1 lies on a paleosol overlying the Rerewhakaaitu tephra. This subunit is a massive, medium ash with rare (5-10 %) fine lapilli. Clasts are sub angular – sub rounded and are moderately sorted. Sub angular lithics make up 5-7 % of the deposit. The thickness of this unit is variable along the dispersal axis.

A_m – 2

A gradational contact with A_m-1 marks the base of this subunit. This unit is the thickest (>40 cm) and coarsest of the medial stratigraphy. According to proximity to the vent, the subunit is a bedded coarse and medium lapilli to a massive medium lapilli with occasional fine lapilli. Vesicular pumice is the predominant component of the unit (85-

90 %) with rare lithics and dense pumice (~10 %). Lithic and dense pumice morphologies are sub angular – angular, while the vesicular pumice is sub rounded.

A_m – 3

A sharp contact exists between this unit and A_m-2. Grainsize ranges from a coarse ash to fine lapilli, with sub rounded to sub angular clast morphologies. The unit is massive and contains 90-95 % vesicular pumice with rare dense pumice and lithics. Free crystals of quartz, hornblende and biotite are rare as well as obsidian fragments.

A_m – 4

A gradational contact exists between this unit and A_m-3. The deposit is variable in thickness, ranging from a ~35 cm medium - coarse lapilli to a 10 cm fine lapilli. Lithic concentrations are higher than the underlying units (~10 %) leading to a grey-tan colour. Componentry is dominated by vesicular pumice (85 %) with rare free crystals (~5 %). Bedding is massive throughout the medial stratigraphy.

A_m – 5

This subunit is not evident everywhere throughout the medial stratigraphy. The unit is a lithic-rich (20-25 %) medium – coarse ash with rare fine lapilli. A sharp contact on A_m-4 forms the base of this poorly sorted subunit. The bedding is variable and ranges from a finely bedded, coarse ash to a massive fine lapilli. Dense pumice clasts and obsidian form a small percentage (10 %) of the medium ash-sized portions of the deposit. Clast morphologies are sub angular and sub rounded for the lithic and vesicular pumice clasts respectively.

A_m – 6

This subunit is evident throughout the medial stratigraphy. Varying in thickness between 20 and 30 cm, this moderately sorted unit forms the top of the tephra sequence. Massively bedded, the unit ranges in grainsize from fine to coarse ash with rare fine lapilli. Lithics are rare (~5 %) with sub angular to angular morphologies. Sub rounded vesicular pumice is the dominant component of this unit. The top of this subunit weathers progressively into the developing soil. The Waiohau tephra is the succeeding eruption.

2.8 Rotorua Tephra Distal Stratigraphy (A_d)

2.8.1 General Description

Distal sites involve locations as far north as Auckland (Sandiford *et al.,* 2001). These data along with the Waikato lake cores (Lowe, 1988) has increased the mapped area of tephra dispersal. The distal stratigraphy (3 subunits) on the Mamaku plateau can be correlated with the deposit in the Lake Okoroire core in the south Waikato region (Figure 2.5).

A_d – 1

The base of this subunit forms a sharp contact with the paleosol of the Mamaku Ignimbrite. The orangey-brown basal unit is a well-sorted, coarse ash - fine lapilli. Lithics and dense pumice are rare (~5 %) in this vesicular pumice-rich unit. Bedding is massive. Clast morphology is sub rounded.

A_d – 2

A gradational contact with A_d-1 marks the boundary between the subunits. This unit is a massive, fine and medium lapilli with sub rounded pumice clasts. The deposit is predominantly vesicular pumice (95 %) with rare lithics and dense pumice (5 %). This subunit represents the coarsest of the three distal subunits.

A_d - 3

A sharp contact marks the transition from an orangey-brown unit (A_d-2) to this tan-grey, uppermost unit. Grainsize ranges from fine to medium ash and sorting is moderate. Sub rounded pumice clasts are dominant in this lithic-poor deposit. Rare dense pumice is evident (5 %). A gradation into the paleosol marks the limit of this massive unit.

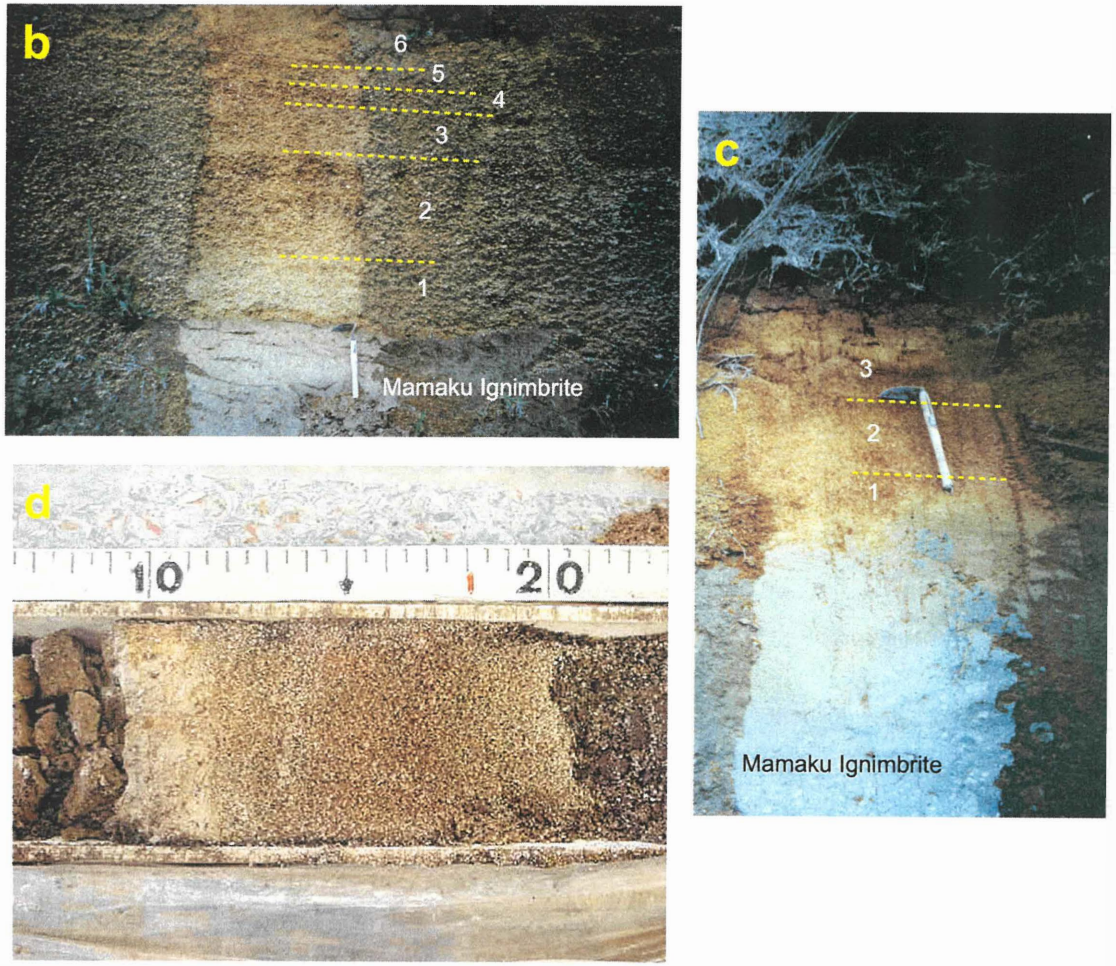

Fig. 2.5 (a) Proximal Rotorua Tephra at the type locality in the Okareka Quarry. **(b)** Medial Rotorua Tephra deposit at U15/ 896406 exhibiting the six medial (A_m) subunits. **(c)** Distal Rotorua on the Mamaku Plateau at U15/ 765473 exhibiting three subunits (A_d). **(d)** A core from Lake Okoroire at T15/ 555612.

2.9 Proximal – Medial – Distal Correlations

Correlations of the subunits are based on grain size, componentry (lithic and dense pumice abundances relative to vesicular pumice) and clast morphology. Columns were drawn and correlated along the dispersal axis to examine the changes in the deposit characteristics, as shown in Figure 2.6.

2.10 Eruption Chronology

The age of the Rotorua eruptive episode has been determined by ^{14}C. However, past dates have not separated the distinct phases of the eruptive episode, as determined by this study.

Nairn (1980) sampled charcoal within a pyroclastic surge deposit from the Rotorua B phase (his 'Upper Rotorua Tephra'), which occurred after the Rotorua A phase, based on stratigraphy. This date was incorporated with Rotorua Tephra (Rotorua A) charcoal and peat samples (Froggatt & Lowe, 1990 and references therein). The sample collected by Nairn (1980) in addition to a sample collected in this study (which obtained a date of 12,941 ± 75 ^{14}C yrs BP), should ideally not be pooled with the Rotorua A dates due to the distinct phases of the eruptive episode. However, a distinction between the two events using ^{14}C is not possible due to the inherent errors in the age determination (as shown in Table 2.1). This in conjunction with the lack of stratigraphic evidence for paleosol development suggest the maximum time break between A and B phases was no more than in the order of tens of years.

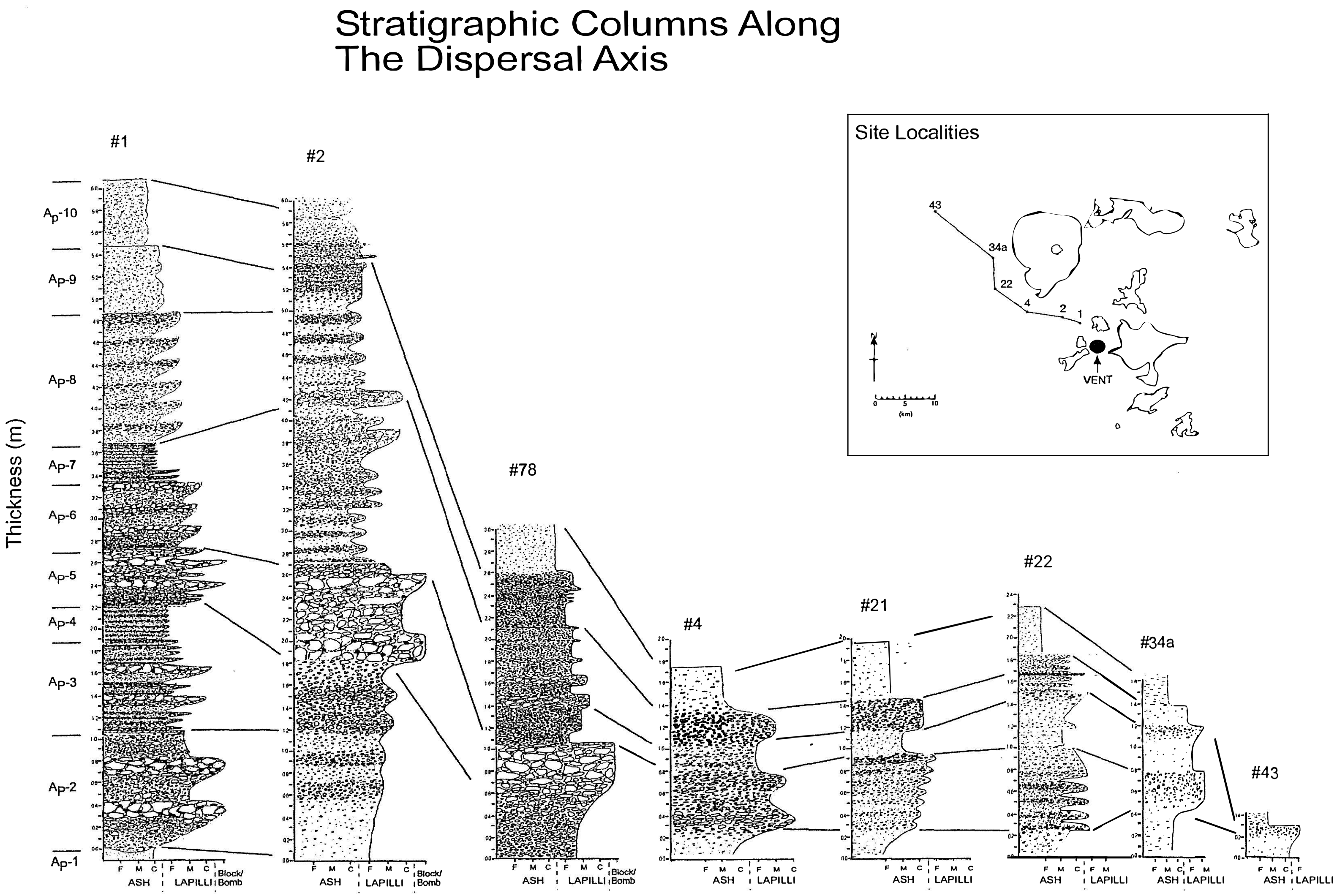

Fig 2.6 Stratigraphic correlations of the plinian fall component of the eruptive episode. Correlations were achieved from the proximal-site #1 (U16/ 018315) to distal locations-#43 (U15/ 814471). Other site location grid references are given in Appendix I.

Table 2.1 Pooled radiocarbon dates with corrected calendar ages from the Rotorua A and B events based on the revised stratigraphy of the Okareka Embayment, as determined in this study. Dates collated from, (ʕ) Topping & Kohn (1973), (#) Nairn (1980), (‡) Hogg *et al.* (1987) and (β) this study. Note: Topping & Kohn data is likely to have been misidentified.

Eruption Phase	Age Determined
Rotorua A	13150 ± 300[ʕ]
	12810 ± 580[ʕ]
	12900 ± 310[‡]
	12800 ± 150[‡]
	13300 ± 110[‡]
	12950 ± 110[‡]
Rotorua B	13450 ± 250[#]
	12941 ± 75[β]
Pooled Age ^{14}C	13020 ± 49
Corrected Cal yrs BP	15700

2.11 Isopach / Isopleth Dispersal Maps

Isopach maps were constructed for the assigned subunits of the medial stratigraphy (A_m-1 to A_m-6) (Figure 2.7) in order to examine the dispersal of the main plinian phases of the eruption over the widest possible area. All subunit isopach maps have a distinctive NW dispersal, with little variation from the whole deposit isopach. Small variations in the dispersal axis do occur but do not significantly deviate from the general dispersal axis. Site localities to the SE of the vent contain only trace amounts of the plinian fall deposit, suggesting a strongly demarcated upwind margin to the plinian plume. Field evidence around the vent suggests the dome building pyroclastics of the Rotorua B phase were extremely localised proximal to the vent and are dispersed to the S and E only. Topographic controls from the older Te Rere related dome (25 ka) to the NW provided an obstacle for density currents and vulcanian fall. Deposits associated with the Rotorua B phase are not evident within the quarry, 3.7 km NW of the vent.

The total dispersal of the Rotorua Tephra has been extended from incorporation of core data from the Waikato (Lowe, 1988) and Auckland (Sandiford *et al.,* 2001). The dispersal of the tephra does not extend east off the Coromandel Peninsula (Carter *et al.,* 1995), therefore eliminating the previously described northern lobe of Vucetich & Pullar (1964) and Nairn (1980). Trace amounts have been identified to the SE of Ruapehu on the ring plain (T19/ 489238) (Donoghue *et al.,* 1995). These data have lead to a more accurate account of the primary pyroclastic coverage over the North Island (Figure 2.5).

a

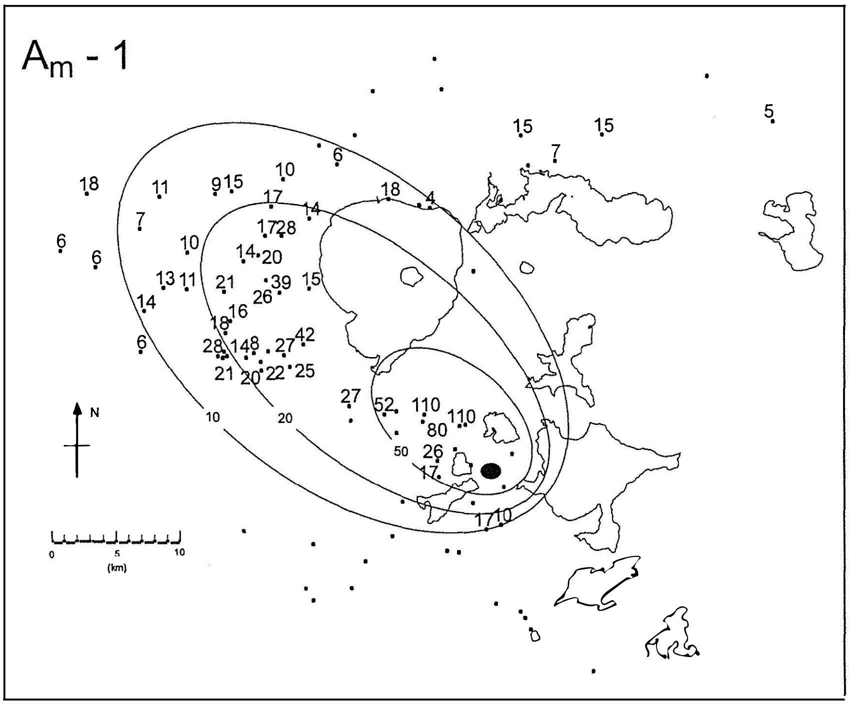

Fig. 2.7 (a-g) Subunit isopach maps based on the medial stratigraphy (A_m-1 - A_m-6). Each subunit is given (a-f) along with a total isopach (g). Thickness contours are in cm. Black dot represents the vent location in all maps.

b

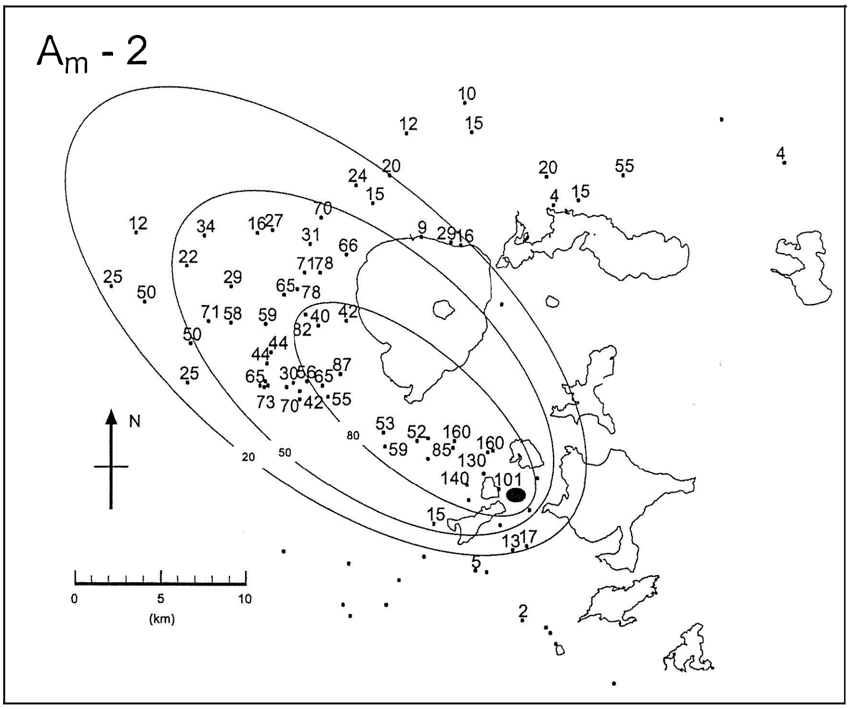

c

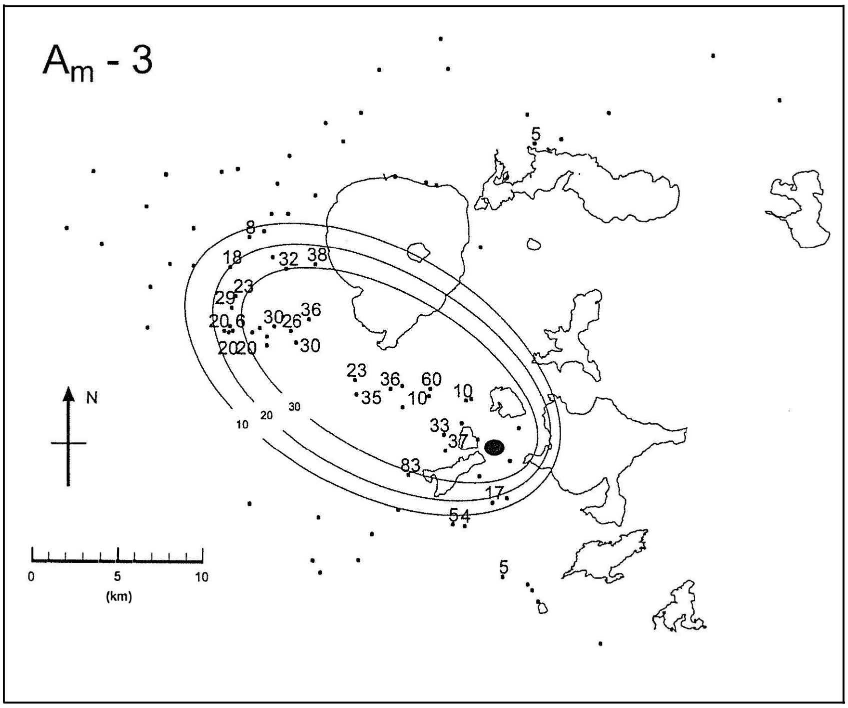

d

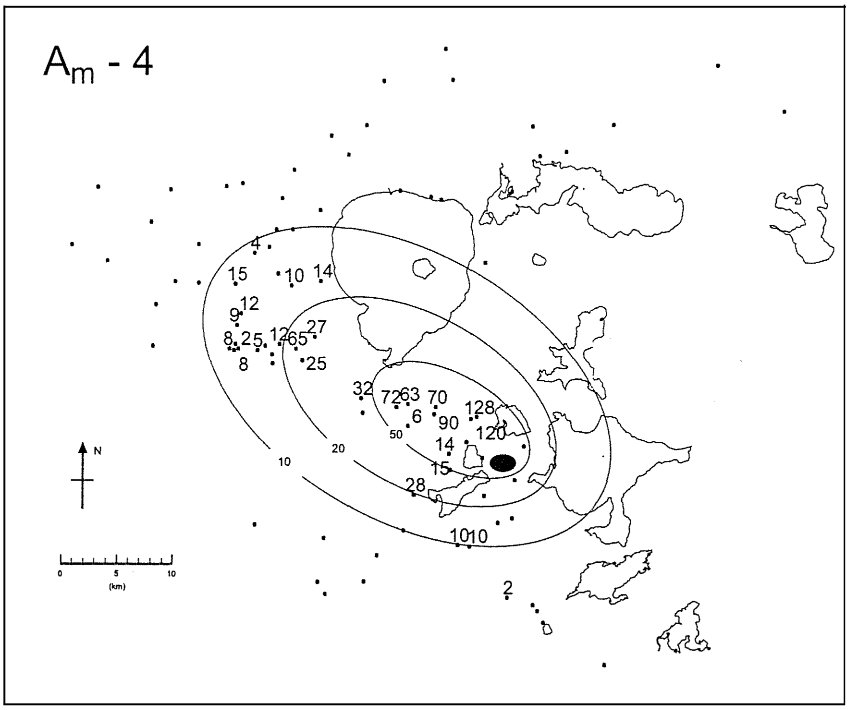

e

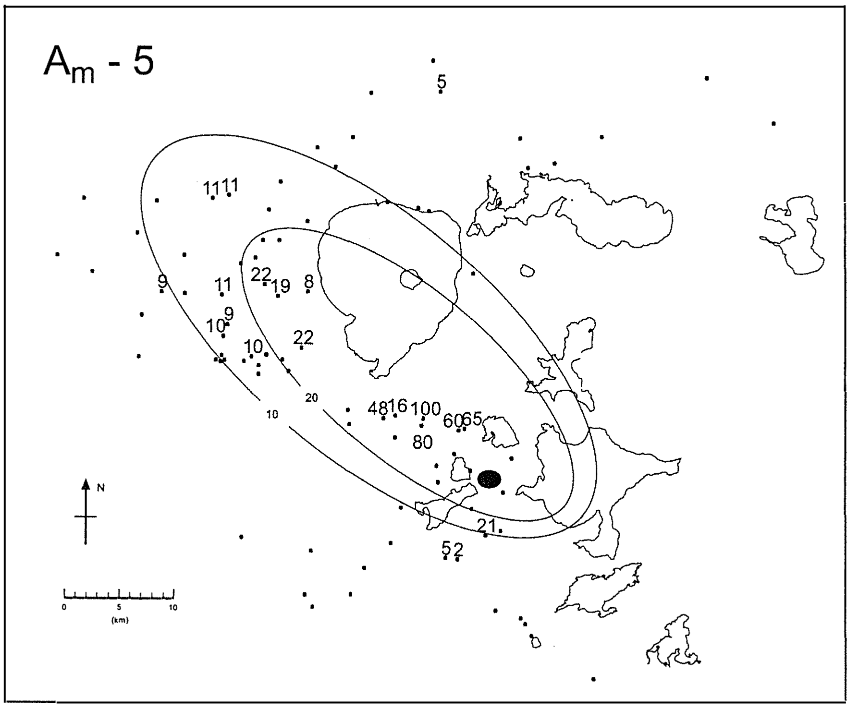

f

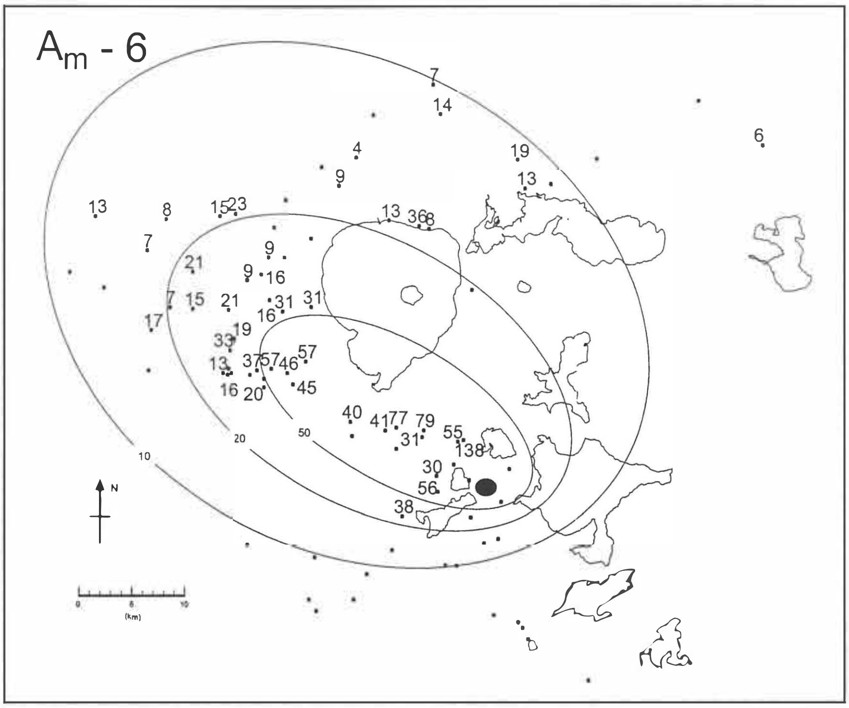

g

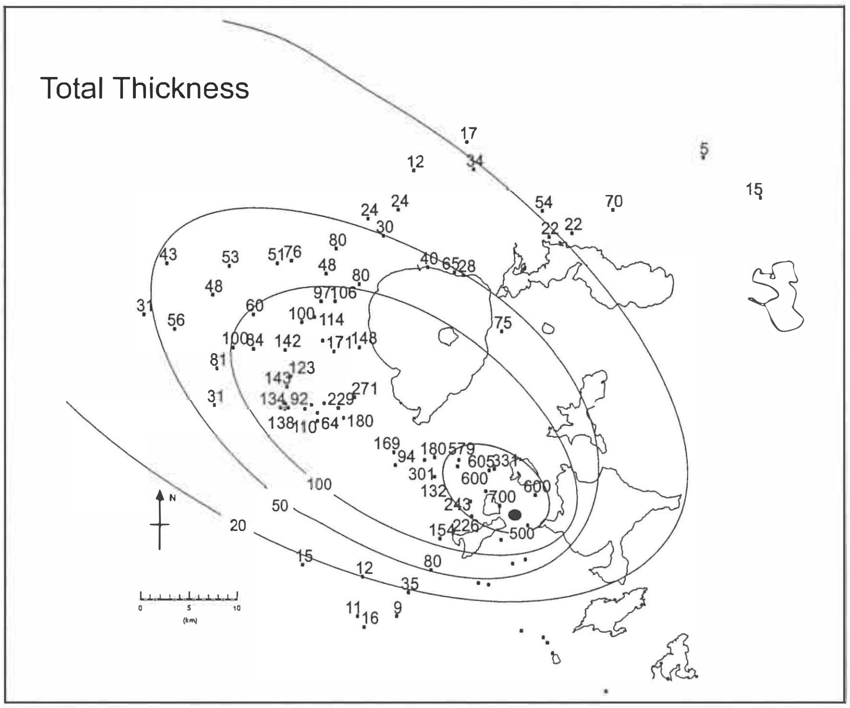

2.12 Volume Estimate – Pyroclastic

2.12.1 Rotorua Tephra

Due to the unform dispersal of the subunits in the NW direction, the volume of the Rotorua Tephra can be accurately calculated on the basis of the whole unit dispersal rather than the sum of the subunits. Using the method of Pyle (1989), tephra volume requires a plot of *ln* thickness versus square root of area enclosed in the isopachs. This method assumes an exponential decay from the vent. Four isopachs were used in the volume calculation based on the ability to adequately define the contours. The Geographic Information System (GIS) program ArcView calculated the isopach area, by calculating the area of a manually drawn polygon. This was chosen due to the accuracy of the GIS program.

The calculated volume of the tephra in this study was expected to be less than that estimated by Nairn (1980) which was based on the mapping of Vucetich & Pullar (1964) who included paleosol thickness in deposit measurements. As shown in Figure 2.8, the dispersal of Nairn (1980) covers a much greater area for the 20 cm isopach than this study's 10 cm isopach. Therefore the volume calculation of Nairn's is likely to be overestimated.

The data produced (Figure 2.9) lead to a straight-line relationship for the four isopachs, indicating an exponential decay in thickness. However, the core data from Waikato and Auckland appear over thickened relative to the more proximal exponential decay. This may be explained by the fine ash component of the tephra being more mobile in the atmosphere (Bonnadonna *et al.,* 1998). The Waikato cores contain fine to medium ash, which is easily transported by slight wind currents. This will lead to an underestimate of the volume using a simple exponential decay model. This is evident in large volume eruptions (Fierstein & Nathenson, 1992) exhibiting three straight segments due to (1) near vent ballistic fall (2) deposition from the convecting column and (3) deposition of lapilli and ash from the umbrella cloud.

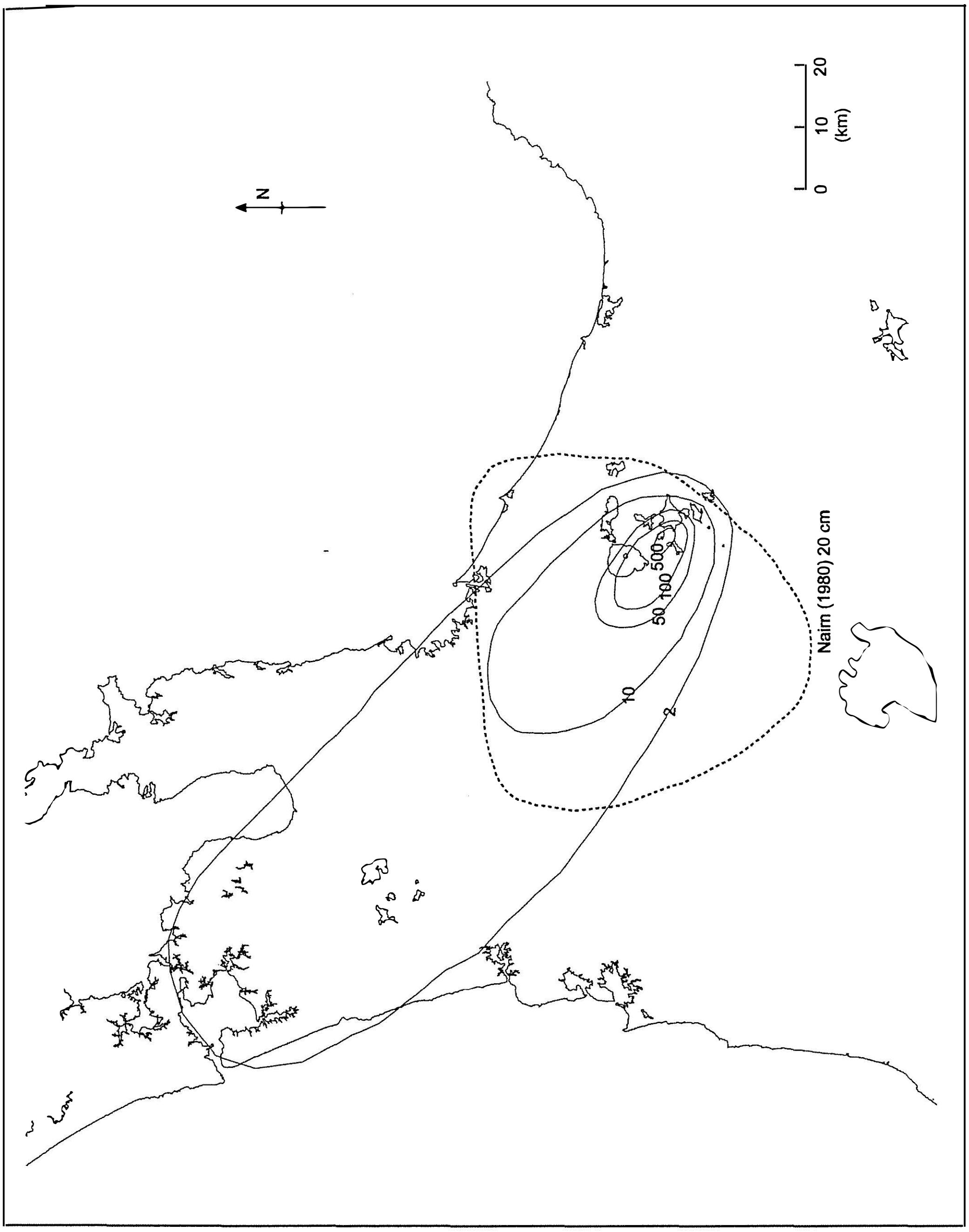

Fig. 2.8 Isopach map of the Rotorua Tephra determined by this study (solid line), with Nairn (1980) for comparison (dashed line). Thicknesses in centimetres.

Volume was calculated using the formula of Pyle (1989):

$$\text{Volume} = 2T_0/k^2$$

Where T_0 = extrapolated maximum thickness at vent

k = slope of the best fit line on the *ln* thickness versus square root of isopach area

The new volume obtained for the Rotorua Tephra is calculated here as 1.61 km^3. Other well-known eruptions for comparison are Taupo lapilli – 9.00km^3 and Mt. St. Helens – 1.22km^3 (Pyle, 1989). The overlying Waiohau tephra has a volume of 4.53 km^3 (Speed, 2001). This volume of tephra equates to an equivalent magma volume of 0.4 km^3 (using a DRE of 2350 kg/m^3).

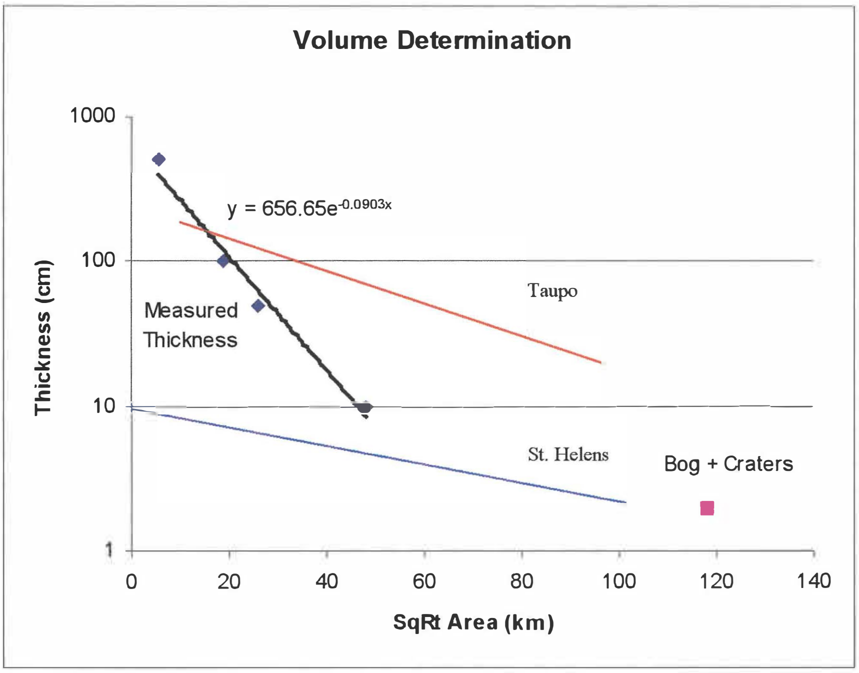

Fig. 2.9 Volume determination for the Rotorua Tephra using the method of Pyle (1989). Data from this study (measured thickness-black) form a single straight line segment. These data were used to determine the volume of the deposit. Distal data from Waikato and Auckland cores (Bog + Craters) are included to show the volume determined is underestimated and considered to be a minimum volume. Taupo (Red) and May 18, 1980 Mount St. Helens (blue) tephra thickness decay included for comparison (Pyle, 1989).

2.12.2 Upper Rotorua Tephra

Due to the extremely localised dispersal and poor exposure of the Upper Rotorua Tephra, an exact volume cannot be calculated. The volume is estimated to be minimal.

2.13 Rotorua A - Isopleth Maps

The maximum dimensions of pumice and lithic clasts are used to model vent location, eruptive energy and wind strength (Carey & Sparks, 1986; Sparks *et al.* 1997). The average maximum dimensions of the five largest clasts within a subunit were used to construct isopleth maps. Initially, the clasts were measured in the three principal axes in order to quantify average clast shape. Pumice and lithic clasts exhibited little variation throughout the dispersal; therefore the largest axis was measured to produce the isopleth maps. Maximum pumice and lithic clasts were measured in the six subunits of the medial stratigraphy (see section 2.6). Three subunits were used to model eruption dynamics based on confidence of isopleth contours. The two coarsest units (A_m-2 and A_m-4) and a fine unit (A_m-6) provided a spectrum of dispersal, stratigraphic position and grainsize for modelling purposes (Figure 2.10 a-f) . The isopleth maps exhibit dispersal axes in similar azimuths to the isopach maps, indicating factors controlling dispersal were constant throughout the plinian phase of the eruptive episode.

Models have been developed by Carey & Sparks (1986), Wilson & Walker (1987) and Pyle (1989) to quantify tephra deposits. Of these, plume height, eruption intensity and duration have been calculated using the method of Carey & Sparks (1986) as it is most commonly used in the literature, and therefore allows for easier comparison of results from other examples globally.

To model the column height and wind speed, the method of Carey & Sparks (1986) requires a measure of down and crosswind axis measurements of the 8 mm lithic isopleth (Figure 2.11). This produced column heights of 20, 17 and 13 km for subunits A_m-2, 4 and 6 respectively, with an average wind speed of 25 m/s. These column height values indicate the plume waned from the early climax of A_m-2 to the later stage deposits of A_m-6. The vertical wind profile in the atmosphere is a function of geographic position and the day of eruption; therefore wind speed is a semi-quantitative or qualitative interpretation (Sparks *et al.,* 1997). However, it is a useful indicator of conditions during the eruption, accounting for the narrow isopach and isopleth contours.

Peak eruption intensity was calculated using the buoyant plume rise model of Sparks (1986). Intensities were calculated (Figure 6b from Sparks (1986)) assuming an average magma temperature of 800 °C with a maximum column height of 20 km (from Carey & Sparks, 1986). Eruption intensities are determined by the maximum height of the plume (during A_m-2), therefore the calculation leads to a peak eruption rate. As indicated by the grain size variations of the deposit, the peak intensities were achieved early in the eruption sequence; therefore, intensities for the later stages of the eruption are not accounted for in the model. This has implications for the inferred plinian eruption duration (3.5 hours), which will be underestimated (based on the maximum discharge rate of 1.0×10^8 kg/s). Quantitative eruption dynamics are summarised in Table 2.2 with comparisons of deposits elsewhere.

a

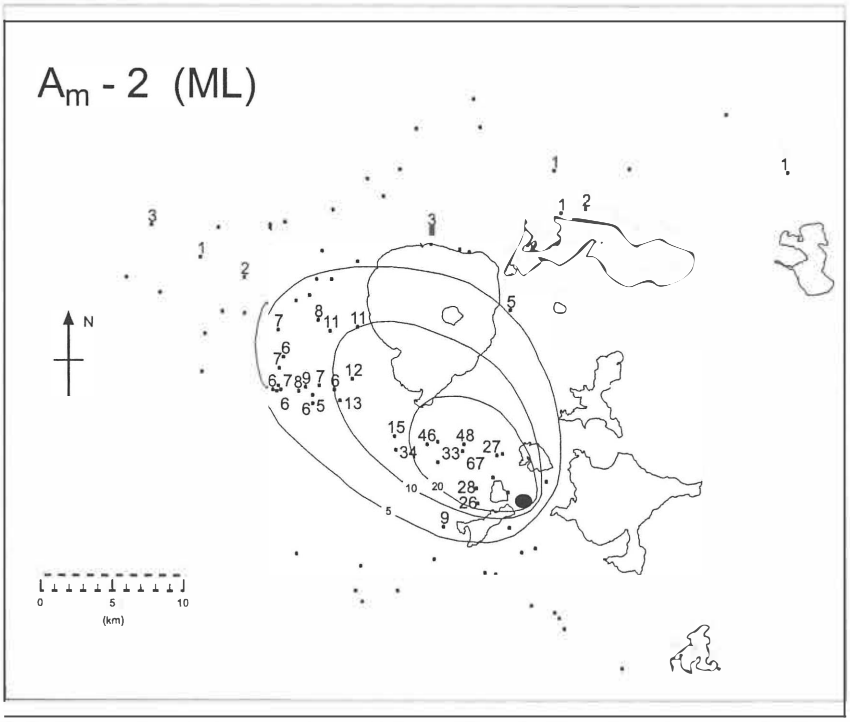

Fig 2.10 (a-f) Isopleth maps of maximum pumice (MP) and lithics (ML) for units A_m-2, 4 and 6. Contours are in mm. Black circle marks the vent location in all isopleth maps.

b

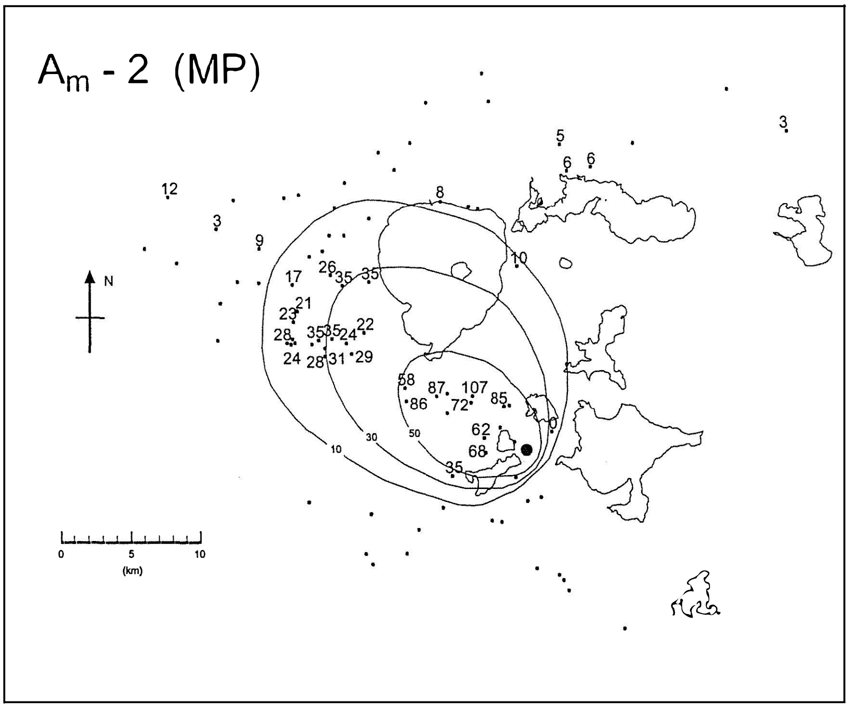

c

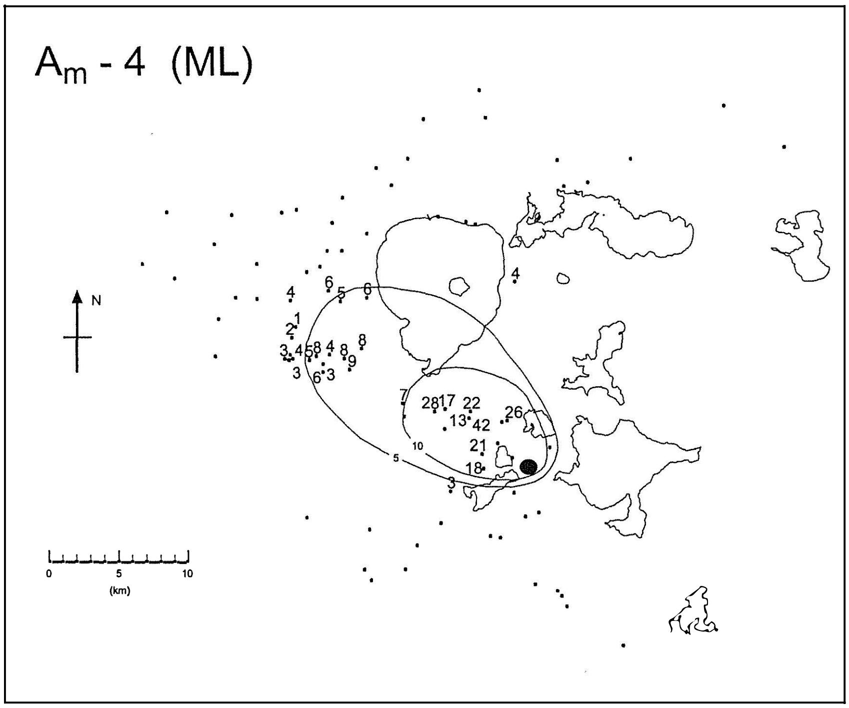

d

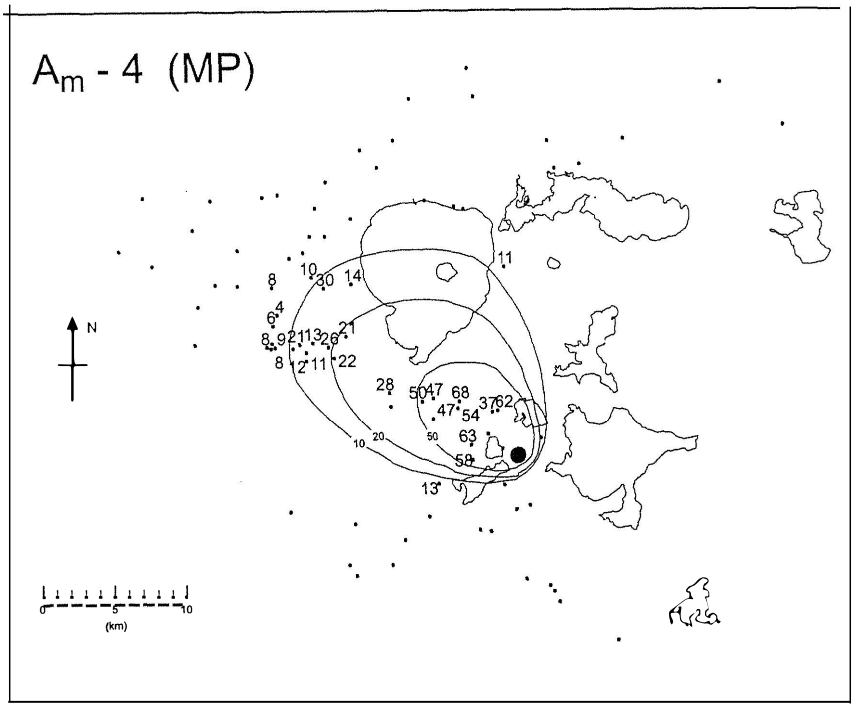

e

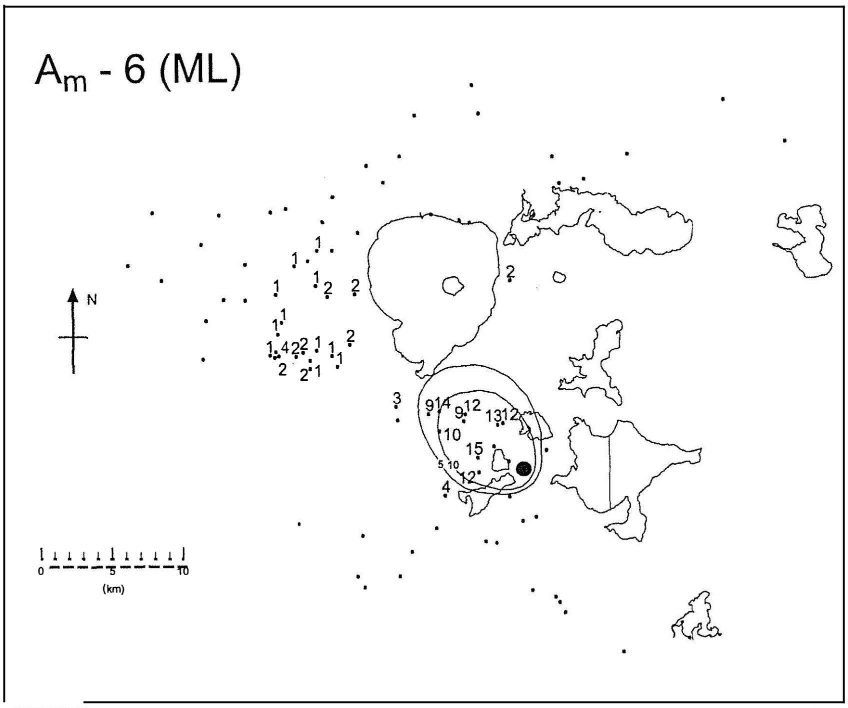

f

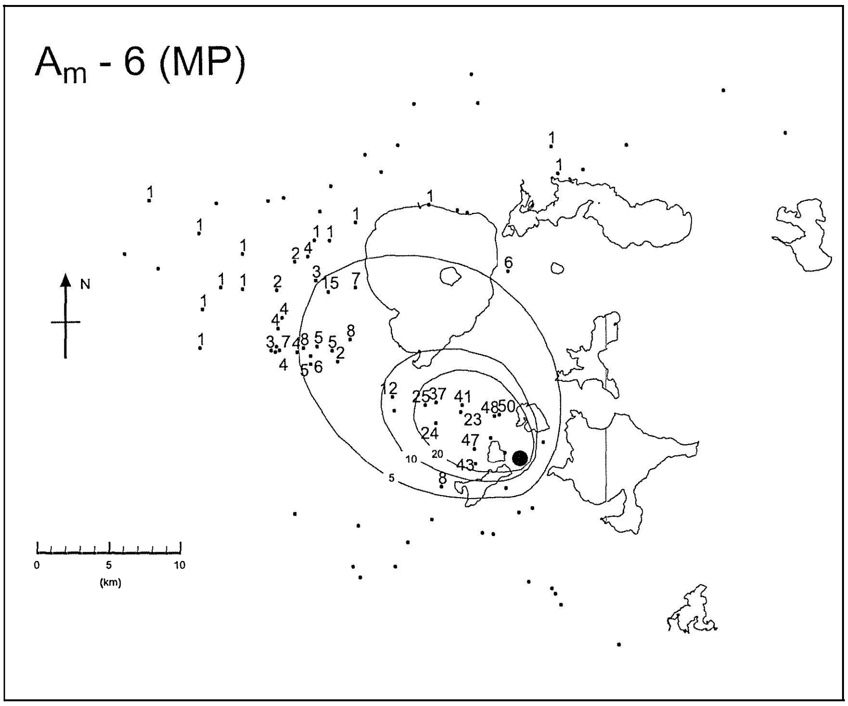

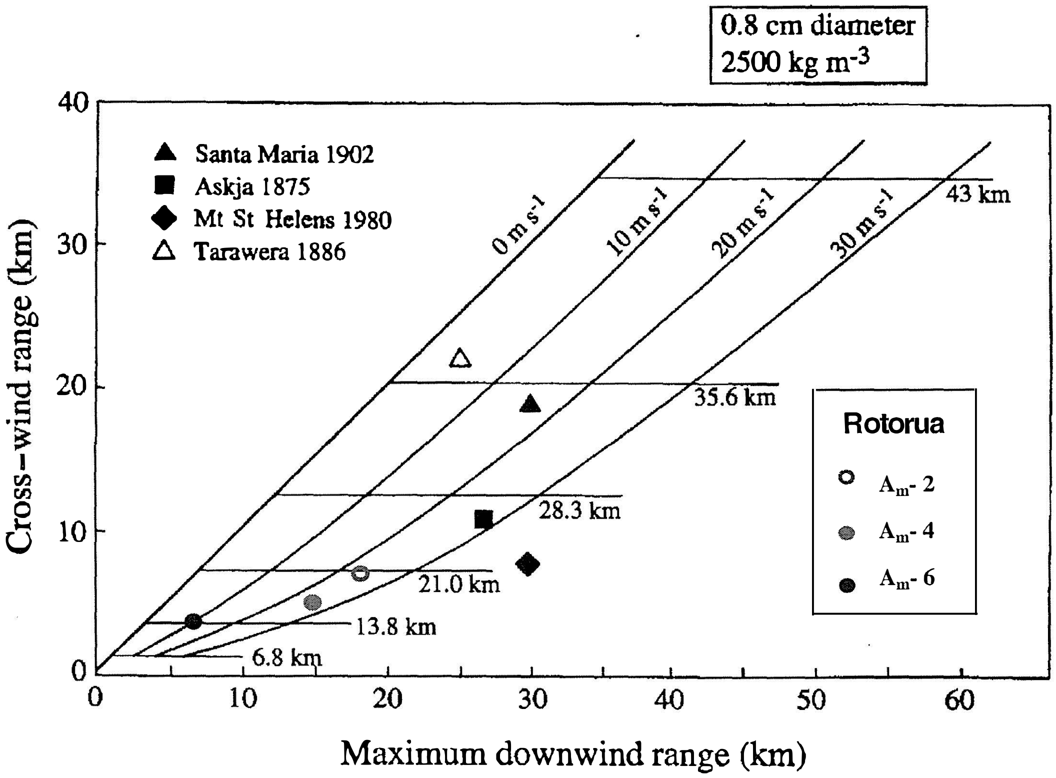

Fig 2.11 Column height and wind speed estimation of the Rotorua Tephra based on down and crosswind range of the 8 mm maximum lithic (ML) isopleth contours (with an estimated density of 2500 kg/m^3) of (Rotorua A medial subunits) A_m-2, 4 and 6 (circles). Historic eruptions for comparison fit well with the modelled predictions (after Carey & Sparks, 1986).

Pyle (1989) provides a reclassification scheme for eruption styles of pyroclastic fall deposits (Fig 2.10). This is based on the relationship between the half distance of the deposit thickness (b_t) and clast size (b_c). The total deposit plots within the plinian field with values b_t = 7.5 km, b_c/b_t = 0.6. This compares well with the smaller eruptions of A, G, H, J and L of the Mangaone subgroup (Jurado-Chichay & Walker, 2001a), and unit E of the Waiohau eruption (Speed, 2001).

To calculate the mass of the plinian fall deposit, the bulk density was measured to quantify the mass of the deposit. The bulk density ranged from 600 – 900 kg/m^3 (due to the predominance of coarse and fine clasts respectively) with an average density of 700 kg/m^3. In order to convert the bulk volumes to dense rock equivalent (DRE), a density of 2350 kg/m^3 was used.

Table 2.2 Summary table of the modelled parameters using the methods of Carey & Sparks (1986) and Pyle (1989). DRE is the dense rock equivalent using a magma density of 2350 kg/m^3. Mass is calculated with an average bulk density of 700 kg/m^3. Duration is based on a peak eruption discharge. Data (+) from Carey & Sparks (1986), (*) Mangaone data from Jurado-Chichay & Walker (2001b) and (#) Mt St Helens data from Carey & Sigurdsson (1986).

		Pyle		-1989			Carey &	Sparks	-1986
Eruption	b_t (km)	b_c (km)	b_c/b_t	Fall vol (km^3)	DRE (km^3)	Mass (kg)	Ht (km)	Intensity (kg/s)	Duration (h)
Rotorua 15 700 BP	7.5	4.5	0.6	1.61	0.4	1.28×10^{12}	20	4.0×10^7	8.9
Unit G *	8.3	7.9	0.9	2.5	0.63	1.5×10^{11}	32	1.44×10^8	2.9
Unit J * (*) Mangaone	5.9	5.9	1	0.77	0.23	5.5×10^{11}	25	6.24×10^7	
Tarawera + 1886							34	1.8×10^6	4
Mt St Helens # 1980					0.3	6.3×10^{11}	19		9.1
Taupo + 181 AD							51	1.1×10^9	3.8

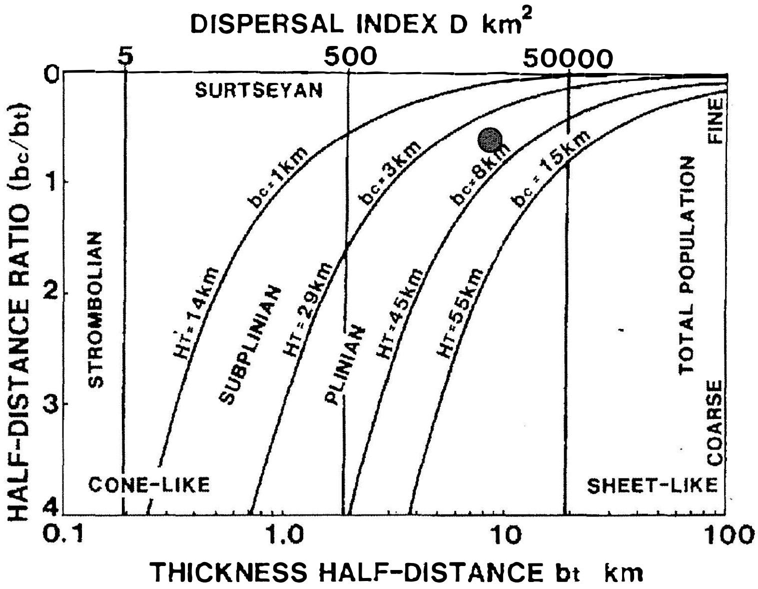

Fig 2.12 Revised classification scheme of Pyle (1989). The half distance ratio (b_c/b_t) represents the total grainsize population and the thickness half distance (b_t) represents the dispersal. Grey dot is Rotorua Tephra.

2.14 Volume Estimate – Dome

2.14.1 Eastern Dome (Rotorua A)

Eastern dome is interpreted in this study to be the product of an effusive phase following the main plinian eruption of Rotorua A. The volume of Eastern dome is calculated by taking the inferred surface area of the dome, extending beneath Trig 7693 and Middle domes, multiplied by the average elevation of the dome, estimated from contour data. Using ArcView to determine the area of the dome, using the polygon function lead to the calculation of the area (Figure 2.13). The dimensions are as follows:

Area = 12.51 km^2

Average thickness of the dome = 60 m (0.06 km)

Volume = Area x Height

= 12.510 km^2 x 0.6 km

= 0.75 km^3

2.14.2 Trig 7693 and Middle Domes (Rotorua B)

Two coalescing domes (Trig 7693 and Middle Rhyolite) are located immediately west of Lake Tikitapu and extend to the western shores of Lake Tarawera (as shown in Figure 2.12). These domes, on the basis of geochemistry and stratigraphy are inferred to be part of the Rotorua B, later-stage dome-building phase.

Froggatt & Lowe (1990) calculated the volume of the domes to be 1 km^3. The volume of the domes was recalculated using the formula of a frustrum (Figure 2.14). Due to the coalescing nature of the domes, the volume was calculated using two frustrum, both for the Trig 7693 and Middle Rhyolite domes. This formula is used to best represent the dome morphology as seen at the youthful Wahanga Dome of Mt Tarawera.

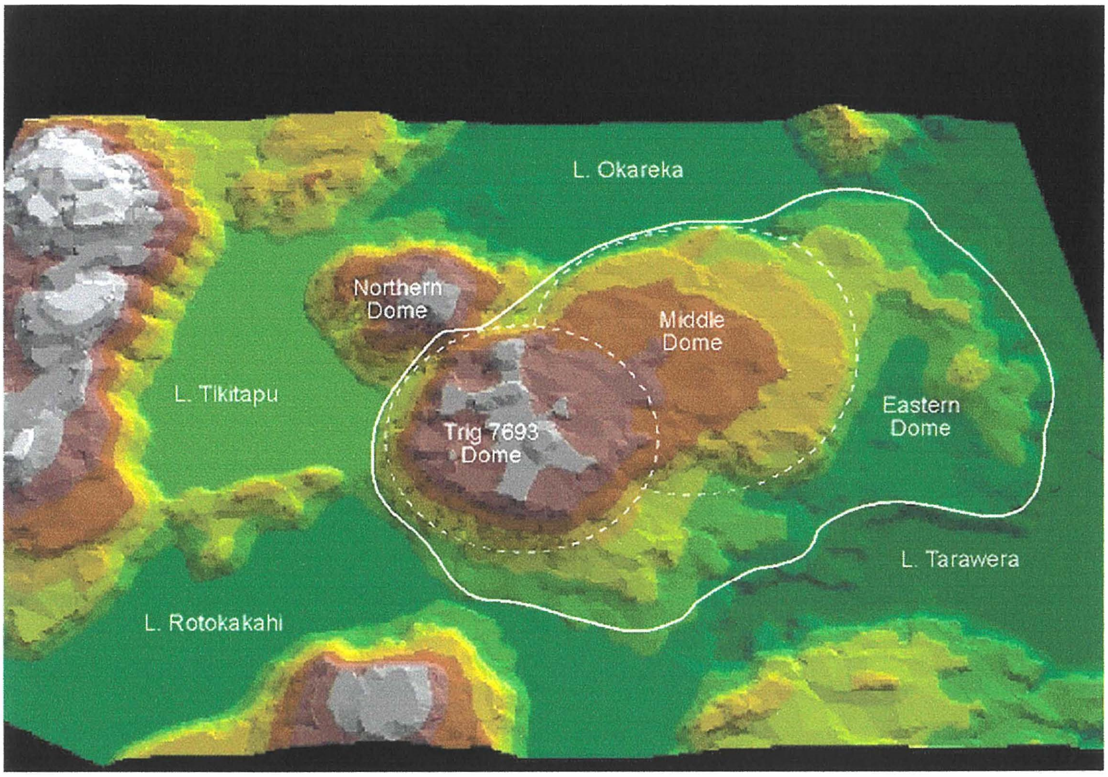

Fig. 2.13 Oblique view of a Digital Elevation Model (DEM) of the vent area. The margins of the domes are dashed according to morphology and Nairn (1980). White dashed lines mark the outline of the two frustrum. The solid white line demarcates the boundary of Eastern dome.

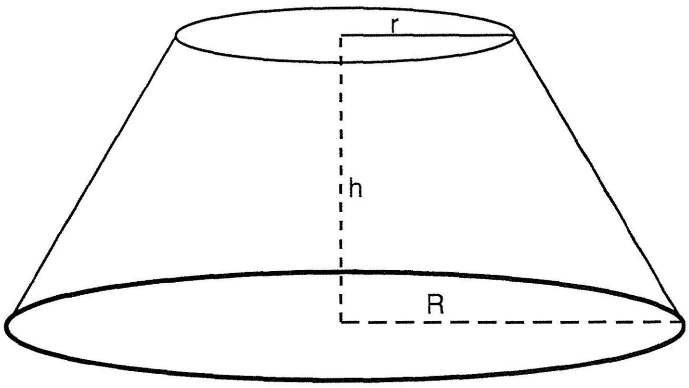

Fig. 2.14 Frustrum dimensions used to calculate the formula of the two rhyolite

The volume calculated using the frustrum equation is:

$$\text{Volume} = \frac{\pi h}{3}(R^2 + Rr + r^2)$$

Using the dimensions of the Middle Rhyolite:

h = 160 m, R = 1000 m, r = 400 m

Volume = 0.26 km^3

Trig 7693:

h = 180 m, R = 900 m, r = 700 m

Volume = 0.36 km^3

Therefore the total volume of the coalesced dome is 0.62 km^3.

Wahanga dome in comparison has dimensions:

h = 520 m, R = 1375 m, r = 625 m

Volume = 1.71 km^3

c.f. 2.0 km^3 of Nairn *et al.,* (2001) This method assumes the base of the dome is at the transition from dome slope to the surrounding surface. This may lead to an underestimation of the erupted magma, due to subsequent burial. No account has been made of the associated block and ash flows generated during dome growth. This has been difficult to quantify due to lack of exposure in the proximal locations. Due to the topographic controls surrounding the vent, the likely flow directions would have been dominantly to the S and E. Due to the age of the dome (15.7 ka), erosion has incised the edifice, which may have lead to an underestimation of the dome volume.

2.15 Eruption Duration

Historic growth rates of andesite and dacite domes (eg. Mt St Helens, Pinatubo and Montserrat) are the best analogues for rhyolite dome growth. Observations of historic dome building eruptions have found extrusion rates of 1-10 m^3/s (Wolfe & Hoblitt, 1996). The mean discharge rate observed at Montserrat is 3 m^3/s (present annual rate), which compares well with Newhall & Melson (1983) who examined the discharge of 67 dome eruptions of dacitic and andesitic composition.

2.15.1 Eastern Dome (Rotorua A)

Eastern dome has an estimated volume of 0.75 km^3. Therefore assuming an average discharge rate of 3 m^3/s, Eastern dome would have taken over 8 years to be extruded. The presence of Rotorua B pyroclastics overlying this dome suggests Eastern dome was extruded before the later dome-building and explosive phases of the Rotorua B event.

2.15.2 Trig 7693 and Middle Dome (Rotorua B)

The total volume of Trig 7693 and Middle domes is estimated at 0.62 km^3. Assuming the 3 m^3/s growth rate, the domes would have been extruded over approximately 6.5 years. The presence of Trig 7693 derived tephra on Middle dome, suggests extrusion of the Trig 7693 dome was still occurring after the cessation of Middle dome growth. Middle dome with a volume of 0.26 km^3 extruding at 3 m^3/s could have taken at least 2.7 years, while the 0.36 km^3 Trig 7693 dome could have been extruded over 3.8 years.

2.16 CONCLUSIONS

- The stratigraphy of the plinian Rotorua Tephra (Rotorua A) is normally graded with cm-scale bedding demonstrating the widely varying eruption intensities. The thickness distribution maps indicate a strongly directed fall deposit to the NW with trace amounts of Upper Rotorua Tephra (Rotorua B) to the S and E of the vent.

- In the proximal sites, there is no evidence for widespread pyroclastic density currents, probably due to the older rhyolite domes surrounding the vent (to the NW, W and NE) creating a topographic barrier. This forced block and ash flows and pyroclastic density currents to the S and E of the vent.

- Dispersal of the plinian fall to the NW extends to Waikato and Auckland.

- Using the method of Pyle (1989), the Rotorua plinian tephra volume is calculated at 1.61 km^3 with an equivalent magma volume of 0.4 km^3 for this, the main explosive phase of the Rotorua eruptive episode. This is likely to be a minimum value due to the effect of distal fine ash being difficult to model.

- Isopleth maps were used in plume modelling. The maximum height of the eruption plume was reached early in the Rotorua A eruption at 20 km, with a maximum discharge rate of 1.0×10^8 kg/s. This equates to a minimum eruption duration for the plinian phase at 3.5 hours.

- Dome volume calculation using the formula for a frustrum results in a total volume of 1.37 km^3. This volume includes Eastern dome (0.75 km^3) and the coalescing Trig 7693 (0.36 km^3) and Middle (0.26 km^3) domes. The total DRE volume for the eruptive episode (Rotorua A and B) is 1.37 km^3 (dome) + 0.4 km^3 (pyroclastics) = 1.77 km^3. The inclusion of Eastern dome in the volume calculation increases the amount of magma erupted during the Rotorua eruptive episode. The pyroclastic volume is significantly smaller than previous estimates and may represent a minimum volume. Interestingly, the volume of magma erupted explosively is less than 25 % of the total eruptive episode.

- A total eruption duration of at least 15 years is calculated for the entire eruptive episode assuming a constant dome growth rate of 3 m^3/s. The lack of a significant paleosol suggests the eruption phases of A and B were closely spaced in time.

- Such long eruption durations have implications for civil defence authorities as shown at Montserrat (see Chapter 6).

Chapter Three
Textural and Component Analysis

3.1 Introduction

Textural and component analysis provides a quantification of the nature and dynamics of the eruption. The plinian fall component of the eruptive episode provides a well exposed deposit to analyse the textural characteristics. Grainsize, componentry, vesicularity, petrography and SEM were used to describe the deposit in detail, both spatially and temporally. Samples for componentry, vesicularity, petrography and SEM were taken from proximal sites in order to record the temporal changes within the eruption sequence. Grainsize samples were taken from a transect down the dispersal axis in order to quantify the change in the deposit with distance from the vent. Figure 3.1 indicates the location of the samples obtained for textural analysis.

3.2 Grain Size

3.2.1 Methods

Samples for grain size were collected on the basis of the assigned stratigraphy from a proximal site (#2 – Red Tank Road) and down the dispersal axis (Figure 3.1) to examine the change in grainsize with distance from vent (37 samples). Vertical collection at individual sub-units was achieved by creating a trench from the top of each section to the base, thus eliminating the collection of foreign grains. Samples were then oven-dried to eliminate coagulation of grains at 60 °C. Using standard Endacott sieves, the samples were sieved at 0.5 ϕ intervals, from -4.0 ϕ down to 4.0 ϕ (Walker 1971; Cas & Wright, 1987). For sieves coarser than -1.0 ϕ, hand sieving was used, while for finer sieves ie. –0.5 ϕ and finer, the mechanical shaker was used at a low amplitude to limit abrasion of clasts. Each sieved sample weight was recorded and kept for componentry analysis. Inman (1952) parameters were determined graphically to obtain descriptive statistics ie. Mean diameter, sorting, kurtosis and skewness (Appendix 2).

3.2.2 Results and Discussion

Grain size distributions of the Rotorua plinian fall samples are entirely unimodal and well sorted (1.7-1.1 ϕ) for pyroclastic deposits, (Walker, 1971) although classed as poorly sorted in sedimentological classifications (Folk & Ward, 1957) (see Appendix II). The normal size distribution enables the samples to be characterised by the median phi value, which is plotted in Figure 3.2 to indicate the trend of changing grainsize within the stratigraphy. The tephra is reverse to normally graded, ranging from a medium lapilli (–2.0 ϕ) – block-sized unit (-5.0 ϕ) – coarse ash (0.0 ϕ). The coarsest grainsize of the tephra is in the lower third of the deposit. This trend of reverse to normal grading is seen at proximal to distal locations. However the fine scale variations seen in the proximal sites are not evident further from the vent (Figure 3.1).

As the distance from the vent increases, along the dispersal axis, the tephra exhibits progressive changes in grainsize characteristics as would be expected. In proximal sites, the tephra contains coarse pumice (up to 1 m) and lithic clasts due to ballistic fall from the low portion in the column. Fine scale bedding is also evident due to highly variable syn-eruptive winds close to the vent. This leads to the relatively poor sorting (1.7 ϕ) in comparison to the medial and distal sites (1.1 ϕ). As distance increases from the vent, the premature fall-out is reduced due to equilibrium fall from the umbrella region of the plume causing a progressive fractionation of the deposit (Sparks *et al.,* 1997).

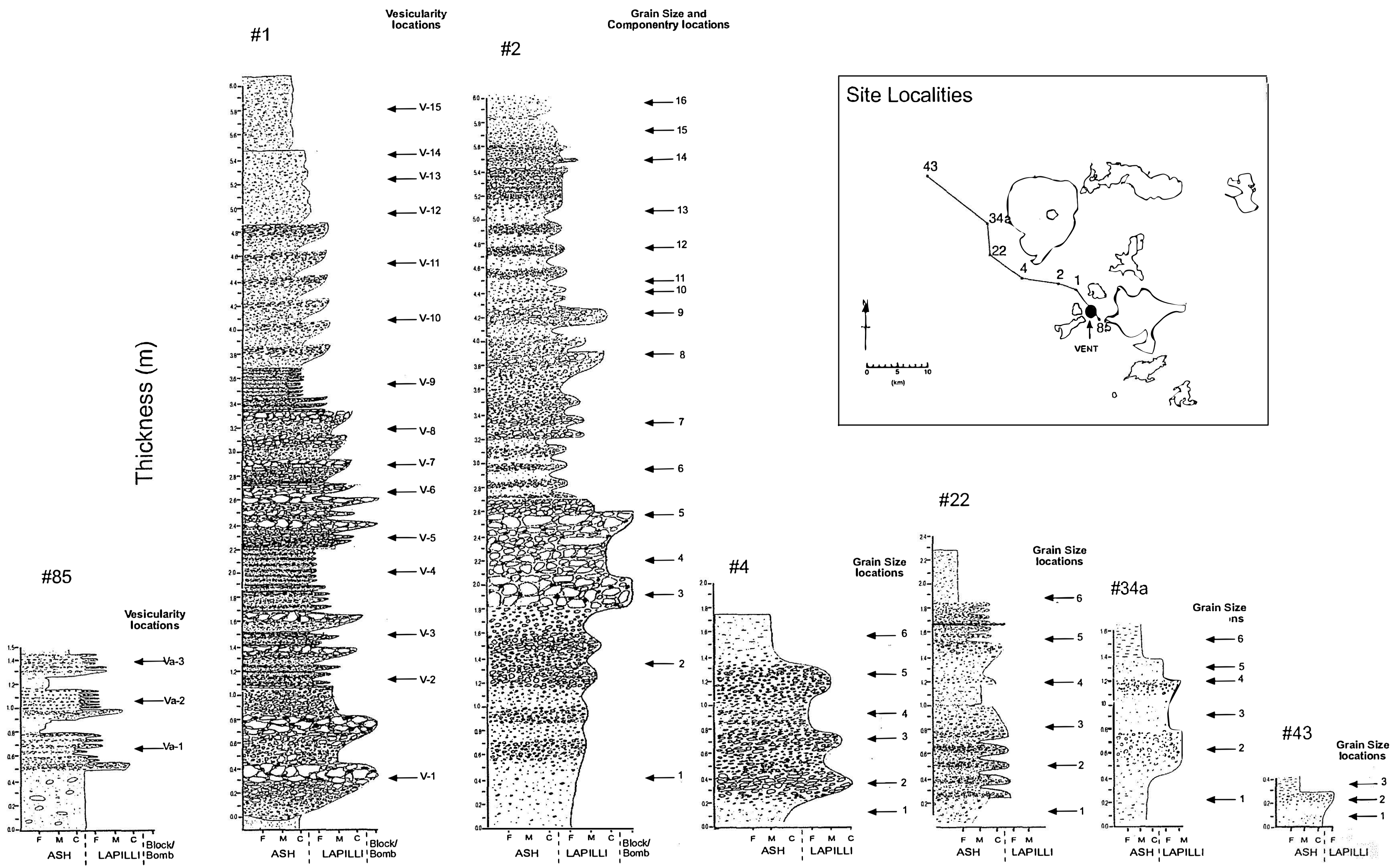

Fig. 3.1 Sample locations for textural analysis along the dispersal axis. Arrows mark sample collection for the various laboratory techniques. Inset indicates location of stratigraphic columns with grey circle representing the location of the vent.

Also, better sorting can result from the increase in pumice density as particle size decreases (Walker 1971). This acts to reduce the density contrast as settling velocity becomes approximately equal to grain size.

The skewness of the tephra samples throughout the deposit is near symmetrical or finely skewed. This indicates the deposit follows a normal distribution curve and does not involve a significant population of fine particles. At one location (# 4), the deposit has been hydrothermally altered leading to an increase in fines.

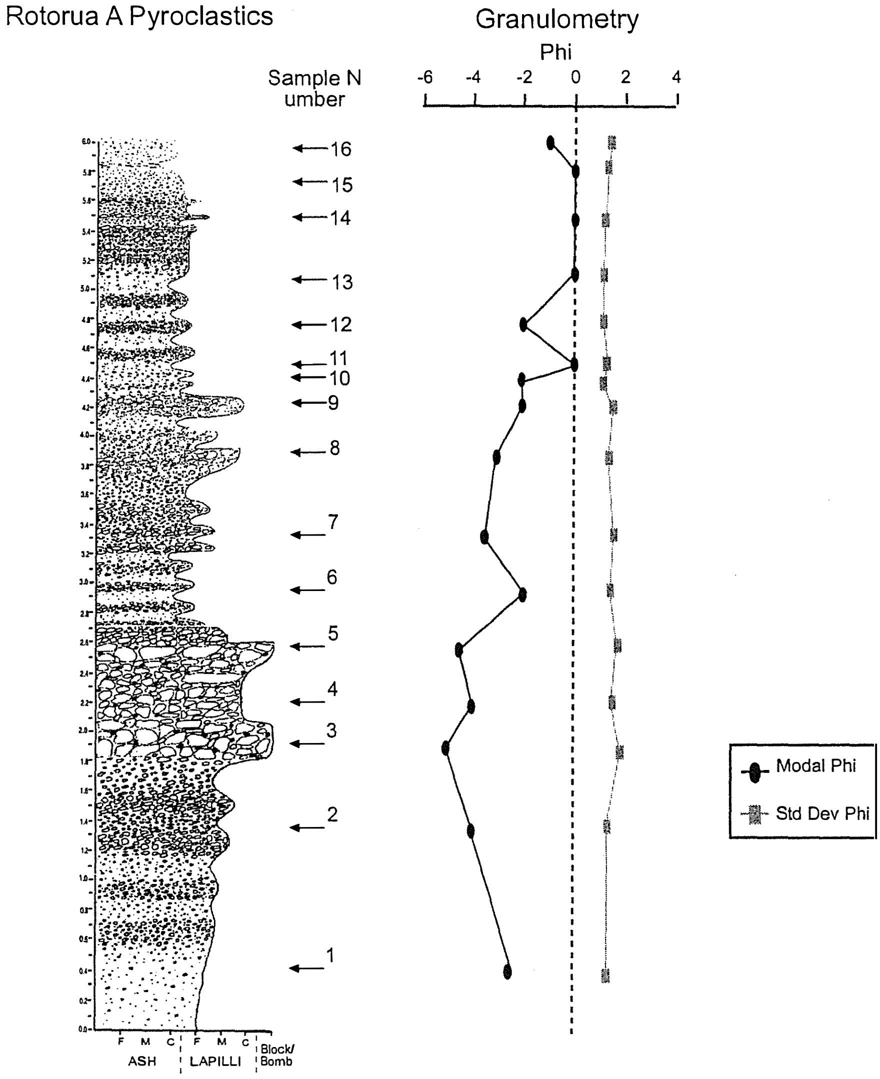

Fig. 3.2 Median and sorting values through a proximal site (Red Tank Road). Site locations marked with arrows with corresponding grainsize data.

3.3 Componentry

3.3.1 Methods

One site was chosen for detailed componentry analysis, being the proximal Red Tank Road site (site # 2). The individual samples for the section were analysed by hand picking (-5.0 to –1.0 ϕ) and under a binocular microscope (<-0.5 ϕ) to determine the proportions of the various constituents. The coarse samples (>-1.0 ϕ) were weighed to 0.01 g and the finer fraction (<-1.0 ϕ) on a 0.0001 g scale due to the small amount of sample separated. Samples well below the grain size median were not analysed and for analysis, the median grainsize was used to quantify the componentry of the subunits. This was based on the unimodal distribution of the grainsize samples. Problems were encountered when distinguishing components finer than 1.0 ϕ, due to the subtle differences in pumice vesicularities.

Walker (1971) divided the components of tephra into pumice, lithics, obsidian and crystals, however due to the spectrum of dense pumice observed, it was necessary to quantify the proportions of the various juvenile components. Samples were separated into 7 categories: 1) vesicular pumice (~75 % vesicles) 2) dense pumice – low density (~50 % vesicles) 3) dense pumice – medium density (~30 % vesicles) 4) dense pumice – high density (~ 10 % vesicles) 5) lithics 6) obsidian and 7) free crystals. The free crystal component consisted of plagioclase, quartz, hypersthene, hornblende and biotite. The range of dense pumice clasts was classified according to the vesicle morphology and colour. Vesicles of the very dense pumice exhibited collapsed morphologies and clasts are dark grey in colour. The range of juvenile clast vesicularity was quantified where possible in order to determine the relative proportions of the juvenile clasts. Determining the proportions of the variously dense pumice clasts was possible for grains coarser than 0.0 ϕ, however finer clasts were difficult to separate due to the inability to closely examine the vesicle morphology and colour was not a sole indicator of apparent density.

3.3.2 Results and Discussion

As Figure 3.3 shows, the variability of componentry data is a function of position in the stratigraphy and modal grainsize. Componentry data can be a valuable tool in determining the character of eruptions. Trends of componentry data within a complete proximal section indicate changes in the eruption evolution through time.

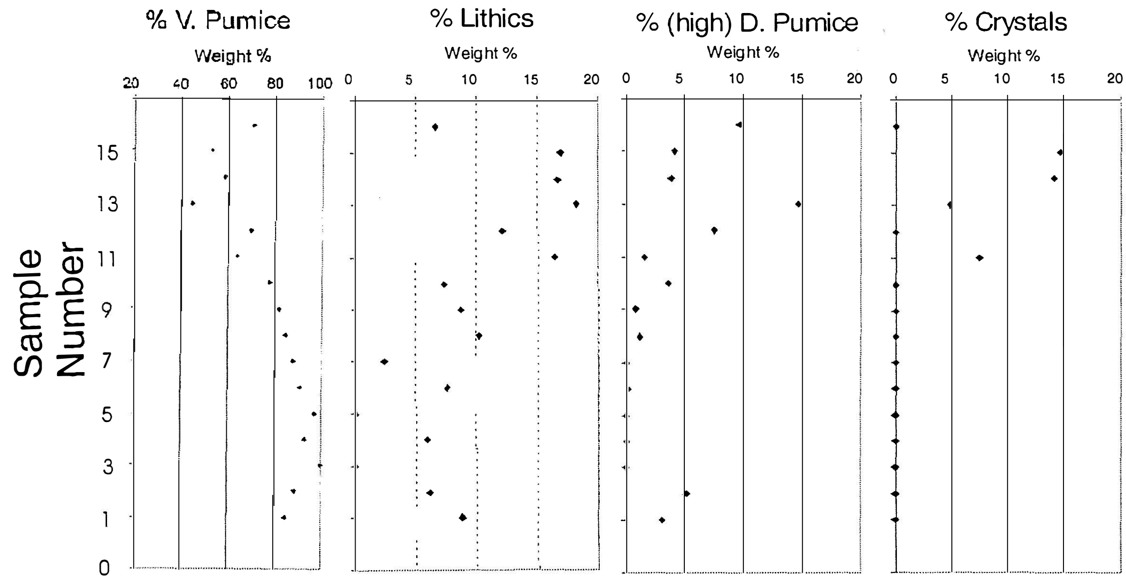

Fig 3.3 Componentry data from the four major categories of the Rotorua tephra. Data collated from modal phi samples from the grainsize samples. Samples taken from the proximal site and locations of Fig. 3.2. V. Pumice represents the vesicular pumice component, (high) D. Pumice represents highly dense (~10 % vesicles) pumice.

Vesicular pumice abundance as determined by componentry, decreases with time, from 80-100 % to ~45 %. This indicates a steady decrease in gas-charged magmatic input during the eruption. This trend is mirrored in the clast vesicularity data (see 3.4) and the median grainsize trend (Figure 3.2).

Lithics within the Rotorua tephra are ~100 % rhyolite lava. Very rare (< 0.05 %) diatomite was found in the lower portions of the tephra, indicating magma ascent through lake sediments early in the eruptive episode. Lithic proportions are inversely related to the vesicular pumice trend ie. as vesicular pumice abundances decrease, lithics increase. An increase in lithic percentages may suggest the progressive widening of the vent or a change in vent location. However, the systematic nature of the increase in lithics suggests progressive vent widening occurred rather than an abrupt change in vent position. The lithic proportions in the early stage of the eruption decrease from 10-0 %. This indicates that after initial conduit development and the ejection of moderate amounts of lithics, the conduit appears to have stabilised. The steady increase in lithics to 15 wt % from 2.6 m (12 on Figure 3.2), corresponds to the climax in grainsize, suggesting greater vent erosion due to increased eruption intensity.

Very dense pumice and free crystals contribute minor components of the tephra. The dense pumice and free crystals exceed 5 wt% at three samples of the proximal stratigraphy. Although in small volume, the dense pumice may indicate particular conditions existed in the conduit and around the vent walls during eruption. Hammer *et al.,* (1999) have shown that the presence of dense pumice (with collapsed vesicle walls) indicates an open degassing system (Figure 3.4), in which the upper portion of the magma chamber forms a degassed and permeable cap, which facilitates degassing. This leads to a gradation of dense pumice capping the gas-rich centre. Therefore the dense pumice may represent episodes of degassing during the eruption as seen at Mt St Helens (Klug & Cashman, 1994) and Mt Pinatubo (Hammer *et al.,* 1999).

3.4 Vesicularity

3.4.1 Methods

To determine the vesicularity of the pumice within the deposit, the Archimedes method (Houghton & Wilson, 1989) was employed (as seen in Figure 3.5). Samples were collected over narrow stratigraphic levels at the proximal type locality (Okareka Quarry). This involved wrapping medium lapilli-sized (16-32 mm), vesicular pumice (refer to 3.3.1) clasts in parafilm to ensure a watertight outer surface. The parafilm was moulded into surface irregularities that were not vesicles and covered the edges of larger vesicles. It was important to eliminate the introduction of pore spaces on the outer portions of the pumice clast in order to gain accurate vesicularity results. Once

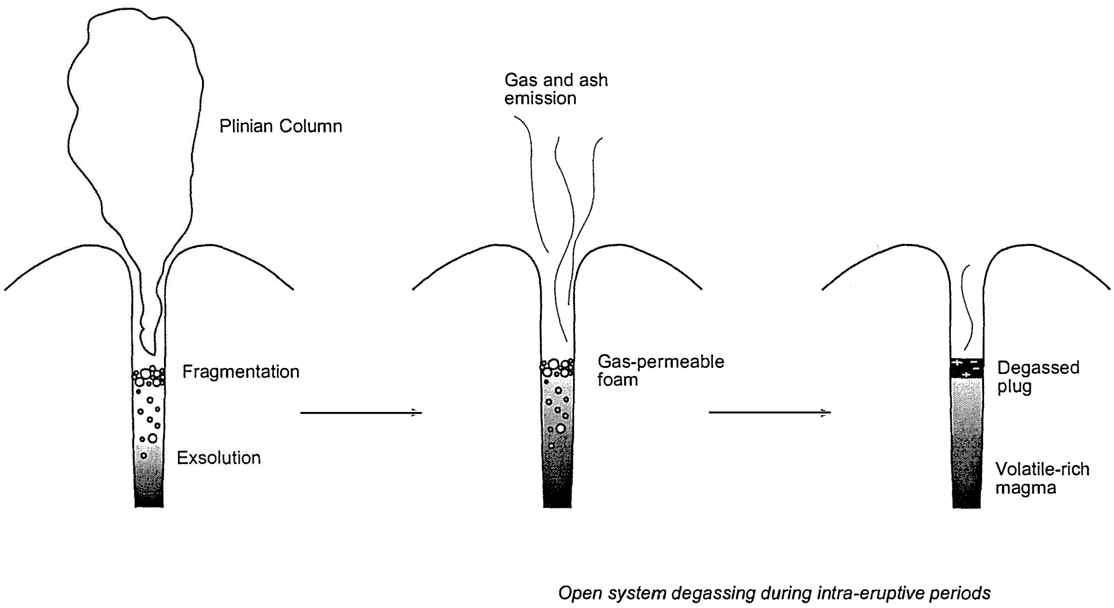

Fig. 3.4 Model of degassing leading to the arrange of densities in pumice clasts. Degassing occurs during repose periods between explosive events. Redrawn from Hammer *et al.,* (1999)

wrapped, the clast was weighed first in air (dry), then weighed in water. A lead weight (of known mass) prevented the buoyant pumice from floating.

Vesicularity was calculated on a crystal free basis. To measure the crystal content of the pumice, large clasts were weighed and crushed to free the crystals. The crystals were separated by wet-sieving, then weighing the remaining crystals as a proportion of the original clast weight.

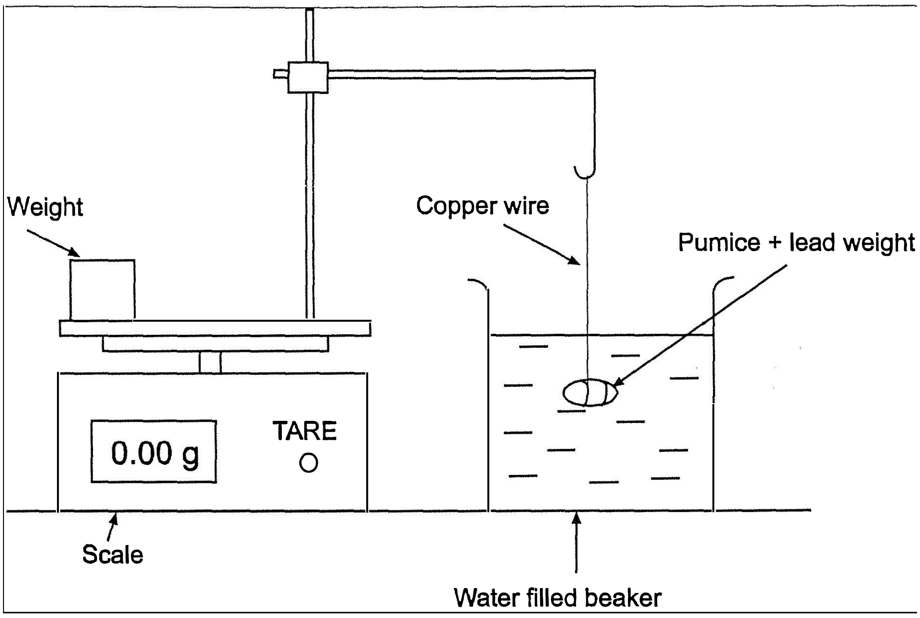

Fig 3.5 Schematic diagram of the Archimedes method for the determination of pumice clast vesicularity (redrawn from Houghton & Wilson, (1989).

To calculate the vesicularity, first the clast density and dense rock equivalent are required:

Clast Density =

$$Clast_{air}/\{(Clast_{air}+Sheet_{water})-(Clast+Sheet+Sinker_{water})-Sinker_{water}\} \quad (1)$$

(using a sinker)

Then to convert to vesicularity:

Assuming a dense rock equivalent (D.R.E) of 2.4 g/cm^3

Vesicularity = 100 (D.R.E. dnsity - clast density)/ D.R.E. density (2)

3.4.2 Results and Discussion

Temporal changes in vesicularity indicate changing eruption dynamics, such as the involvement of water in driving the eruption. Several authors have reported on the implications of pumice vesicularity in describing the eruption dynamics, which leads to information on the state of the magma at fragmentation (eg. Thomas *et al.,* 1994; Kaminski & Jaupart, 1997; Tait *et al.,* 1998). The vesicularity of the juvenile component of the Rotorua tephra is approximately 75 % throughout the plinian phase of the eruptive episode until the uppermost subunit, where a sudden drop to ~65-45 % vesicles is obtained. The tight range of values around the mean suggest the driving force for the eruption was sourced predominantly from gases within the magma (Houghton & Wilson, 1989). This is due to the equilibrium fragmentation level (~75 %) reached just prior to eruption compared with magma: water interaction creating a wide vesicularity range in each sample (Houghton & Wilson, 1989). Although the range in vesicularity increases at the top of the section, the range in values is a result of varying clast densities of suitable size for the laboratory method. However, the coarsest clasts are ~60 % vesicular. Therefore, the plinian phase exhibits a slow decline in mean vesicularity with little variation within each sample (Figure 3.6), indicating the magmatically driven eruption tapped steadily gas-poor magma.

The Te Mu Road section contains pyroclastics of the Rotorua B phase of the eruptive episode. Due to the increased crystal content, the density is much higher than that of the Rotorua A phase juveniles. Vesicularities range from 50-20 %, suggesting the involvement of gas-depleted magma in the later phase of the eruption. There is no major decrease in vesicularity through the short sequence indicating similar eruptive processes were occurring within this period of time. The trend of these samples indicates small (vulcanian) magmatic explosions through a growing dome complex lead to their emplacement on the south and east vectors of the vent (see Chapter 2).

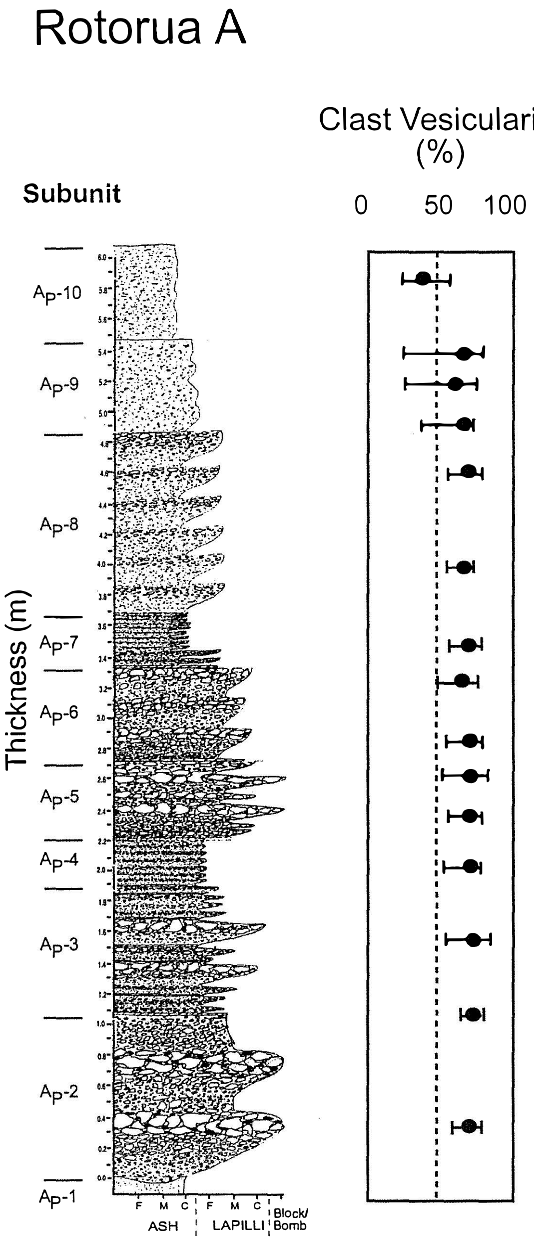

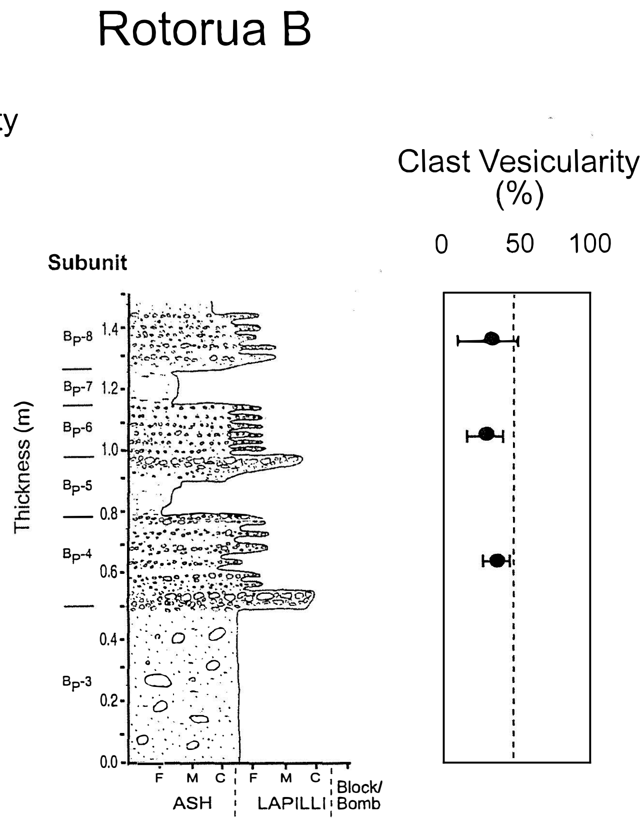

Fig. 3.6 Juvenile clast vesicularity data for proximal locations at (a) Okareka Quarry (plinian phase) and (b) Te Mu Road section (dome building phase). The black circles and bars represent, respectively, the mean and range of vesicularities within the sample population.

3.5 Scanning Electron Microscope (SEM)

3.5.1 Methods

To analyse the pumice textures of whole clasts and vesicle morphology, SEM was used to produce images of the juvenile clasts. Ash-sized samples from the Te Mu Road section were analysed under reflected light to examine edge modification, and other aspects of ash morphology. Also a spectrum of dense pumice clasts, representative of the deposit, were made into thin-sections and polished in order to examine bubble wall morphology under backscattered imaging.

3.5.2 SEM – Reflected Light Images

Reflected light was used to examine the morphology of ash-sized juvenile clasts sampled from pyroclastic flow, surge and fall units in the proximal site in the Rotorua B phase. The proximal site sampled is located within 1.5 km of the vent (Te Mu Road section). Images in Figure 3.7, indicate the presence of subtle edge modification in density current deposits. Density current deposits indicate that edge modification has occurred due to grain-grain interaction during transport. Rounding of the density deposits is seen at a range of grain sizes (fine ash to fine lapilli) and reflects the energy contained in the flow to cause friction and collision of grains. Fall deposits exhibit angular margins with fragile edges still intact. Some fall derived clasts show signs of minimal edge modification probably due to turbulence in the eruption plume, or derivation from co-surge plumes.

a

b

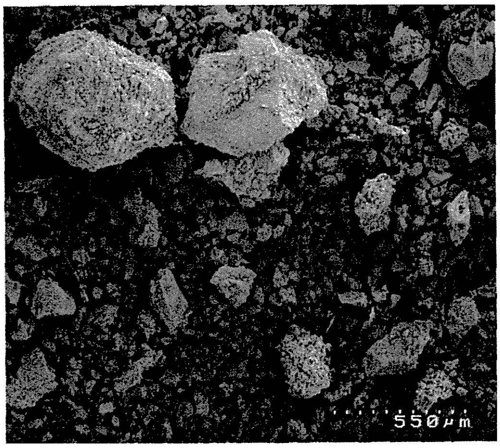

Fig. 3.7 SEM images of Rotorua B ash-sized juvenile clasts sampled from (a) pyroclastic fall (b) pyroclastic flow, and (c) a pyroclastic surge deposit at the Te Mu Road section. Subtle edge modification is evident in the density current deposits. Due to the proximity to source, the degree of clast rounding is minimal.

c

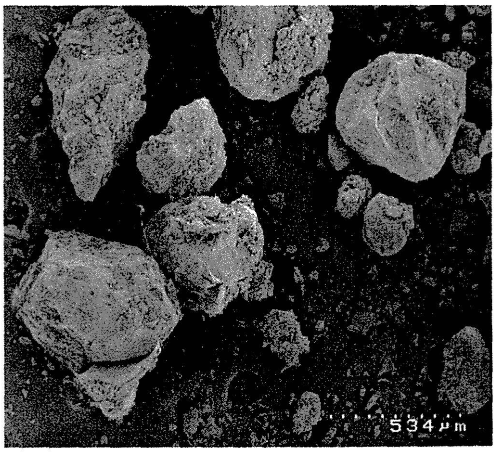

3.5.3 SEM – Backscatter Images

Representative samples of the lapilli-sized juvenile component of the Rotorua eruptive episode were examined under the SEM using backscatter imaging. Backscatter imaging assesses the vesicle morphology and can be used to determine the record of magmatic processes preserved in the juvenile clasts

The vesicular pumice of the Rotorua Tephra (Rotorua A) exhibits unimpeded growth of vesicles, leading to bubble coalescence. The growth of vesicles has lead to the ~ 75 % vesicularity of the crystal-poor Rotorua A pyroclastic deposit (Rotorua Tephra). Due to the low crystal content (<5 %), the vesicle walls are free to grow and are therefore not retarded due to the presence of crystals. Vesicles can be deformed according to the position in the conduit, however the predominant vesicle morphology is sub rounded and vesicles are of approximately equal size (Figure 3.8 a).

Dense pumice clasts of the Rotorua A pyroclastics exhibit ~ 0 % vesicularity due to the complete collapse of pre-existing vesicles (seen in hand specimen). Under backscatter, the dense clasts exhibit perlitic cracks. Crystals are rare (< 5 %), however microlites (seen in petrographic thin sections) are not evident, even at high magnification (Figure 3.8 b).

Rotorua B pyroclastics are crystal-rich (~ 20 %) and exhibit bubble wall modification in backscatter images. Vesicles in the Rotorua B pyroclastics have been deformed around large phenocrysts (Figure 3.8 c, d) leading to elongation of flattened vesicles. Vesicularity is significantly lower in the Rotorua B compared to Rotorua A pyroclastic deposits.

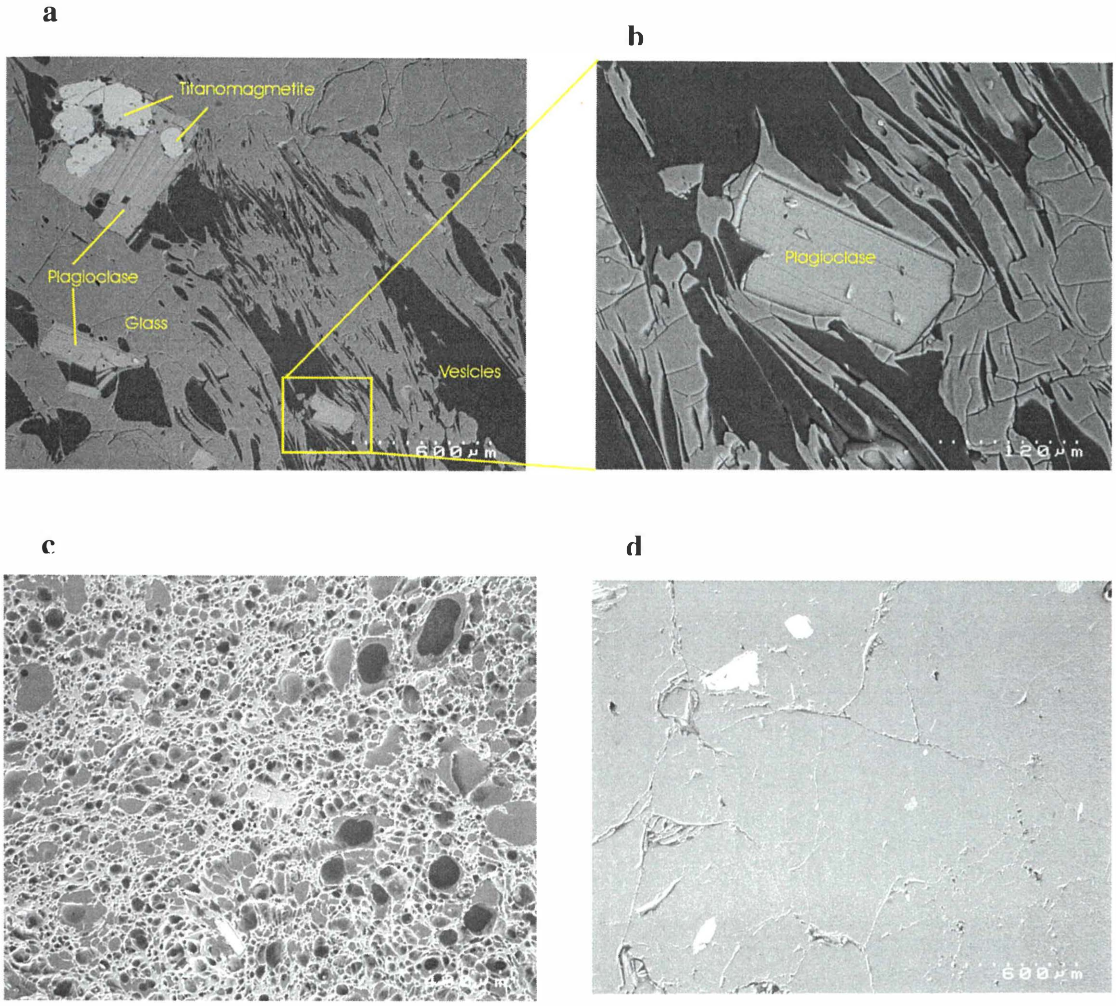

Fig. 3.8 SEM backscatter images of representative samples from (a) Rotorua B pyroclastics indicating bubble deformation around rigid crystals, (b) Rotorua B pyroclastics at a higher magnification showing vesicle growth modification around single crystals, (c) Rotorua A pyroclastic fall (Rotorua Tephra) exhibiting unimpeded vesicle growth leading to bubble coalescence, (d) a dense pumice clast from the Rotorua A fall deposit, with completely collapsed vesicles.

3.6 Conclusions

- Grainsize for the Rotorua A (Rotorua Tephra) pyroclastics ranges from a block/bomb basal sub unit to a medium ash upper sub unit. Maximum grainsize (and intensity) was achieved early in the plinian phase of the eruption. Fine scale bedding on a cm scale is evident throughout the deposit and indicates eruption intensity fluctuated significantly over very short intervals of time.

- The deposits of the Rotorua A pyroclastic phase are well sorted (1.7-1.1 ϕ). All sub units exhibit a normal grainsize distribution indicating the explosive Rotorua A phase was driven by magmatic gases.

- Componentry analysis on the Rotorua A pyroclastic phase indicates a trend of increasing lithic content with stratigraphic height, suggesting the conduit was becoming increasingly unstable.

- Vesicularity of the plinian juvenile clasts in much of the deposit is constant at ~ 75 %. However in the uppermost sub units (A_p-9 and A_p-10) clast vesicularity decreases to ~ 50 % vesicles. This indicates the eruption tapped progressively gas-poor portions of the magma.

- SEM images of whole clasts from the Rotorua B phase indicates subtle edge modification occurred in density current derived deposits. Fall deposits have maintained their angular margins.

- Backscatter images under the SEM, indicate vesicle growth was unimpeded during the Rotorua A pyroclastic phase. Dense pumice clasts from the Rotorua A phase exhibit completely collapsed vesicles leading to a perlitic glassy texture. In contrast, Rotorua B pyroclastic deposits show that growth of vesicles was retarded due to the presence of crystals. This has led to significant elongation of the vesicles.

Chapter Four
Mineralogy and Geochemistry

4.1 Introduction

Detailed studies of mineralogy and geochemistry of pyroclastic deposits can provide important constraints on magmatic evolution and petrogenesis. Pumice clasts and accessory lithics were sampled for geochemical analysis at two proximal locations (Red Tank Road – Whakarewarewa Forest and Te Mu Road). Samples of the dome lavas in the Okareka Embayment collected by Bowyer (*in prep*) were used to compare with the pyroclastic deposits collected in this study. These proximal sites were chosen to determine whether the magma supplying the Rotorua eruption was the source for both the Rotorua A (Rotorua Tephra) and the Rotorua B ('upper Rotorua' of Nairn, 1980). The Rotorua Tephra was sampled at closely spaced stratigraphic intervals through the sequence to determine whether the magma was compositionally zoned prior to eruption. Dunbar *et al.*, (1989) showed that many TVZ magmas are compositionally heterogeneous, while more recent investigations (eg. Briggs *et al.*, 1993; Sutton *et al.*, 1995) have shown that compositionally zoned magma chambers are common in TVZ rhyolitic eruptions.

Pumice clasts were examined petrographically to determine the mineral assemblage of the Rotorua A and B phases. Samples were collected in stratigraphic sequence through the A and B phases to determine whether any mineralogical changes were occurring during the eruption.

4.2 Mineralogy

The Rotorua A and B phases of the Rotorua eruptive episode can be distinguished based on their distinct mineral assemblages. Representative samples were pooled and used to describe the nature of the juveniles from each phase of the eruptive episode.

4.2.1 Rotorua A Pyroclastics

Thin sections of the Rotorua A pyroclasts exhibit a mineral assemblage of plagioclase, quartz, orthopyroxene, hornblende, biotite, opaques, augite, apatite and zircon. Phenocrysts make up ~2-5 % of the pumice clasts and are constant in abundance throughout the deposit. Phenocryst descriptions are given below.

- Plagioclase is the dominant mineral (~ 70 % of the total phenocryst abundance) in the Rotorua Tephra. Morphology of the minerals is generally subhedral with rare euhedral boundaries. The size of the crystals ranges from 1-2 mm. Plagioclase crystals are predominantly twinned and commonly zoned. In some zoned plagioclase crystals, the core is resorbed with a euhedral overgrowth. Apatite forms tiny asicular inclusions in plagioclase crystals.
- Quartz crystals (1-1.5 mm) are estimated to be 15 % of the total phenocryst abundance in the plinian pumice clasts. The morphology of the crystals is generally anhedral with subconchoidal fracture. Common embayments of the crystal margins are common.
- Orthopyroxene abundance is estimated at 8 %. Generally, orthopyroxene phenocrysts are subhedral and prismatic, and range in size from 0.5 to 0.75 mm.

- Hornblende phenocrysts range in size (1-2.5 mm) and abundance (2-5 %). They are subhedral and are free from opacite rims.
- Opaque crystals of predominantly titanomagnetite, and occur as subhedral phenocrysts. Their abundance is estimated at 2 %.
- Biotite phenocrysts are rare (~ 1 %) and are found as small (0.25 mm) anhedral-subhedral flakes.
- Accessory minerals of augite, apatite and zircon are rare, totalling less than 2 % of the phenocryst abundance.
- Some of the crystals within the pumice clasts show a jigsaw-fit texture indicating that they have been fractured *in situ*.
- The glass of the plinian pumice clasts is clear and white, and contains perlitic cracks. Vesicles are abundant (75 %) and are rarely infilled with crystals.
- Dense pumice clasts exhibit similar mineralogy to the vesicular pumice clasts, however microlites are abundant. Plagioclase microlites occur throughout the dense pumice, but are extensive (50 %) in bands of concentrated regions within a given pumice clast.
- Apparent 'mingled' pumice clasts are evident within the plinian phase pyroclastics. These clasts are characterised by similar mineralogy, however the banding occurs due to the presence of altered glass.
- The mineral assemblage of the Rotorua A pyroclasts is similar to that of Eastern dome.

4.2.2 Rotorua B Pyroclastics

The mineral phases present in the Rotorua B eruptives are plagioclase, quartz, biotite, orthopyroxene, augite, apatite and zircon. Phenocrysts consist ~15-20 % of the pumice clasts and their descriptions are given below.

- Plagioclase consists ~80 % of the total phenocrysts within the pyroclastic deposits. Plagioclase phenocrysts are dominantly subhedral, commonly zoned, and some show evidence of resorption in their cores. Plagioclase crystals are the largest phenocryst in the pumice clasts and range from 1.25-3.25 mm.

- Quartz crystals exhibit rounded anhedral and embayed crystal margins. They commonly display subconchoidal fracture and abundance ranges from 5 to 15 %.
- Biotite phenocrysts occur as flakes with subhedral habit, ranging in size from 0.25 to 1.0 mm, and 5 to 10 % in abundance.
- Orthopyroxene, hornblende, augite, apatite and zircon are rare and make up 1-2 % of the total phenocrysts observed.
- Glass is clear and contains perlitic cracks.

4.3 Geochemical Methods

The proximal section at Red Tank Road (Rotorua A) was sampled at ca. 30 cm intervals (Figure 4.1). Sampling at the Te Mu Road site (Rotorua B) included a pyroclastic flow and three fall units, which were extremely local in their dispersal. Where available, a single pumice clast was used, although this was often not possible due to the medium lapilli-sized samples available. If samples were combined, they were extracted from a narrow stratigraphic horizon.

Preparation of the clasts involved removal of the outer, weathered portion of the clast. Samples were then individually placed in a sonic bath of distilled water for at least 5 minutes in order to extract fine material within vesicles. If the samples contained a significant amount of fines, the samples were rinsed with distilled water, then returned to the sonic bath. After a period of 3-4 days in a 110°C oven, the samples were crushed for approximately 30 seconds by a tungsten-carbide head in a ring mill. Pressed powder pellets and fusion beads were analysed by XRF at the University of Canterbury, Christchurch.

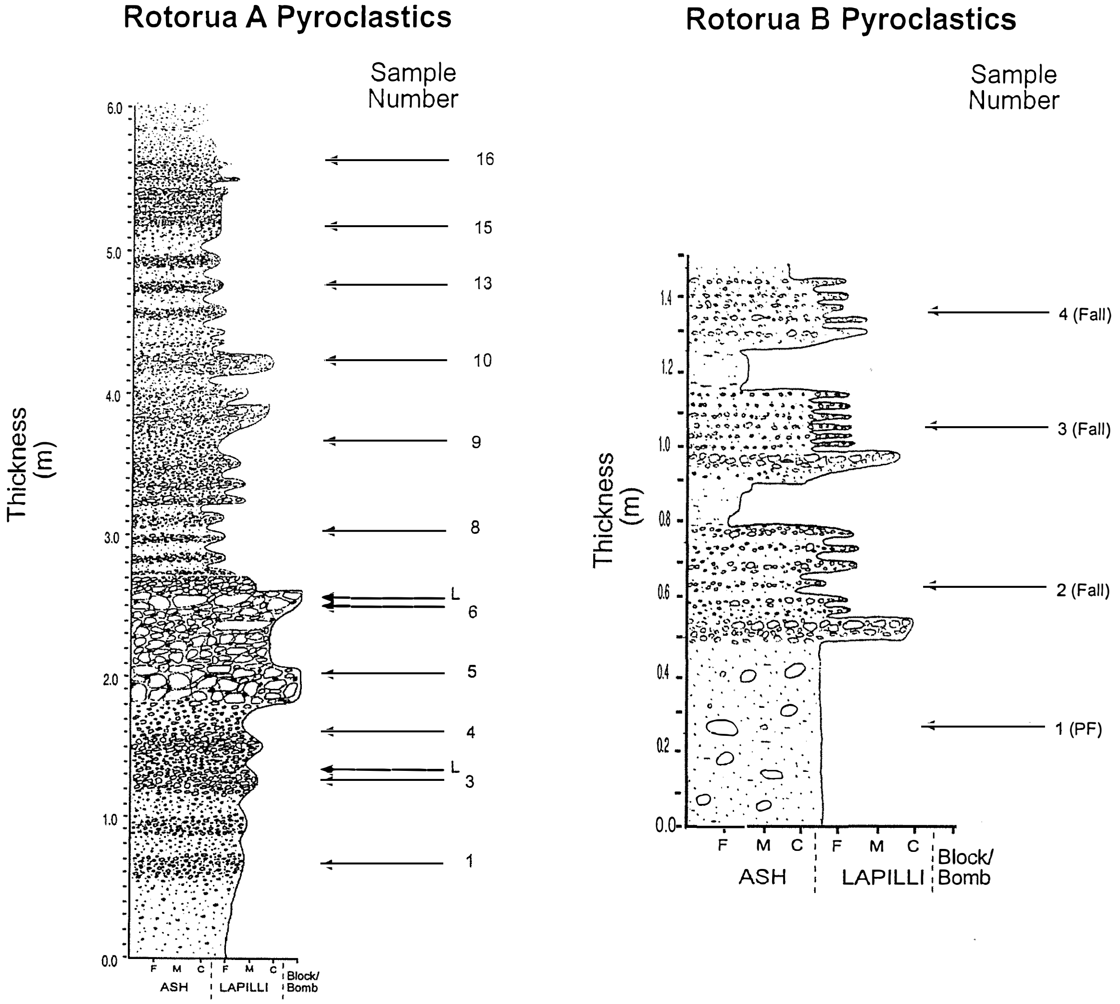

Fig 4.1 Sample locations from two proximal sites for geochemical (XRF) and mineralogical analysis. Numbers on the Red Tank Road section (Rotorua A) represent stratigraphic level of Rotorua Tephra single pumice clasts. (L) represents accessory lithics. A pyroclastic flow (PF) and three fall (Fall) deposits were sampled from Rotorua B at the Te Mu Road, Rotorua B site.

4.4 Geochemical Classification

The Rotorua eruptive episode involved two geochemically distinct populations, classified as Rotorua A and B. Rotorua A deposits consist of the Eastern dome and the plinian deposits known as the Rotorua Tephra, while the Rotorua B deposits consist of Trig 7693 and Middle domes, and associated pyroclastics 'Upper Rotorua Tephra' of Nairn (1980). The deposits of this eruptive episode are chemically similar to the average TVZ rhyolites as indicated by the total alkali (Na_2O + K_2O) and K_2O vs SiO_2 plots (Figure 4.2 and 4.3). The pyroclastic deposits are classified as medium-K rhyolites and range from 73 to 76 wt % SiO_2.

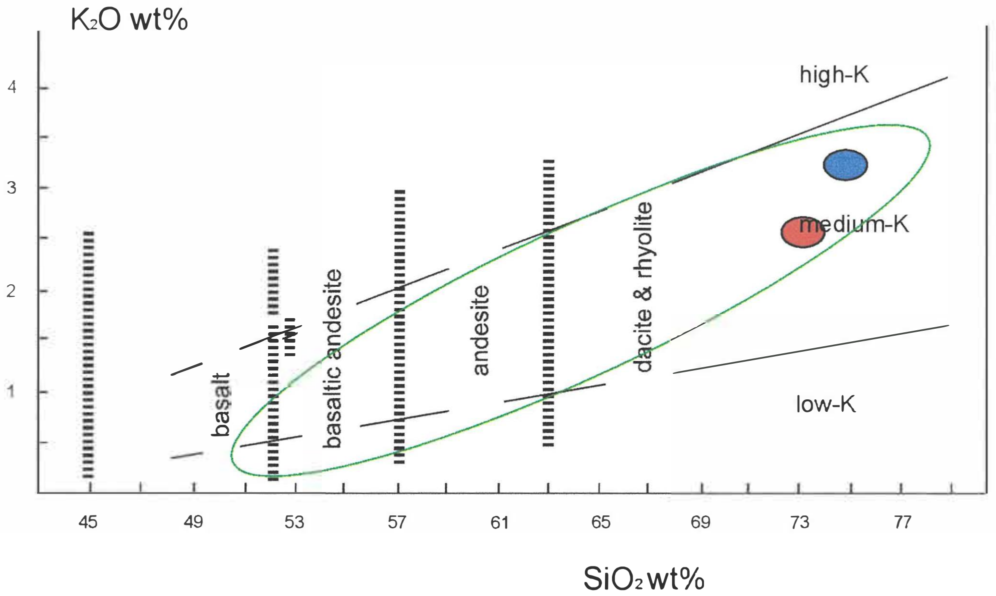

Fig. 4.2 K_2O vs SiO_2 plot indicating the deposits of the Rotorua episode (Rotorua A - Red, Rotorua B - Blue) lie within the range of TVZ magmas (green outline) (classification fields from Le Maitre, 1989; TVZ data from Graham *et al.*, 1995).

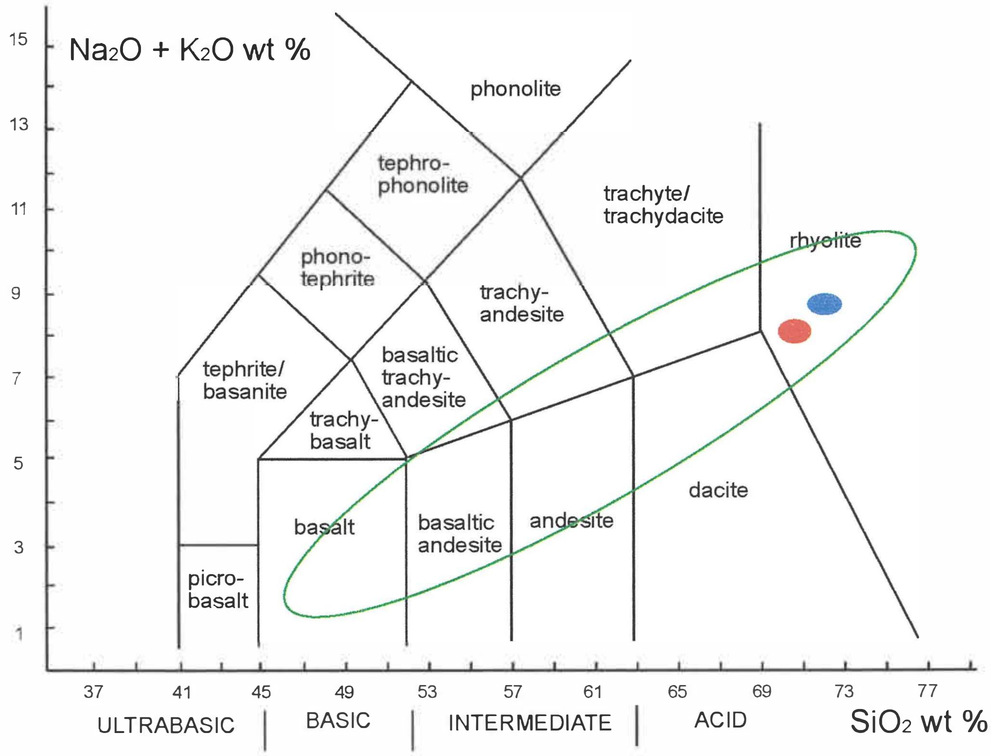

Fig. 4.3 Total alkali vs SiO_2 indicating the Rotorua episode (Rotorua A - Red, Rotorua B - Blue) lies within 'normal' TVZ (green outline) calc-alkali fields (fields from Le Bas *et al.*, 1986; TVZ data from Graham *et al.*, 1995).

4.5 XRF – Whole Pumice Analysis

4.5.1 Major Elements

Analyses of pumice clasts from the plinian deposit of Rotorua A plot as an apparent trend of 1) relative decrease in compatible elements and 2) an increase in incompatible elements with an increase in SiO_2 content (Figure 4.5). On a plot of Al_2O_3 versus SiO_2 (wt %) (Figure 4.4), there is an apparent trend in the data, but there is no systematic trend with stratigraphic height. Briggs *et al.* (1993) have shown that trends in geochemical plots, randomly positioned according to stratigraphic height, indicate the magma was compositional zoned prior to eruption. These data indicate the original zonation of the magma was disturbed during or immediately prior to eruption.

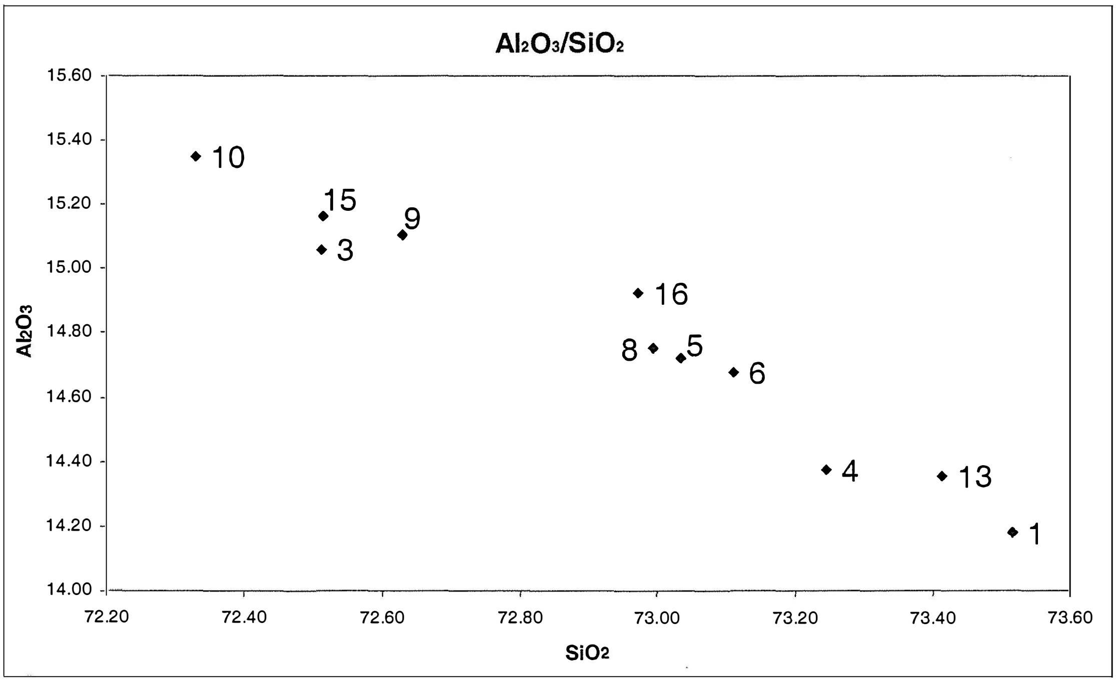

Fig. 4.4 Al_2O_3 vs SiO_2 binary plot of single pumice clasts in the Rotorua Tephra at the Red Tank Road section. Sample numbers refer to relative stratigraphic height in the section (not in metres).

Table 4.1 Whole rock geochemistry data on the Rotorua eruptive episode. Samples were taken from the plinian deposits of Rotorua A (Rr Tephra)a, upper Rotorua Tephra, and a site (U16/ 067279) on the margin of Eastern dome containing an obsidian block with Rotorua B pyroclastics underneath. Major elements are recalculated to anhydrous values (wt %), based on a volatile-free basis.

Sample type	Rotorua A											Rotorua B				U16/ 067279	
Sample number	G1	G3	G4	G5	G6	G8	G9	G10	G13	G15	G16	PF	Pre 1	Post 1	Post 2	Fall (RrB)	Obsid (RrA)
Major elements (wt %)																	
SiO2	73.52	72.51	73.25	73.03	73.11	72.99	72.63	72.33	73.41	72.52	72.97	74.67	75.38	75.76	75.20	75.30	74.05
TiO2	0.35	0.37	0.36	0.36	0.33	0.36	0.37	0.38	0.34	0.37	0.35	0.24	0.20	0.20	0.21	0.19	0.34
Al2O3	14.18	15.06	14.38	14.72	14.68	14.75	15.11	15.35	14.36	15.17	14.92	13.80	13.68	13.30	13.60	13.55	13.71
Fe2O3	2.24	2.47	2.37	2.39	2.23	2.36	2.43	2.52	2.26	2.46	2.36	1.91	1.55	1.62	1.77	1.63	2.20
MnO	0.07	0.08	0.08	0.08	0.07	0.08	0.08	0.08	0.07	0.08	0.08	0.06	0.06	0.06	0.06	0.06	0.07
MgO	0.47	0.51	0.51	0.51	0.45	0.48	0.49	0.51	0.48	0.52	0.49	0.37	0.28	0.28	0.33	0.28	0.49
CaO	2.06	2.19	2.15	2.07	2.25	2.13	2.08	2.06	2.08	2.11	1.99	1.71	1.50	1.43	1.48	1.47	2.03
Na2O	4.35	4.19	4.20	4.18	4.15	4.18	4.19	4.18	4.23	4.21	4.17	4.02	4.02	4.01	4.05	4.14	4.40
K2O	2.66	2.55	2.62	2.59	2.64	2.59	2.56	2.53	2.70	2.52	2.58	3.20	3.31	3.30	3.29	3.35	2.68
P2O5	0.08	0.08	0.07	0.07	0.06	0.07	0.06	0.06	0.07	0.07	0.07	0.02	0.03	0.03	0.03	0.02	0.04
Total	97.16	96.88	97.37	96.94	96.81	97.20	96.97	96.93	97.23	96.93	96.83	98.25	98.02	98.07	98.24	98.73	99.96
Trace elements (ppm)																	
V	16	17	19	20	20	19	20	17	20	19	18	18	17	16	15	15	21
Cr	4	<3	<3	3	<3	<3	<3	<3	<3	<3	<3	3	<3	<3	<3	<3	<3
Ni	3	<3	3	3	<3	<3	<3	<3	<3	<3	<3	<3	<3	3	<3	<3	<3
Zn	40	49	49	45	46	48	49	50	43	46	45	36	33	32	34	32	43
Zr	233	248	239	242	238	237	245	255	215	240	236	135	129	123	130	135	234
Nb	8	8	7	8	8	8	8	8	7	8	7	7	7	7	7	7	7
Ba	835	864	827	798	852	852	858	888	819	783	798	876	852	837	842	876	799
La	19	21	16	18	19	22	17	16	20	17	23	19	15	19	18	15	14
Ce	62	53	53	52	54	50	53	55	56	58	57	47	53	48	50	48	50
Nd	16	23	35	24	31	19	27	24	13	18	19	13	11	<10	17	24	29
Ga	12	14	14	14	14	14	14	15	14	14	14	13	12	12	13	12	13
Pb	12	12	13	15	15	13	12	12	12	13	14	14	14	16	14	16	13
Rb	91	87	89	86	88	88	87	87	91	85	85	112	112	113	113	114	94
Sr	160	169	168	162	164	165	164	165	160	163	154	133	116	111	115	116	166
Th	10	10	10	8	9	12	12	11	9	10	10	12	13	14	13	15	13
Y	25	26	26	26	26	28	27	27	25	25	25	18	21	21	21	21	24

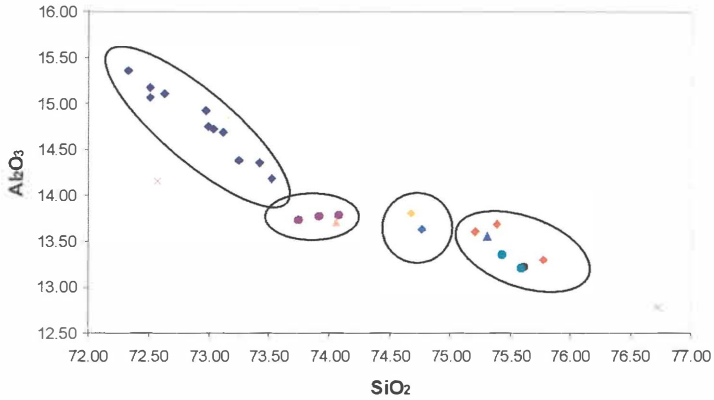

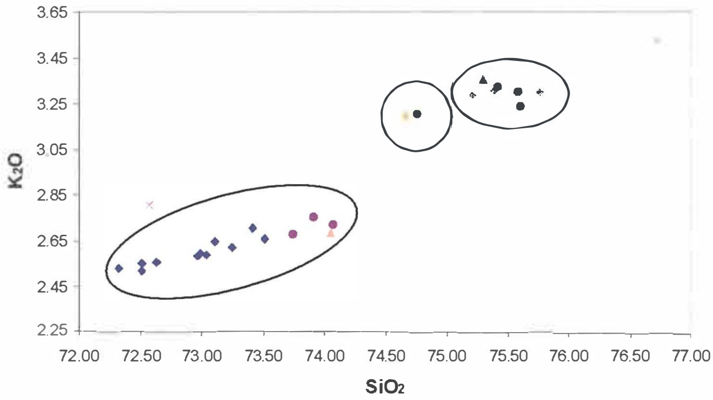

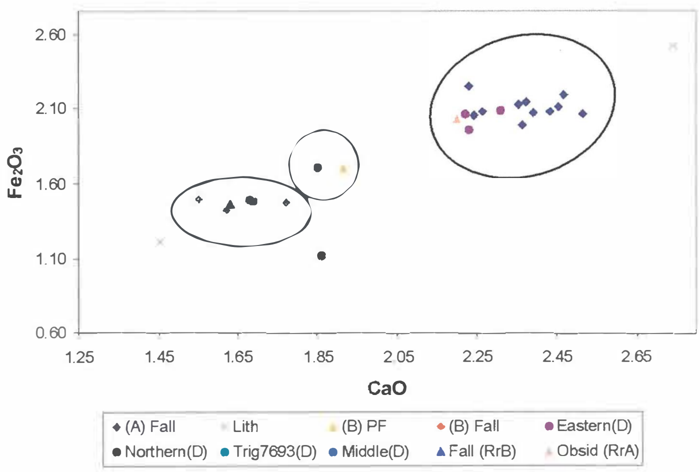

Fig 4.5 Major element binary plots of pumice, lithics and an obsidian block with an underlying tephra (Rr B) (this study) with the Rotorua and Te Rere dome lavas (Bowyer, *in prep*) for comparison. All major elements are recalculated to anhydrous values. Major elements are expressed as wt %. Legend is constant for all geochemical plots.

If the apparent trend of decrease in compatible elements with an increase in SiO_2 is projected further, it corresponds with the Eastern dome lavas in all major element binary plots (Figure 4.5), and in some cases overlaps (eg. Fe_2O_3 vs. CaO). The Rotorua B deposits (Te Mu Road) have significantly higher SiO_2 (~74.8-75.5 wt %) compared to the Rotorua A deposits (~72.3-73.5 wt %). The Rotorua Tephra has high Al_2O_3 (14-15.5 wt %), Fe_2O_3 (2.0-2.25 wt %) and CaO (2.25-2.5 wt %) compared to the Rotorua B pyroclastics (13-13.8, 1.5-1.7 and 1.65-1.8 wt % respectively). The SiO_2 vs K_2O and Al_2O_3 plots show the distinctive chemistry of the Rotorua Tephra from the Rotorua B pyroclastics, also the distinction between Te Rere and Rotorua related domes. The Rotorua B pyroclastics correlate well with the Trig 7693 and Middle dome lavas in all major element plots, while the Northern and Eastern domes show a significant separation. These have been previously identified as Te Rere related domes by Nairn (1980; 1992). The debris flow deposit correlates well with the Eastern dome, while the underlying tephra has similar composition to the Rotorua B pyroclastics.

4.5.2 Trace Elements

The Rotorua deposits exhibit similar trends in trace element compositions to the major elements (Figure 4.6). The Rotorua A and B deposits plot in two distinct clusters in all trace element plots (Sr vs Rb, Y vs Zr and Zr vs SiO_2). Rotorua A deposits have higher contents of Zr (215-255 ppm), Y (25-28 ppm) and Sr (152-170 ppm) compared to the Rotorua B eruptives (120-135, 18-21 and 110-132 ppm respectively). Rotorua A deposits plot in a very tight cluster in the Sr vs Rb and Y vs Zr plots while the Rotorua B deposits show more scatter.

A close correlation exists between the Rotorua B pyroclastics and the Rotorua dome samples (Trig 7693 and Middle domes), as shown in both the Y vs Zr and Sr vs Rb plots. Eastern dome and the Rotorua Tephra (Rotorua A) exhibit tight clustering in all trace element plots, but Northern and Eastern domes show a significant separation.

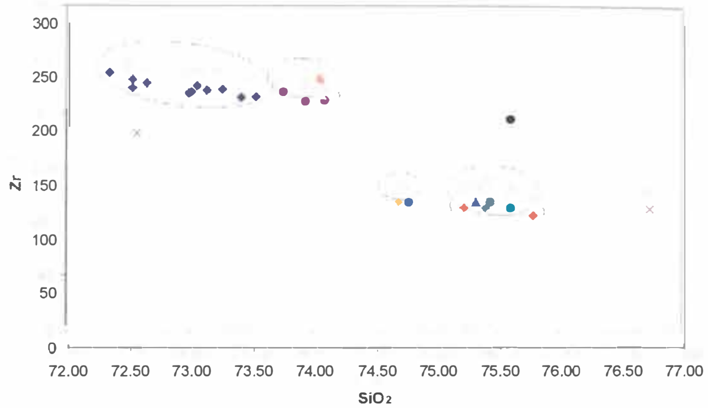

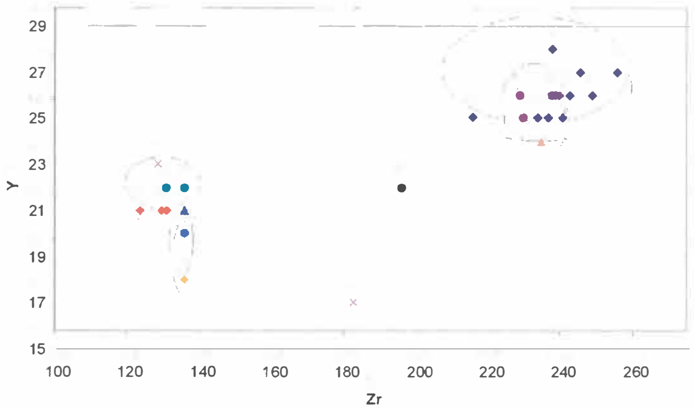

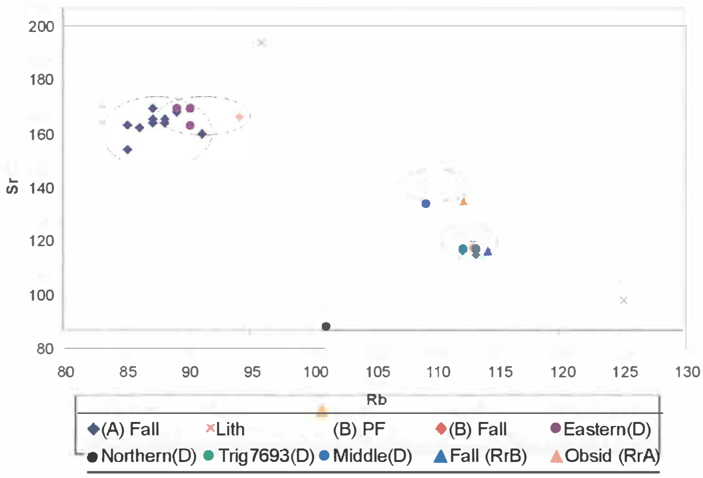

Fig 4.6 Trace element binary plots for the Rotorua A and B phases, with an obsidian block and underlying tephra (this study), and the Te Rere (D) and Rotorua (D) (Bowyer, *in prep*) dome lavas for comparison. Trace elements are expressed as ppm.

4.6 Intensive Parameters

The composition of iron-titanium (Fe-Ti) oxides in silicic volcanic rocks is sensitive to magmatic properties, such as chemistry, temperature (T) and oxygen fugacity (fO_2). Subtle changes in Fe-Ti oxides can be used to distinguish deposits from a similar or common source (Shane, 1998).

Shane (1998) sampled numerous pyroclastic deposits from the TVZ including Okataina. That study involved the distinction of pyroclastic units based on intensive parameters. Bowyer (*in prep*) analysed the rhyolite domes of Okataina, including a study on Fe-Ti oxides. Both studies calculated T and fO_2 using the method outlined by Ghiorso and Sack (1991). Data from Bowyer (*in prep*) shows that the Eastern dome lavas have eruption temperatures (T°C) and oxygen fugacities (Δlog fO_2) of ~ 850 °C and 2.0 respectively, while the Rotorua lavas (Trig 7693 dome) have modelled parameters of ~ 650 °C and 0.75. When the data are combined (Figure 4.7) the pyroclastic samples plot closely with the Eastern dome lavas. The Rotorua Tephra sampled by Shane (1998) has modelled intensive parameters of 856 °C and 1.8 based on six samples.

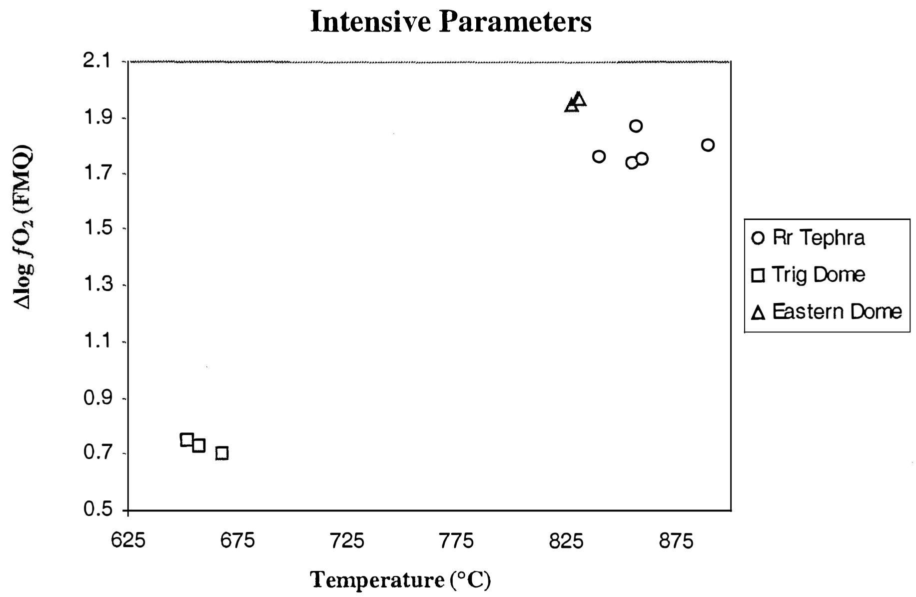

Fig. 4.7 Temperature and Δlog fO_2 (FMQ) estimates for the Rotorua Tephra (Shane, 1998) with Eastern and Trig 7693 Domes (Bowyer *in prep*) for comparison.

4.7 Isotopic Data

Isotopic data on lavas can be used to determine whether the magma feeding two eruptions can be linked by a common source. Bowyer (*in prep*) used samples from Eastern and Trig 7693 rhyolite domes to quantify the differences between the two lavas. The isotopic data indicated the two lavas were sourced from a different magma batch due to their distinct isotopic composition.

4.8 Conclusions

- Mineralogy of the pyroclasts and lavas of the Rotorua A and B phases are distinct. The Rotorua A tephra contains abundant orthopyroxene, hornblende ± biotite, while the Rotorua B pyroclastics contain abundant (15 %) biotite with rare orthopyroxene and hornblende.

- The average composition of the Rotorua A deposits is 73 wt % (SiO_2) compared to the Rotorua B deposits of 75.5 wt % (SiO_2).

- Major and trace element data suggest that the explosive phase of the Rotorua eruptive episode tapped a compositionally heterogeneous and zoned magma chamber.

- The distinct geochemical population cluster of the Rotorua A and B pyroclasts and lavas indicates they are the product of separate eruption phases.

- Major and trace element geochemistry, isotopic and intensive parameter analyses suggest the Rotorua A tephra was associated with growth of Eastern dome, while the 'upper Rotorua Tephra' of Nairn (1980) (Rotorua B – this study) is distinct and related to the growth of the Trig 7693 and Middle domes.

Chapter Five
Eruptive History

5.1 Introduction

The various forms of data obtained and analysed in this study leads to the production of an eruptive history for the Rotorua episode. Each technique has been used to quantify the deposits of the eruption in order to evaluate the conditions of the magma and the sequence of events that occurred during the eruption. Geochemical analysis was used to examine the state of the magma immediately prior to eruption, indicating whether the magma was compositionally zoned or homogeneous. The stratigraphy records the nature of the eruption, such as the initiating conditions, plume stability, column height, eruption duration and intensity. Dispersal of the lithic portion of the plinian tephra indicates the inclination of the plume, the wind speed and direction, at the time of the eruption. Textural analysis determined the process of fragmentation, explosivity and the role external water played in driving the eruption.

In this chapter, a modelled eruption chronology is provided, based on the compilation of the data collected from the various aspects of this study. The eruption chronology models the magmatic, vent and atmospheric processes acting during the eruptive episode.

5.2 Geochemistry and Mineralogy

Geochemical and mineralogy data collected on the Rotorua eruptive episode products describe the magmatic conditions prior to and during the eruption. With stratigraphic control and high resolution sampling, geochemical plots of major and trace elements can be used to constrain changes in magmatic conditions during the eruptive episode.

5.2.1 Geochemistry

Both the major and trace element plots exhibit similar trends in compositional variability. The chemical composition of the Rotorua A and B eruptives is distinct on geochemical plots. The trends in the data of the two deposits are significantly offset, indicating that there was probably two phases of the eruptive episode. The clustering of the Rotorua A pyroclastics (previously 'Rotorua Tephra') with the Eastern dome lavas in the major and trace element plots, implies the source of this plinian deposit was compositionally related to Eastern dome. Trig 7693 and Middle dome lavas plot closely with the Rotorua B pyroclastics (previously 'Upper Rotorua Tephra') indicating that they are probably genetically related and derived from the same batch of magma that was spatially distinct from the Rotorua A batch.

5.2.2 Mineralogy

The mineralogy of the Rotorua A tephra consists of plagioclase, quartz, orthopyroxene, hornblende ± biotite. The mineralogy of the plinian deposit is similar to Eastern dome lavas. Rotorua B pyroclastics consist of plagioclase, quartz and biotite. Orthopyroxene and hornblende are rare to absent in the biotite-bearing Rotorua B pyroclastic deposits. Biotite flakes exceed 1 mm in the Rotorua B deposits compared to the 0.2 mm flakes in samples from the Rotorua A tephra. The clear difference in mineralogy between these two phases suggests the eruptions were sourced from a distinct magma body.

Hornblende phenocrysts are unstable at low temperatures and are therefore key indicators of the residence time of magma at shallow levels (Rutherford & Devine, 1988). The absence of a reaction rim suggests the magma rose rapidly, as found at

Mount St Helens, 1980 (Rutherford & Hill, 1993). Opacite rims on hornblende are indicative of magma residence at low pressures but are absent from hornblende crystals in the Rotorua A tephra. This implies the plinian eruption was sourced by a magma that did not reside at shallow levels for an extensive period of time. Hornblende is rare within the Rotorua B pyroclastic deposits.

Zoned plagioclase crystals are common in the Rotorua tephra samples. A euhedral outer rim often surrounds a resorbed core. This indicates the crystal periodically went into and out of equilibrium to create the zoned crystals. This phenomenon could be facilitated by relative rise and fall of magma within the vent prior to eruption or influxes and mixing of new magma into the system.

The presence of abundant microlites in dense pumice clasts of the Rotorua A tephra suggests short-term residence occurred at very shallow levels periodically during the eruption. The development of permeability in degassing magma leads to the growth of microlites (Hammer *et al.*, 1999). This leads to a reduction in vesicularity due to the collapsing of vesicle walls and infilling of pore spaces.

5.2.3 Intensive Parameters

Modelled eruption temperature (T°C) and oxygen fugacity (fO_2) data from the Rotorua A tephra and Eastern dome plot in a tight cluster. Similar eruption temperatures and fO_2 of the Eastern dome and the Rotorua A tephra indicate a strong petrogenetic relationship. The large difference between the Rotorua tephra and the Trig 7693 domes, previously attributed to the source of the plinian tephra (Nairn, 1980; 1992), suggests the Eastern dome more likely represents an effusive episode of the Rotorua A phase.

5.2.4 Isotopic Data

Data from Bowyer (*in prep.*) indicate the Eastern and Trig 7693 lavas are isotopically different, which indicates the Rotorua A and B phases were sourced from distinct magma batches. This is unexpected due to the close temporal and spatial relationship of the vent areas and resulting deposits.

5.3 Stratigraphy and Dispersal

The stratigraphy of the Rotorua eruptive episode has been reinterpreted from Nairn (1980). Stratigraphic information provides an account of the series of events that occurred during the eruption. By examining the sub unit stratigraphy of the plinian fall deposit, the dynamics of the Rotorua A tephra of the eruptive episode can be estimated. Detailed stratigraphy also provides a basis for quantitative techniques such as geochemistry, mineralogy, vesicularity, grainsize and componentry.

The dispersal of the Rotorua eruptive episode deposits is used to identify the syn eruptive conditions, such as atmospheric effects and intensity. Dispersal maps of sub unit and total thickness, maximum pumice and maximum lithics provided data to model the eruption using accepted models from the literature (eg. Carey & Sparks, 1986; Pyle, 1989). Estimates of parameters such as plume height, erupted volume, eruption duration (Rotorua A and B phases) and wind speed, were made to quantify conditions during the eruption.

5.3.1 Stratigraphy

The stratigraphy of the Rotorua eruptive episode was described using data from > 80 sites ranging from proximal to distal locations. Based on stratigraphic control, the Rotorua A phase occurred before the Rotorua B phase.

The Rotorua A phase included an explosive plinian event followed by dome-building (Eastern rhyolite dome), which is a common sequence for silicic eruptions in TVZ eg. Puketarata (Brooker *et al.*, 1993) and globally eg. Mount St. Helens (Newhall &

Melson, 1983). A variably distributed phreatomagmatic unit, found in rare locations to the NW, marks the base of the plinian fall deposit. This represents the precursor to the plinian eruption. Significantly, there is no evidence of a basalt trigger to the plinian phase, in the stratigraphy or mineralogy. Basalt triggers have been noted in other studies at Okataina eg. Kaharoa (Nairn *et al.*, 2001) and Okareka (Nairn, 1992) eruptive episodes. The Rotorua A tephra is reverse to normally graded, with the maximum grainsize occurring very early in the eruptive sequence. This suggests the climax of eruptive energy occurred early in the eruptive sequence. Fine scale bedding is a key feature of the Rotorua A proximal fall stratigraphy indicating the plume height was variable and discharge rate fluctuated throughout the eruption. 10 sub units have been defined in the proximal stratigraphy (A_p-1 to A_p-10) based on grainsize and componentry, while 3 sub units are mappable in the distal stratigraphy (A_d-1 to A_d-3).

Dome building of the Rotorua A phase occurred at the cessation of the plinian phase. This led to construction of Eastern Dome. During dome growth, limited block and ash flows were produced (compared to the later B phase of the eruption) due to the low angle flow fronts of the dome margins.

The Rotorua B phase primarily involved dome building. This involved tapping of a compositionally distinct magma batch to the Rotorua A phase. Soon after the cessation of the Rotorua A phase (based on a lack of paleosol development), growth of Middle Dome ensued. During dome growth, periodic expulsion of gas-rich portions of the magma generated vulcanian-style explosions of crystal-rich pumice to the south and east of the vent.

5.3.2 Dispersal

The precursor to the Rotorua A tephra was a small phreatomagmatic event that was locally dispersed. The dispersal of the Rotorua A tephra was predominantly to the NW in a well-defined lobe (> 25 000 km^2) reaching as far north as Auckland (Sandiford *et al.*, 2001) and Northland (D. Lowe pers comm.). Isopach maps were constructed largely from data obtained in this study and supplemented by distal data in the literature eg.

Lowe *et al.*, (1988) and Sandiford *et al.*, (2001). These data enable the completion of more robust contours, which are then used to determine the tephra volume (Pyle, 1989). Eruption modelling using widely accepted formulae (Carey & Sparks, 1986; Pyle, 1989) has quantified the eruption dynamics for comparison with other Okataina eruptions and global examples. The modelled eruption dynamics for the Rotorua A plinian phase are:

Maximum plume height	= 20 km
Eruption intensity	= 4 x 10^7 kg/s
Eruption duration	= 8-9 h
Volume	= 1.62 km^3 (bulk volume)
Wind speed	= 25 m/s (SE)

Subsequent to the Rotorua A phase (and Eastern dome growth), Rotorua B dome growth occurred with sporadic pyroclastic eruptions. These pyroclastic eruption deposited Rotorua B tephra to the S and E. The deposits of these sporadic eruptions are dispersed up to 8 km SE of the vent. Local pyroclastic density currents are observed within 3 km of the vent but do not extend beyond this. Topographic controls of the older, surrounding domes to the N and W are the likely cause of this limited dispersal. Volumetrically, the Rotorua B pyroclastics are a minor portion of the total magma erupted during the Rotorua eruptive episode.

5.4 Textural and Component Analysis

The analysis of the Rotorua A and B pyroclastics can be further quantified by the use of textural and component analysis. Textural data are used to determine the processes of fragmentation, vent processes and the state of the magma immediately prior to eruption. These data are collated and compared with observed eruptions to understand the timing of events and eruption dynamics. Grainsize samples were collected along the dispersal axis to determine the median size and sorting downwind. Componentry indicates the relative abundances of pumice (in its various densities), lithics, obsidian and crystals. Vesicularity indicates the presence or absence of magma-water interaction and the extent magmatic gases were driving the eruption.

5.4.1 Grainsize

A range in grainsize exists throughout the Rotorua A tephra. The initial sub unit (A_p-1) is –2 ϕ. The deposit reversely grades into the coarsest sub unit (–5 ϕ) (A_p-2) ~2 m from the base. The deposit is then normally graded (with fine scale bedding) to an upper fine lapilli/medium ash (0.5 ϕ). The Rotorua A tephra is well sorted in a volcanological context (Cas & Wright, 1987) with sorting values of ~1.5 ϕ, indicating deposition involved discrete clast fallout from a relatively dry plume. The vertical grainsize variations in proximal deposits indicate that the peak eruption intensity was achieved early in the plinian sequence and waned unsteadily throughout the eruption sequence.

5.4.2 Componentry

Samples for componentry analysis were obtained from the retained proximal grainsize samples of Rotorua A pyroclastics. Vesicular pumice clasts (~ 75 % vesicles) were the most abundant component of the tephra (~ 95 %), however the juvenile clasts were not of uniform density. The separation of variably dense pumice clasts into categories was necessary to quantify the range in densities. A spectrum from ~ 75 % vesicular pumice to high-density (obsidian-like) pumice was observed containing variably collapsed vesicles. This indicates that perhaps periodic capping of a gas-rich magma occurred during quiescence, with a degassing plug of formally exsolved magma residing below. This phenomenon has been observed during the 1991 eruption of Mt. Pinatubo (Hammer *et al.*, 1999).

The lithic component of the Rotorua A tephra consists of (~ 95 %) rhyolite lava. Lithic abundances increase steadily through the deposit. Due to this steady trend, it is likely that progressive vent erosion occurred during the Rotorua A explosive phase. Rare lake deposits (< 5 %) are evident in the basal portions of the Rotorua A tephra, suggesting the eruption initiated through or in close proximity to a lake or paleolake.

5.4.3 Vesicularity

The vesicularity of the plinian tephra clasts are predominantly constant (~ 75 %) throughout the deposit. A tight range of vesicularity values exists in the lower portions of the tephra indicating a constant level of fragmentation. In the upper portions of the tephra (sub units A_p-9 and A_p-10), the vesicularity decreases (~ 60 %) and the range increases. This progressive increase in density suggests the eruption tapped progressively gas-poor portions of the Rotorua A magma.

5.5 Eruption Chronology

The chronology of the Rotorua eruptive episode is based on data obtained and interpreted in previous chapters. The eruptive sequence is given graphically in Figure 5.2. The eruption chronology as determined by data collected in this study is as follows:

1. Rapid convection of the initially heterogeneous Rotorua A magma occurred beneath a shallow lake situated immediately SE of the pre-existing Northern dome. Vigorous earthquakes rupturing the zoned magma chamber may have caused convection. The Rotorua B magma batch was located within 1 km of the Rotorua A magma.

2. The rise of Rotorua A magma led to short-lived magma-water interaction with groundwater and/or a shallow lake. This lead to the production of a small phreatomagmatic eruption during winds from the SE. This phase of the eruption established the conduit for the later-stage phases to occur.

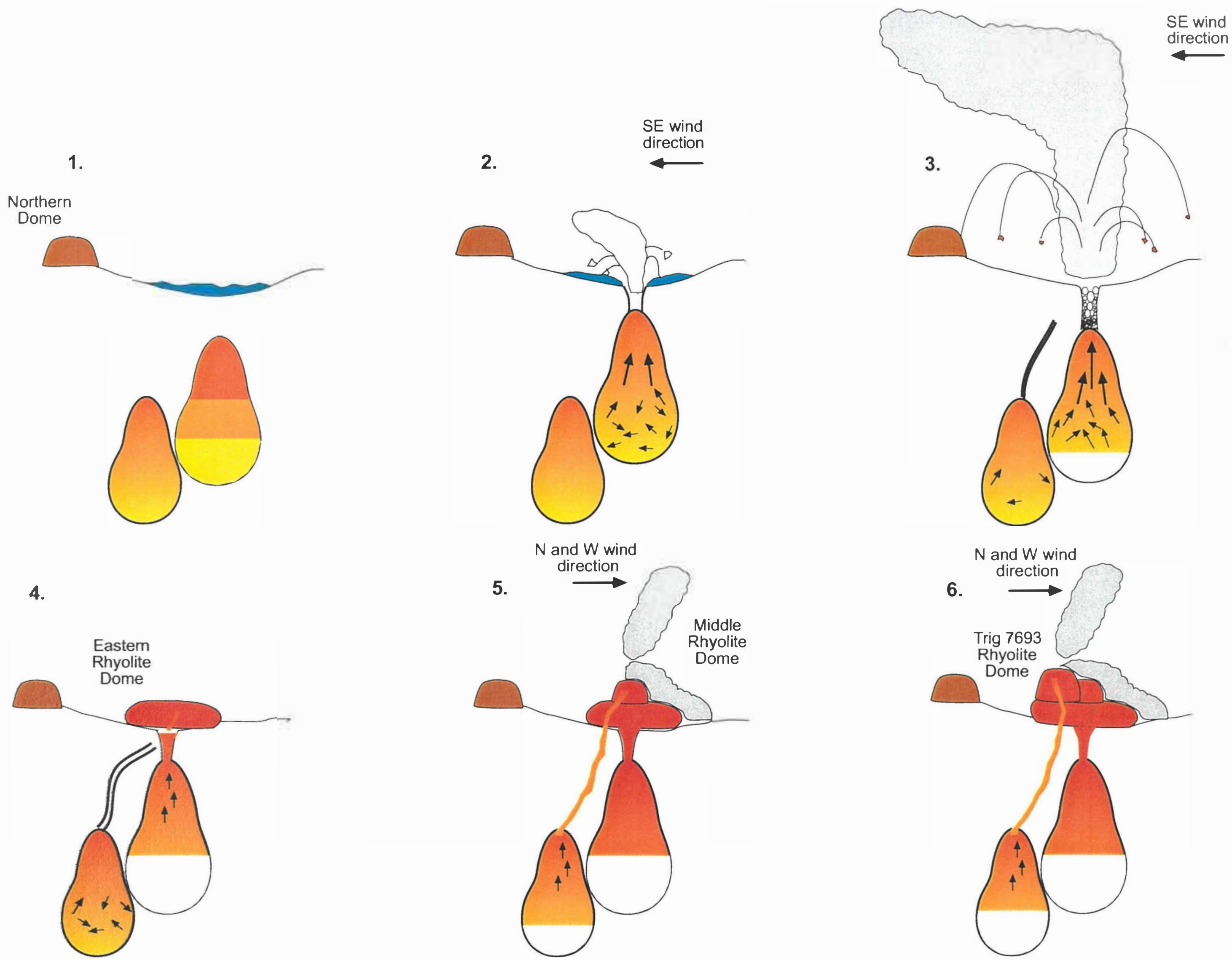

Fig. 5.1 Modelled eruption history of the Rotorua eruptive episode. Refer to section 5.5 in the text for explanation of the eruptive processes with time. Figure not drawn to scale. Magma batches are representative of relative volume.

3. Soon after the phreatomagmatic phase (minutes to hours), rapid rise of the Rotorua A, (0.4 km^3) gas-rich magma produced a high, buoyant but unsteady plinian eruption column. This phase soon waxed and reached a climax consisting of a 20 km high plume. Strong SE winds (~25 m/s) distributed the tephra in a well-confined lobe to the NW. The eruption began to wane unsteadily, tapping gas-poor magma until the cessation of activity. No evidence exists for a widespread ignimbrite accompanying the plinian phase indicating that although eruption intensity was widely variable, the plume remained buoyant throughout. The duration of the plinian phase is estimated at 8-9 hours.

4. At the cessation of explosive activity the remaining gas-poor portions of the Rotorua A magma slowly ascended. The high temperature and low SiO_2 content of the lava being extruded created the (0.75 km^3) laterally extensive and low-lying Eastern dome. The extent of the dome reached what now occupies the barrier to lake drainage between Lakes Okareka, Tikitapu, Rotokakahi and Tarawera.

5. The cessation of Eastern dome growth (after a period of several years) enabled the rise of Rotorua B magma at a similar vent location to the Rotorua A phase. Passive degassing of this magma may have been facilitated by extensive rupture during the Rotorua A pyroclastic phase. The Rotorua B magma supplied a long-lived (at least 8 years), predominantly effusive phase of eruption leading to the construction of Middle rhyolite dome. Periodic failure of the dome and the rapid rise of gas-rich portions of the magma led to vulcanian-style pyroclastic eruptions. Block and ash flows were produced radially from the vent during periods of instability during dome construction. Topographic barriers (older domes) to the N and W directed density currents to the S and E. Middle dome took at least 3.5 years to be constructed.

6. A resurgence in Rotorua B magma upwelling at a similar vent location led to the growth of the steep-sided Trig 7693 rhyolite dome. The Trig 7693 dome produced block and ash flows and pyroclastic density currents due to periodic sector collapse during dome construction. The Trig 7693 dome produced vulcanian-style, locally dispersed pyroclastic eruptions to the S and SE as indicated. The Trig 7693 dome erupted over a period exceeding 2.5 years.

5.6 Comparisons With Other Examples

The Rotorua eruptive episode is a unique example of two distinct rhyolitic magma batches erupting in close temporal and spatial dimensions. Magma mixing is a common phenomenon (eg. Briggs *et al.*, 1993) however, the Rotorua eruptive episode appears to have involved the eruption of two compositional distinct magmas in succession without a significant time break. Both eruption phases were sourced from a similar vent location.

The eruption chronology of the Rotorua eruptive episode involved three main phases. The explosive emplacement of the Rotorua A tephra was followed by effusive growth of Eastern dome. The Rotorua A magma became exhausted or inactive, allowing the predominantly dome building period of the Rotorua B phase to ensue with periodic explosive events.

The 1980, Mount St. Helens eruption provides an analogy for the chronology of the Rotorua A phase of the eruptive episode. In the Mount St. Helens eruption, a 9 hour plinian event was the initial phase of the eruption (Crisewell, 1987). Soon after the cessation of explosive activity, a series of dacitic domes grew and were later destroyed by later collapse events. This is a likely series of events for the Rotorua A phase, due to the chronology of initial plinian phase followed by dome growth. A similar volume of magma was erupted in the Mount St. Helens eruption to the Rotorua A phase.

The A.D. 1305 Kaharoa eruptive episode is the most recent rhyolitic eruption from the TVZ. This eruption was initiated by a basalt trigger, unlike the Rotorua episode, that lead to a plinian eruption depositing the widespread Kaharoa Tephra to the NW and SE (Nairn *et al.*, 2001). The Kaharoa eruption involved the growth of a series of rhyolite domes in a NE-trending fissure. The chronology interpreted for the Kaharoa eruptive episode from the pyroclastics and lavas indicates that a rhyolitic eruption (especially the Rotorua A phase) is commonly initiated by a plinian phase, then succeeded by an effusive dome growth phase.

The Rotorua B phase is a predominantly effusive series of events leading to the construction of the coalesced Trig 7693 and Middle domes. Such long-lived effusive activity is seen at Montserrat, where effusive activity has constructed a dome initiated in 1995. Sector collapse and minor upwelling of gas-rich portions of the magma have triggered periodic explosive events.

Although there are modern analogues for the general chronology of explosive events followed by effusive events, the Rotorua eruptive episode involved two distinct magma batches residing in close proximity prior to eruption. The cessation of the Rotorua A phase was soon succeeded by the more evolved and distinct Rotorua B phase. Such a complex magmatic system at depth may be due to a deep-seated structural control in the Okareka Embayment.

6.5 Conclusions

- The history of the Rotorua eruptive episode can be developed according to the information interpreted in this study. The use of multiple analytical techniques provides the framework for the eruptive history of the Rotorua A and B phases.

- The Rotorua eruptive episode was initiated by an explosive plinian eruption (Rotorua A tephra) followed by effusive growth of Eastern dome (Rotorua A magma). Soon after the cessation of Eastern dome growth, the distinct Rotorua B magma batch erupted predominantly effusively. This lead to the construction of the coalesced Trig 7693 and Middle domes. Periodic pyroclastic eruptions were erupted by the rapid rise of gas-rich portions of the magma through the existing domes, or due to sector collapse of the dome margins.

- Comparisons with historic eruptions indicate the chronology of explosive followed by effusive activity to be common, however the eruption of two distinct magma batches from a similar vent location without magma mixing is unique to the Rotorua event.

Chapter Six
Volcanic Hazards

6.1 Introduction

Volcanic eruptions have impacts at a wide range of temporal and spatial scales, from widespread (eg. ash fall) to local (eg. gas emissions and ballistic fall) and from seconds to a number of years. The effect of historic eruptions has highlighted the need for hazard analysis in volcanically active centres, which endanger populated areas. The Okataina Volcanic Centre (OVC) is an important location for hazard analysis due to its proximity to the major cities of Rotorua, Tauranga, Whakatane and Kawerau.

The Rotorua eruptive episode involved two distinct phases (A and B). The Rotorua phase involved a plinian explosive eruption and the growth of Eastern dome. The Rotorua B phase predominantly involved dome growth of the Trig 7693 and Middle domes. The distinct eruption phase produced unique hazards according to the mode of emplacement and proximity to the vent. To analyse the effect of this eruption, a scenario-based approach is given, which quantifies the impacts of a similar eruption today. This approach requires accurate information on the volcanic processes (see chapter 5), population of the region (census information), and economic value of the forestry, agriculture and tourism industries within the effected region.
Using the definition of Blong (1996), risk is defined as:

$$RISK = Hazard \ x \ Vulnerability$$

Where *hazard* refers to the physical events produced by an eruption and *vulnerability* includes the consequences for people, buildings, infrastructure and economy.

The effects of the components of a plinian-dome building eruption will be discussed to describe the specific hazards posed by pyroclastic fall, flow and surge, block and ash flows and other phenomenon associated with dome growth. Modern examples will provide a basis for effects from each.

6.2 Rotorua A - Plinian Phase

The plinian phase of the eruptive episode produced two main hazards 1) a widespread tephra directed to the NW and 2) proximal ballistic fall. Due to the unusual pattern of dispersal, the Rotorua eruption would cause a large amount of damage to the cities of Rotorua, Hamilton and Tauranga (Figure 6.1) if this event occurred today.

6.2.1 Ballistic Fall

Proximal to the vent, both ballistic clasts and juvenile clasts from the outer margins of the plume are deposited. Clasts from the outer margins of the plume fall close to the vent due to eruption-induced wind vectors causing the clasts to be deposited close to or inside the vent (Houghton & Smith, 1993). This would lead to the rapid deposition of extremely hot clasts of lithic and pumice blocks and bombs on the settlements surrounding Lakes Okareka and Tarawera. The area affected by ballistic fall is approximately 3 km around the vent although exposures on the south and southeastern margins of the vent do not indicate ballistic fall. This may be a result of both syn – and post-eruption erosion. Lithic and juvenile clasts emplaced ballistically are normally larger than 10 cm diameter and are able to penetrate modern house construction with little difficulty (Blong, 1984). This leads to structural failure caused by impact of supporting structures, and due to the inability of the clasts to reach thermal equilibrium, temperatures of ballistic clasts may reach 200-300°C (Blong, 1984). Ballistic clasts effect vegetation eg. the Whakarewarewa Forest, causing the stripping of branches and due to the heat of the clasts, fires are likely to result.

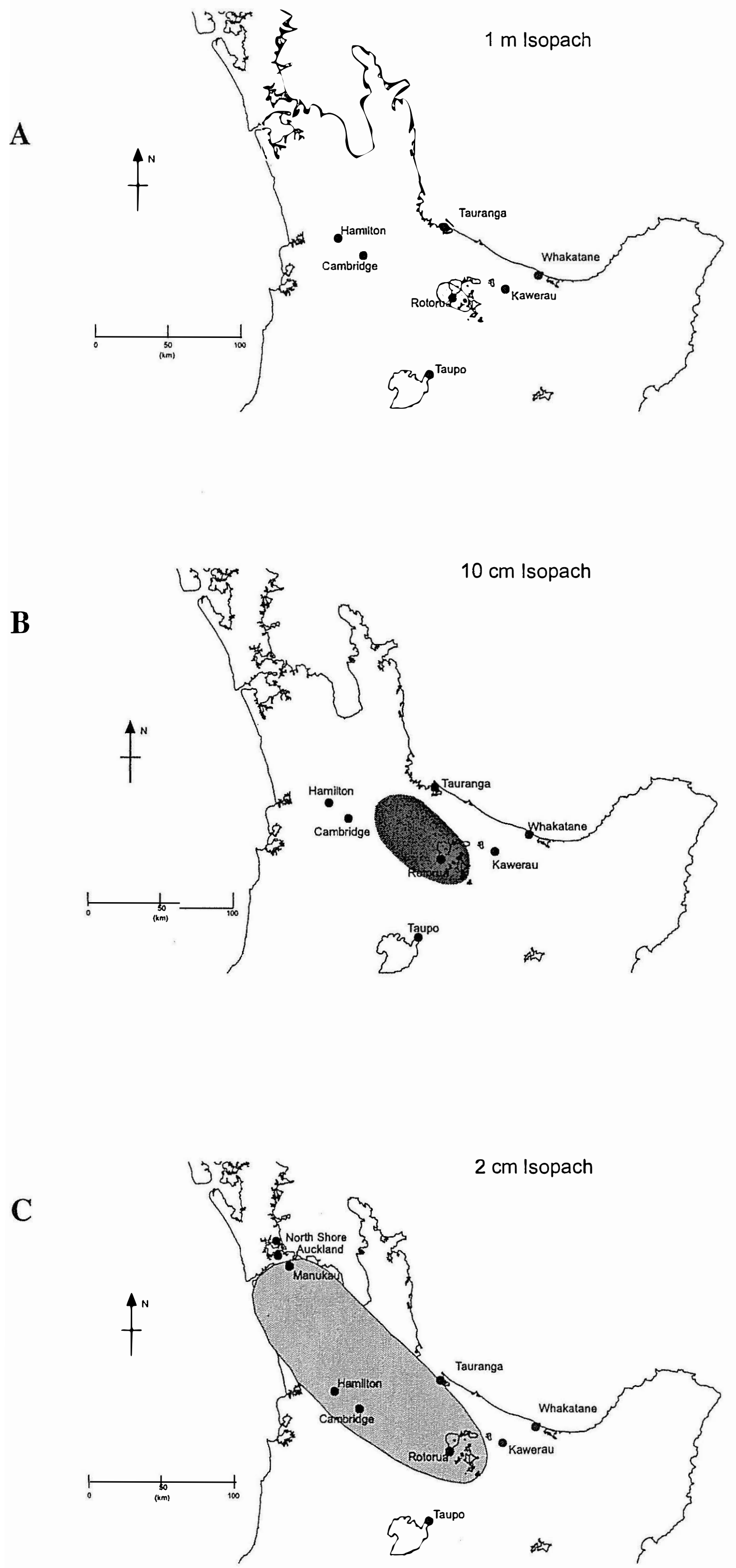

Fig. 6.1 100(a), 10(b) and 2(c) cm isopach maps indicating areas of impact from the plinian fall component of the eruptive episode.

6.2.2 Plinian Fall

The widespread tephra associated with the climactic phase of the Rotorua eruption scenario forms the major hazard to the inhabitants of the Bay of Plenty, Waikato and Auckland regions (Figure 6.1).

In the Rotorua region, the damage to the city would be total. Figure 6.2 highlights the area enclosed by the 100 cm isopach has encompassed the entire Rotorua city and outlying suburbs. The major hazards from the plinian phase of the eruption are given to quantify the effects to aspects of society if a similar eruption occurred today.

Buildings

The main concern for the ca. 50,000 population of Rotorua would be the collapse of houses and other buildings and infrastructure. Blong (1984) quantitatively assessed the amount of loading required before failure in historic eruptions. However the data compiled was based on eruptions primarily prior to 1900 A.D., before modern building design and strength. The results indicate that a tephra thickness of 10-30 cm is required before widespread collapse will occur. Failure depends on the state of the tephra (wet or dry), the angle of the roof and the strength and direction of the wind during deposition (Figure 6.3).

Phreatomagmatic (wet) eruptions (eg. Rotongaio and Hatepe ashes of the Taupo eruption) produce water-laden ash creating a higher specific load than dry tephra. Therefore, the amount of tephra required for failure will be less in phreatomagmatic eruptions, such as at Rabaul in 1994 (Blong, 2001). The Rotorua tephra is the result of a magmatic eruption (see previous chapters), therefore a conservative estimate of complete collapse of buildings is bounded by the 100 cm isopach (Fig 6.1 a). This is assumed due to the required building codes for Rotorua requiring a dead load strength of (50 kg/m^2) (NZS 3604, 1999). Due to the medium lapilli-sized pumice and lithics modelled to affect Rotorua City, the bulk density of the Rotorua A tephra is approximately 400 kg/m^3. Therefore the tephra loading on houses within the 1 m isopach exceeds the standard for snow loading by 8 times. These data suggest all residential buildings will collapse within the 0.5 m isopach.

Depending on roofing styles, deposition of tephra may exacerbate or reduce failure. Flat roofs are more likely to fail with tephra loading due to the rapidly increasing volume of tephra accumulating during the eruption.

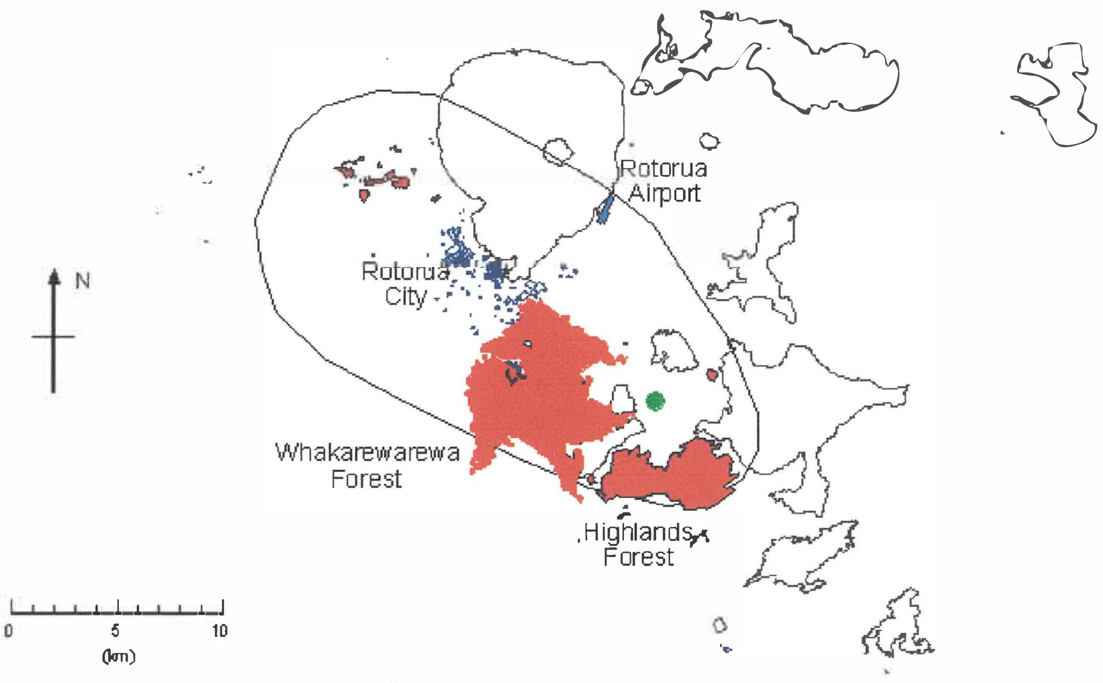

Fig. 6.2 100 cm isopach encompassing two large forestry blocks, the Rotorua airport and Rotorua city. Green – vent location, red – *Pinus radiata* forest, dark blue – buildings, light blue - airport

Conversely, high-angle roofs deflect tephra away from the apex, therefore are less prone to rapid build-up of tephra. During eruptions of small volume, clearing gutters is advised in order to reduce the stress on guttering (FEMA, 1984). However, in the Rotorua eruption scenario, the ability for houses to withstand 100 cm of tephra would be unlikely. The peripheral towns of Putaruru and Tirau would be affected by tephra thicknesses greater than 10 cm (Fig 6.1 b), therefore adequate information regarding the danger of tephra loading would be required to be issued to the communities for proper removal of excess tephra levels.

Wind can affect the ability of structures to withstand the load of tephra. Small-scale redeposition of the finer sized ash particles on the lee side of the wind direction will cause localised regions of increased loading (Blong, 1984). This may lead to preferential failure and may facilitate complete collapse of flat to moderately dipping rooftops.

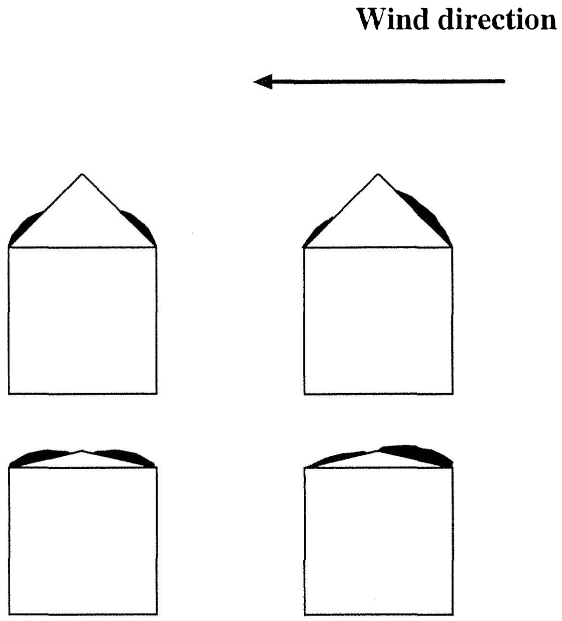

Fig. 6.3 The effect of roof design and wind on roof strength during build-up of tephra during a plinian eruption (redrawn from Blong, 1984). Deposition of tephra on the lee side of a roof may increase the risk of failure to due heightened loading.

Human Health

The effect on human health is likely to be widespread due to the mobility of fine ash (including juvenile material, lithics, obsidian and free crystals) in the atmosphere. Results from the 1995-1996 Ruapehu eruptions suggest a small increase in acute bronchitis was caused by inhaling fine ash particles (Hickling *et al.*, 1999). The study involved subjects living within a region receiving > 0.25 mm of ash as the test case, compared with an unaffected population. While the results showed only a borderline increase in cases of acute bronchitis, the amount of tephra being deposited is considered minimal compared with the Rotorua tephra scenario. Therefore, the effect of volcanic ash on the population's health is likely to be much larger in a plinian eruption. The 2 cm isopach (Figure 6.1c) conservatively indicates the area that may be adversely affected by fine ash. Fine ash may cause the most concern to people with respiratory problems such as asthma and bronchitis. Accounts of historic eruptions indicate that respiratory distress is the main cause for concern in prone patients and fragile individuals ie. the elderly and children (Blong, 1984; Baxter, 1990). Due to the dispersal to the NW, the tephra would have reached south Auckland, home to one of the highest rates of asthma in New Zealand (South Auckland Health Board, 2001). This may create a major logistical problem encountering large patient numbers for respiratory distress. Cases of respiratory distress have been shown to continue well after the cessation of an eruption, up to 1 month as noted from the 1977, Usu eruption (Blong, 1984 and references therein).

Associated with fine ash is the irritation of the eyes, which has lead to discomfort in some individuals (especially those wearing contact lenses) as noted at St Helens, Ruapehu and other historic accounts (Blong, 1984).

Forestry

Forestry is a major industry in New Zealand and one of the most profitable in the Rotorua region. The blocks of forestry to the south (Highlands) and northwest of the vent (Whakarewarewa) account for a large portion of Fletcher Challenge forests in Rotorua. Figure 6.2 indicates that these blocks of forestry would have been inundated with at least 100 cm of tephra during the eruption. The Highlands block to the south would be buried under ca. 200 cm of tephra due to the proximity to the vent. These two blocks of forestry cover an area of ca. 60km^2 (43 km^2-Whakarewarewa Block, 16 km^2-Highlands Block). Current values for forestry are $40,000/ha, therefore the 60 km^2 of forest that would be destroyed would be worth $240 M (NZ Forestry Statistics, 2002). The Waipa sawmill, situated within the Whakarewarewa Forest is also likely to be destroyed, with a current valuation of $15 M (NZ Forestry Statistics, 2002). According to Blong (1984), most vegetation is killed with tephra thicknesses between 100-150 cm, while all vegetation is destroyed with tephra greater than 200 cm thick. These data suggest that the large forestry blocks would be destroyed and deemed unrecoverable for a long period after the eruption (10-20 years). The burial under such large volumes of tephra would limit oxygen influx through the soil. Initial fall of tephra would strip a large portion of the tree's branches rendering the plant ineffective in acquiring energy via photosynthesis (Blong, 1984). Also destruction of surrounding forestry blocks will be increased due to the effect of forest fires, initiated by hot ballistic blocks and bombs.

Agriculture

The hazard to livestock in New Zealand is an important factor to examine due to the reliance on such an industry for nationwide economic prosperity. Historic eruptions such as the 1785 Laki eruption highlight the devastation caused by volcanic eruptions leading to the collapse of agriculture in Iceland. The Rotorua eruption scenario involves burial and inundation of pastureland, and the introduction of minerals and heavy metals into the soil. A widespread tephra blanket over the central North Island would lead to intensive intervention by farmers to remove the tephra for livestock to adequately graze. Depending on the amount of burial, the effectiveness of tephra removal will be greatly decreased in locations within the dispersal axis or close to the vent. In the Rotorua region, the depth of burial will be too great to mitigate against, therefore alternative feed would be required if the property was viable to maintain.

Fluoride is an essential element for animal growth, not readily taken up by plants from soils; however, acute fluorosis in grazing animals has the potential to cause widespread sickness in livestock (Cronin *et al.*, 2000). Fluorosis causes bones to become weak, internal organs to develop ulcers and teeth and gums to become pitted and fragile, as seen at Iceland due to the Laki, 1785 eruption (Blong, 1984). This leads to emaciated herds due to the inability to chew, leading to a slow and painful death.

Tourism

Rotorua is a significant destination for tourists due to the hydrothermal and volcanic activity seen in exhibits and in natural settings. The average yearly income from tourists to Rotorua exceeds $350 M, providing the region with a substantial source of income. The effect of tourism collapse to Rotorua would cause the loss of ~18 % of Rotorua's employment and the loss of $462 M in tourism dependant spending in the Rotorua District (Destination Rotorua, 2002). The numerous events stationed in and around the city provide a destination for a wide range of people from international to national visitors. Therefore due to the volume of tephra deposited in and around Rotorua city, an eruption similar to that of the Rotorua eruptive episode would cause the complete collapse of tourism operations in the Rotorua region. The burial of the city and surroundings would eliminate the chance of a rapid return to the area after an evacuation, due to remobilisation of the tephra, causing unstable foundations for buildings etc. Recovery time of a significant population after a plinian eruption is estimated at over 5 years after the eruption.

Aviation

The effect of volcanic ash on the aviation industry can be extremely costly. Due to the corrosive nature of volcanic ash (carrying a film of corrosive acid) the delicate machinery of jet engines is easily corroded and abraded causing costly engine failure, requiring extensive maintenance (Blong, 1984; Houghton *et al.*, 1988). This requires aeroplanes to be placed in adequate storage hangers to eliminate the corrosive and abrasive nature of volcanic ash on the fuselage, engine and computer equipment housed inside the cockpit. This is a necessary measure due to the ability of fine ash to penetrate small openings within the hanger and the plane itself.

Due to the increased awareness of the effect of volcanic ash on aviation, it is deemed too dangerous to fly when 1 cm of ash is falling on the airport. During a Rotorua-type eruption, this scenario would ground all international and national flights from Rotorua (likely to be destroyed), Hamilton and Auckland airports. This would cause long delays before it would be deemed safe for travel causing extensive economic losses. The ability for flight would be delayed for several days in this scenario due to the ability for fine ash to remain suspended in the atmosphere. The Ruapehu eruption of 1995-1996 caused the grounding of flights in Hamilton and Auckland for at least three days. This was caused by a shift in wind direction causing ash to be deposited towards the NW. Due to this precedent, it would be conceivable to delay flights for at least one week, lasting up to three weeks, depending on the ability to dampen the fine ash (naturally and/or induced).

Hydropower

The Ruapehu 1995-1996 eruption highlighted the need for effective mitigative measures for hydropower stations in the central north island for small-scale eruptions. Considering the volume of the Rotorua eruption, the response of hydropower operators would be required to be implemented very early in the eruption sequence. The amount of abrasive ash and lapilli that would be deposited in the Waikato River, with 9 hydropower stations (Mighty River Power, 2002) would necessitate an early shutdown of operations in order to reduce the input of ejecta into the turbines, causing expensive maintenance as seen in 1995. An eruption of the Rotorua's size would cause a major increase in river turbidity and sediment load, leading to rapid sedimentation behind the dams. This would cause a significant decrease in power production, which may last for several years after the eruption. At maximum output the total power output of the 9 hydropower stations on the Waikato River is approximately 1 GW (Mighty River Power, 2002). The shutdown of these hydropower stations would lead to a major dependence on Huntly power station, which has a similar capacity (Genesis Power, 2002). However, power dependence for both the Waikato and Auckland regions would need to be primarily sourced from Huntly. This would lead to a rapid increase in power output at Huntly placing a major strain on sufficient power generation.

Also affected by the tephra would be the electrical insulators due to conductive ash causing insulator flashover and line breakage caused by loading of the tephra. This will lead to power outages in the Waikato and Auckland catchments (Johnston, 1997).

Drinking Water

The composition of volcanic ash can cause problems with drinking water due to the introduction of increased proportions of heavy metals and gases downwind than would otherwise occur. Metals such as Pb, As, Zn, Mn, Ti, Co, Tl, Se, Mo, Cr, Ni and Cl, F and SO_4 were sampled at Popocatepetl during a period from December 1994 - October

1998 (Armienta *et al.*, 2001). The composition of the ash further from the vent indicated that the concentrations of F and SO_4 increased with distance (Armienta *et al.*, 2001). A number of factors could have exacerbated the trends, but it is necessary to highlight the mobility of metals and gases within a plume to understand the hazard posed by such events. Water tanks on farms surrounding the Rotorua region would be heavily affected and residents would be advised to boil and/or purchase bottled water until a clean water supply is regained. The effect of heavy metals and F can be detrimental to young children and pregnant mothers, in extreme cases causing stillbirth (Blong, 1984). The large amount of fine ash in catchment water will also increase the turbidity of the drinking water requiring expensive filtration systems.

6.3 Dome building of the Rotorua A and B phases

The Rotrua A and B phases both produced voluminous domes; however sites proximal to the vent have not indicated whether the Rotorua A phase produced pyroclastic deposits (upper Rotorua tephra) during dome growth. Therefore, the hazard posed by dome growth has been modelled on the Rotorua B phase, which does show evidence of vulcanian eruptions during lava extrusion. During dome growth, periodic explosive events produced locally dispersed pyroclastic falls, surges, pumice flows and block and ash flows.

The hazard posed by volcanic gases has been modelled on literature from Montserrat and other historical dome-building eruptions.

6.3.1 Pyroclastic fall

Unlike the plinian phase of the eruption, the upper Rotorua tephra has been deposited locally due to small vulcanian-type explosions from the domes late in the eruptive sequence. The area of dispersal is located immediately south and east of the vent, only recorded in 3 site locations. The main hazard with the upper Rotorua tephra is the timing of such events. The plinian phase was over within a matter of hours, while the transition into dome building may have lasted several years, although no soil development is witnessed. There may have been a significant time delay before dome building began (10 years). If a period of years marked the transition between plinian and dome-building phases, the hazard may be due to the determination of local residents to return to what is left of their dwellings. However, with effective emergency management, a perimeter would be introduced as at Montserrat, to eliminate the risk from a localised hazard.

6.3.2 Pyroclastic Flow

Baxter (1990) provides a graphic account of the hazards from pyroclastic flows as seen in historic eruptions. The ignimbrite seen in the Te Mu Road section (see Chapter 2) is the only evidence of pyroclastic flows from the Rotorua eruptive episode. This may be a function of exposure or that the eruption did not produce extensive pyroclastic flows. Due to the small volume of the ignimbrite, the topographic controls of the older domes surrounding the vent would have contained the flow in the valley floors towards the south and southeast eliminating the effect on more populated areas to the east and north. This form of volcanic hazard is the most destructive due to the heat and impact damage caused (Baxter, 1990). Asphyxiation from the fine particles within the dense current has occurred at historic eruptions due to the rapid elutriation of fine ash into the throat and lungs (Baxter, 1990). Due to the evidence of an ignimbrite to the southeast of the vent alone, it is significant from a hazards perspective that there were no large pyroclastic flows produced during either stage of the eruptive episode. If this eruption occurred today, it would be standard procedure to include a probability-based hazard delineation for likely pathways of pyroclastic flows due to complete or partial column collapse.

6.3.3 Pyroclastic Surge

Surge deposits are found within the dome-building sequence at the Te Mu Road section on the southern side of the vent. Surges have devastating consequences due to the abundance of fine material easily transported away from the flow itself. This can lead to a wider hazard due to inhalation of very fine particles elutriated from the flow and deposited downwind. Pyroclastic surges contain more gas, less particles and are more turbulent than pyroclastic flows enabling them to surmount ridges and deposit as veneers on topographic highs (Houghton *et al.*, 1994). The hazard posed by pyroclastic surges is very high due to the turbulent nature creating asphyxiation and burns to those trapped in their path.

6.3.4 Block and Ash Flow

During dome growth, the slopes of the dome become unstable due to the creation of over steepened slopes. This leads to partial collapse of the dome leading to the production of block and ash flows (Cas & Wright, 1987). As shown at Montserrat (1995-present), the collapse of portions of the dome can lead to voluminous and extensive block and ash flows being produced. Tectonic or volcanic related earthquakes and pockets of gas-rich magma erupting periodically can cause these failures. This has a secondary effect of physically crushing the rhyolite into extremely small particles due to grain-grain interaction. This leads to the production of free silica in the form of cristobalite, which in a respirable form ($< 10\ \mu m$) can cause silicosis over long periods of exposure (Blong, 1984; Baxter *et al.*, 1999). However it has been shown from Popocatepetl (1994-1995 eruptions), that short exposure to volcanic ash is associated with reversible inflammation of the airways (Rojas-Ramos *et al.*, 2001).

Nairn *et al.*, (2001) has shown that block and ash flows are able to travel for extensive distances from the Tarawera massif for up to 10 km from the vent, which has implications for hazard zoning, extending restricted zones down likely flow channels. There is limited evidence of block and ash flow generation around the vent area and domes, but it is likely much of the block and ash flow material has been removed or modified.

6.3.5 Debris Avalanche

After the cessation of volcanic activity, dome slopes may be over steepened. This leads to the generation of debris avalanches due to sudden and catastrophic collapse from an unstable portion of a dome. Unlike block and ash flows, debris avalanches are cold and momentum is provided by gravity rather than gas and heat flux within the hot flow. The debris follows valleys and may evolve into a lahar if sufficient water is available (Houghton *et al.*, 1988). After the cessation of Rotorua eruption/s, debris avalanches would have been a common site proximal to the vent. The likely radial dispersal would endanger any residents returning to their dwellings on the shores of Lake Tarawera.

6.3.6 Volcanic Gas

During dome growth (as seen at Montserrat), degassing of the effusive dome creates a series of short and long term health risks to the local residents. The main causes for a health hazard are the enrichment of gases such as CO_2, SO_2, Cl, F (Blong, 1984). These have the ability to cause asphyxiation, irritation to the nose, throat and eyes, and acid rain. CO_2 emissions are a concern due to the odourless nature and slow effect on the brain slowly starving it of oxygen (Baxter & Kapila, 1989). On February 20th, 1979, 142 inhabitants of Dieng Plateau, Indonesia were asphyxiated by what was later determined to be caused by CO_2 (Le Guern *et al.*, 1982). SO_2 when oxidised becomes H_2SO_4 and is the cause of acid rain effecting proximal to distal locations.

During a period of heightened activity at Montserrat, Allen *et al.*, (2000) measured gas levels in the capital of Plymouth (located 5 km southwest of the vent – downwind). Aerosols were found to be highly acidic at source but rapidly neutralised during transport. The concentration of sulphur dioxide was found to be too low to pose a health risk.

6.4 Economic Losses

The cost incurred from the Rotorua eruption in modern terms would be economically devastating. It is difficult to accurately gauge the primary effects and the long-lived secondary effects from an explosive rhyolitic eruption. Forestry and tourism would be the major industries to be affected by a large eruption and an estimated economic loss can be attempted. However, other impacts such as damage to ecology over a wide area of the central north island is difficult to estimate due to the varying ability for biota to adapt to increases in turbidity and acidity (eg. Masaya, Nicaragua) (Delmelle *et al.*, 2001).

The Ruapehu eruptions of 1995-1996 cost over $100 million due to the loss of two ski seasons, rapid tourism decline, hydropower failure and aviation delays. These events involved a relatively small volume of material (0.01 km^3) and the effect of an explosive rhyolitic eruption will be at least an order of magnitude more devastating. It is possible to estimate minimal losses due to the loss of the two large forestry blocks of Whakarewarewa and Highlands to the NW and S of the vent respectively. The estimated loss of ca. 60 km^2 of *Pinus radiata* forest is ca. $200 million at present wood prices, with the loss of two large forestry blocks being difficult to regenerate due to the large volumes of burial. This figure includes the complete destruction of the forest saw mill. The average yearly income from tourism to the Rotorua region is ca. $200 million, which would be expected to be the minimal amount lossed by a Rotorua-type eruption. An estimated cost to the destruction of property and dwellings of ca. 10,000 homes at an average value of $100,000, lends to a loss of over $1 billion. No account has been made of commercial buildings, while infrastructure costs are difficult to obtain and quantify. Therefore the estimates proposed in this study are considered minimal values.

Minimal estimates of economic losses indicates that an eruption similar to the Rotorua episode would cause extensive economic losses, upwards of $1.3 billion. This figure will be greatly increased due to both primary and secondary processes of the eruption. The May 18, 1980 eruption of Mount St. Helens is estimated to have cost Washington State approximately $950 million (MacCready, 1982).

6.5 Conclusions

- The plinian phase of the eruptive episode creates a widespread hazard due to burial from the voluminous tephra, while the dome-building phase creates a more localised but much longer-lived hazard zone.

- The 1 m isopach conservatively estimates the limit of complete building failure, surrounding the city of Rotorua and its suburbs (>50,000 population). Collapse of houses is expected in the communities of Ngongotaha and Hamurana.

- Data from historic eruptions suggest a load of 10-30 cm on a standard roof will cause some collapse. This indicates the extent of roof collapse could extend to Tirau, Putaruru and Cambridge depending on roof construction and style.

- Health effects from the plinian fall are expected to extend to the 2 cm isopach, causing respiratory distress to prone individuals (ie. asthma and bronchitis sufferers). The effect of this health hazard is likely to extend to south and central Auckland.

- Several effects of the plinian fall will cause major economic losses such as:
  - collapse of forestry operations in the Rotorua region,
  - cessation of tourism operations in and around Rotorua for several years,
  - major agriculture losses primarily due to fluorosis and lack of feed and land inundation,
  - lengthy delays to aviation operations on the order of weeks to months,
  - risk to health from drinking contaminated water due to the acidity of the ash and
  - hydropower operations being shut down for long periods due to abrasive and corrosive nature of volcanic ash on turbines.
  - Destruction of infrastructure networks in the central and upper North Island

- The dome-building phase creates a localised hazard from the production of ash plumes and pyroclastic density currents, that are topographically controlled around the vent.

- Economic losses are estimated to exceed \$1.3 billion within hours of the eruption due to rapid burial of Rotorua city causing collapse of the tourism industry and burial of the forestry in the region.

Chapter Seven
Conclusions

7.1 Introduction

The deposits of the (15.7 cal ka BP) Rotorua eruptive episode have been re-examined and re-interpreted in this study. Through detailed stratigraphic, textural and component, and geochemical analysis, the deposits of the Rotorua eruptive episode have been grouped into A and B phases. This distinction between the two phases is based largely on mineralogy, geochemistry and intensive parameters. The result of this study has re-defined the volcanic history of the Okareka Embayment of the Okataina Volcanic Centre. This work has also lead to a more accurate volcanic impact assessment of a similar eruption today. The key findings of this study are summarised below.

7.2 Key Findings

The Rotorua eruptive episode was sourced within the Okareka Embayment of Okataina Volcanic Centre and is the most recent eruption (15.7 cal ka B.P.) from this part of the Okataina caldera complex. Nairn (1980, 1981) identified four rhyolite domes (Northern, Trig 7693, Middle and Eastern) within the embayment. The Northern and Eastern domes were identified as been erupted during the (25 cal ka BP) Te Rere eruptive episode on the basis of stratigraphy, while Trig 7693 and Middle domes were identified as effusive remnants of the Rotorua eruptive episode due to their youthful appearance and lack of older tephra overlying them.

In this study the products of the Rotorua eruptive episode have been grouped into A and B phases. Previous studies (Nairn, 1980; 1992) have indicated that Eastern dome was erupted during the Te Rere eruptive episode, however this study has demonstrated through geochemical analysis and general stratigraphic relationships, that Eastern dome and the plinian Rotorua Tephra have similar compositions and are distinct from the previously inferred vent of Trig 7693 and Middle domes. The Upper Rotorua Tephra of Nairn (1980) has a similar composition to the Trig 7693 and Middle domes. The two distinct compositions identified then are, A) Eastern dome and the Rotorua Tephra and B) Trig 7693 and Middle domes, and the Upper Rotorua Tephra. These data indicate the Rotorua eruptive episode involved a short but intense plinian eruption, followed by long-lived effusive dome growth activity (Eastern Dome). After a brief time break effusive activity resumed involving degassed magma from new vents. This led to the construction of Middle and Trig 7693 domes.

Isotopic evidence suggests that the Rotorua eruptive episode involved the eruption of two magma batches. The location of the effusive domes and volume of the eruptives associated with the A and B phases, indicate the separate magma batches were small (~1 km^3) and resided in close proximity to each other.

Detailed analysis of the Rotorua tephra indicates the deposit was dispersed strongly to the NW at least as far as Auckland and Northland. The dispersal of the tephra was narrowly constrained perpendicular to the dispersal axis. Eruption modelling of the isopleth and isopach maps suggests the tephra was dispersed from a plume up to 20 km high, pushed by strong winds from the SE at approximately 25 m/s.

Geochemical analysis of the Rotorua Tephra indicates the A-phase magma was compositional zoned prior to eruption. During withdrawal of magma in the plinian phase, zones were disrupted and mixing within the plume resulted in variable clast compositions through the stratigraphy.

A scenario-based eruption hazard was based on the volcanological interpretations within this study. Due to the dispersal of the plinian fall to the NW, Rotorua City and District would be heavily impacted during a similar eruption today. The 1 m isopach encompasses Rotorua City and a large portion of the district. Due to such large volumes of pyroclastic material inundating and collapsing buildings, it has been determined that all buildings and infrastructure within this area would be destroyed. An economic loss of $1.3 billion was estimated based on collapse of tourism to Rotorua, job losses, infrastructure failure, complete housing failure, and destruction of forestry operations.

7.3 Recommendations for Future Research

- Due to the lack of proximal exposure, it has been difficult to unequivocally constrain the nature and timing of the relationship between the A and B phases of the Rotorua eruptive episode. Therefore, it is necessary to locate sections that contain both the Rotorua A and B pyroclastics. The identification of a time break (or lack thereof), will determine whether or not the plinian (Rotorua A) event lead to the eruption of Trig 7693 and Middle domes, and the Upper Rotorua Tephra. This has implications for the hazard assessment, due to the extension of the modelled eruption duration. These data may model the dynamics of small magma batches residing in close proximity and may lead to a re-appraisal of active volcanic centres due to the danger of discrete magma batches erupting soon after each other.

- More detailed geochemistry is required to determine the relationships between the A and B phase magma batches. Important issues include whether the plumbing systems of these two, apparently distinct batches were interconnected and under what conditions the B-batch magma was able to passively degas.

- The Rotorua eruption represents a credible medium return period scenario for a volcanic disaster in the Rotorua District. Therefore further study of the economic effects of relatively small (<1 km^3) plinian eruptions is required to determine the cost of an explosive rhyolitic eruption on today's society.

References

Allen, A.G.; Baxter, P.J.; Ottley, C.J. 2000. Gas and particle emissions from Soufriere Hills volcano, Montserrat, West Indies: Characterization and health hazard assessment. *Bulletin of Volcanology 62(1)*: 8-19.

Armienta, M-A; de la Cruz-Reyna, S.; Morton, O.; Cruz, O.; Canceros, N. 2001. Compositional variations of ash deposits as a function of distance at Popocatepetl volcano. *In*: Stewart, C. (*ed*), *Proceedings of the Cities on Volcanoes 2 Conference, Auckland, New Zealand, 12-14 February 2001.* Institute of Geological and Nuclear Sciences Limited. 158p.

Baxter, P.J. 1990. Medical effects of volcanic eruptions I. Main causes of death and injury. *Bulletin of Volcanology 52*: 532-544.

Baxter, P.J.; Kapilla, M. 1989. Acute health impact of the gas release at Lake Nyos, Cameroon, 1986. *Journal of Volcanology and Geothermal Research 39(2-3):* 265-275.

Baxter, P.J.; Kohn, S.C.; Murphy, M.D.; Nichols, A.; Nicholson, R.A.; Norton, G.; Searl, A.; Sparks, R.S.J.; Vickers, B.P.; Bonadonna, C.; Dupree, R.; Hards, V.L. 1999. Cristobalite in volcanic ash of the Soufriere Hills volcano, Montserrat, British West Indies. *Science* 283(5405): 1142-1145.

Blong, R.J. 1984. *Volcanic Hazards: A sourcebook on the effects of eruptions*. Academic Press, Australia. 424p.

Blong, R.J. 1996. Volcanic hazards risk assessment. *In*: Scarpa, R. and R.I. Tilling (*eds.*), *Monitoring and Mitigation of Volcano Hazards*. Springer - Verlag, Berlin. P 675-700.

Blong, R.J. 2001. Building damage in Rabaul, Paua New Guinea, 1994. *In*: Stewart, C. (*ed*), *Proceedings of the Cities on Volcanoes 2 Conference, Auckland, New Zealand, 12-14 February 2001.* Institute of Geological and Nuclear Sciences Limited. 158p.

Bonadonna, C.; Ernst, G.G.L.; Sparks, R.S.J. 1998. Thickness variations and volume estimates of tephra fall deposits: the importance of the particle Reynolds number. *Journal of Volcanology and Geothermal Research 81:* 173-187.

Bowyer, D. *(in prep).* PhD Thesis. Petrologic, geochemical and isotopic evolution of rhyolite lavas from the Okataina, Rotorua and Kapenga Volcanic Centres, Taupo Volcanic Zone, New Zealand. University of Waikato, New Zealand.

Briggs, R.M.; Gifford, M.G.; Moyle, A.R.; Taylor, S.R.;Norman, M.D.; Houghton, B.F.; Wilson, C.J.N. 1993. Geochemical zoning and eruptive mixing in ignimbrites from Mangakino volcano, Taupo Volcanic Zone, *New Zealand. Journal of Volcanology and Geothermal Research. 56.* 175-203.

Brooker, M.R.; Houghton, B.F.; Wilson, C.J.N.; Gamble, J.A. 1993. Pyroclastic phases of a rhyolitic dome–building eruption: Puketarata tuff ring, Taupo Volcanic Zone, New Zealand.

Carey, S.N.; Sigurdsson, H. 1986. The 1982 eruptions of El Chichon volcano, Mexico (2): observations and numerical modelling of tephra fall distribution. *Bulletin of Volcanology 48*: 127-141.

Carey, S.N.; Sparks, R.S.J. 1986. Quantitative models of the fallout and dispersal of tephra from volcanic eruption columns. *Bulletin of Volcanology 48*: 109-125.

Carter, L.; Nelson, C.S.; Neil, H.L.; Froggatt, P.C. 1995. Correlation, dispersal and preservation of the Kawakawa tephra and other late Quaternary tephra layers in the southwest Pacific Ocean. *New Zealand Journal of Geology and Geophysics 38(1):* 29-46.

Cas, R.F.; Wright, J.V. 1987. *Volcanic successions, modern and ancient.* Allen and Unwin, England. 528p.

Crisewell, C.W. 1987. Chronology and stratigraphy of the May 18, 1980, eruption of Mount St. Helens, Washington (USA). *Journal of Geophysical Research 92(B10)*: 10,237-10266.

Cronin, S.J.; Manoharan, V.; Hedley, M.J.; Legonathan, P. 2000. Fluoride: A review of its fate, bioavailability, and risks of fluorosis in grazed-pasture systems in New Zealand. *New Zealand Journal of Agricultural Research 43(3)*: 285-321.

Delmelle, P.; Garcia-Alvarez, J.; Barquero, J.; Stix, J.; Bourque, C.P.; Baxter, P.J. 2001. Dry deposition and heavy acid loading in the vicinity of Masaya volcano, a major sulphur and chlorine source in Nicaragua. *Environmental Science and Technology 35(7):* 1289-1293.

Donoghue, S.L.; Neall, V.E.; Palmer, A.S. 1995. Stratigraphy and chronology of late Quaternary andesitic tephra deposits, Tongariro Volcanic Centre, New Zealand. *Journal of the Royal Society of New Zealand 25(2)*: 115-206.

Dunbar, N.W.; Kyle, P.R.; Wilson, C.J.N. 1989. Evidence for limited zonation in silicic magma systems, Taupo Volcanic Zone, New Zealand. *Geology 17*: 234-246.

Ewart, A.: Healy, J. 1965: Rotorua volcanic geology. In New Zealand volcanology, Central Volcanic Region. New Zealand. DSIR Information Series 50: 10-26.

Federal Emergency Management Agency. 1984. *The Mitigation of Ashfall Damage to Public Facilities. Lessons learned from the 1980 eruption of Mount St. Helens, Washington.* Federal Emergency Management Authority, Region X. 70p.

Fierstein, J. Nathenson, M. 1992. Another look at the calculation of fallout tephra volumes. *Bulletin of Volcanology 54*: 156-167.

Folk, R.L.; Ward, W.C. 1957. Brazos river bar: a study of the significance of grainsize parameters. *Journal of Sedimentary Petrology 27*: 3-26.

Froggatt, P.C.; Lowe, D.J. 1990. A review of late Quaternary silicic and some other tephra formations from New Zealand: their stratigraphy, nomenclature, distribution, volume, and age. *New Zealand Journal of Geology and Geophysics 33*: 89-109.

Genesis Power, 2002. www.genesispower.co.nz

Ghiorso, M.S.; Sack, R.O. 1991. Fe-Ti oxide geothermometry: thermodynamic formulation and estimation of intensive variables in silicic magmas. *Contributions to Mineral Petrology 108:* 485-510.

Graham, I.H.; Cole, J.W.; Briggs, R.M.; Gamble, J.A.; Smith, I.E.M. 1995. Petrology and petrogenesis of volcanic rocks from the Taupo Volcanic Zone: a review. *Journal of Volcanology and Geothermal Research 68:* 59-87.

Grange, L.I. 1929. A classification of the soils of Rotorua County. *New Zealand Journal of Science and Technology 11:* 219-228.

Grange, L.I. 1937. The geology of the Rotorua -Taupo Subdivision. *New Zealand Geological Survey Bulletin 37*: 138.

Hammer, J.E.; Cashman, K.V.; Hoblitt, R.P.; Newman, S. 1999. Degassing and microlite crystallization during pre-climactic events of the 1991 eruption of Mt. Pinatubo, Phillipines. *Bulletin of Volcanology 60(5):* 355-380.

Hickling, J.; Clements, M.; Weinstein, P.; Woodward, A. 1999. Acute health effects of the Mount Ruapehu (New Zealand) volcanic eruption of June 1996. *International Journal of Environmental Health Research 9(2):* 97-107.

Hogg. A.G.; Lowe, D.J.; Hendy, C.H. 1987. University of Waikato radiocarbon dates 1. *Radiocarbon 29*: 263-301.

Hogg, A.G.; Palmer, J.; Lowe, D.J.; Reimer, P.; Higham, T.F.G.; Newnham, R.M. (in press). Wiggle match date for Polynesian 'settlement layer' (Kaharoa Tephra) of New Zealand. *Antiquity.*

Houghton, B.F.; Smith, R.T. 1993. Recycling of magmatic clasts during explosive eruptions: estimating the true juvenile content of phreatomagmatic volcanic deposits. *Bulletin of Volcanolgy 55(6):* 414-420.

Houghton, B.F.; Wilson, C.J.N. 1989. A vesicularity index for pyroclastic deposits. *Bulletin of Volcanology 51*: 451-462.

Houghton, B.F.; Latter, J.H.; Froggatt, P.C. 1988. Volcanic Hazard in New Zealand: Identifying the problem and practical measures to mitigate the risk. *Geological Society of New Zealand Miscellaneous Publication 41d.* 54p.

Houghton, B.F.; Wilson, C.J.N.; Weaver, S.D.; Lanphere, M.D.; Barclay, J. 1994. Volcanic Hazards at Mayor Island. Ministry of Civil Defence, *Volcanic Hazards Information Series No. 6.* 23p.

Houghton, B.F.; Wilson, C.J.N.; McWilliams, M.O.; Lanphere, M.A.; Weaver, S.D.; Briggs, R.M. and Pringle, M.S. 1995: Chronology and dynamics of a large silicic magmatic system: Central Taupo Volcanic Zone, New Zealand. *Geology. 23.* 13-156.

Inman, D.L. 1952. Measures for describing the size distribution of sediments. *Journal of Sedimentary Petrology 22:* 125-145.

Johnston, D.M. 1997. The impact of recent falls of volcanic ash on public utilities in two communities in the United States of America. *Institute of Geological and Nuclear Sciences Science Report 97/5.* 21p.

Jurado-Chichay, Z.; Walker, G.P.L. 2000. Stratigraphy and dispersal of the Mangaone Subgroup pyroclastic deposits, Okataina Volcanic Centre, New Zealand. *Journal of Volcanology and Geothermal Research 104:* 319-383.

Jurado-Chichay, Z.; Walker, G.P.L. 2001a. The intensity and magnitude of the Mangaone Subgroup plinian eruptions from Okataina Volcanic Centre, New Zealand. *Journal of Volcanology and Geothermal Research 111:* 219-237.

Jurado-Chichay, Z.; Walker, G.P.L. 2001b. Variability of plinian fall deposits: examples from Okataina Volcanic Centre, New Zealand. *Journal of Volcanology and Geothermal Research 111:* 239-263.

Kaminski, E.; Jaupart, C. 1997. Expansion and quenching of vesicular magma fragments in plinian eruptions. *Journal of Geophysical Research 102(B6):* 12187-12203.

Klug, C.; Cashman, K.V. 1994. Vesiculation of May 18, 1980, Mount St. Helens magma. *Geology 22(5):* 468-472.

Le Bas, M.J.; Le Maitre, R.W.; Streckeisen, A.; Zanettin, B. 1986. A Chemical Classification of Volcanic Rocks based on the Total Alkali-Silica Diagram. *Journal of Petrology 27:* 745-750.

Le Guern, F.; Tazieff, F.H.; Favre Pierret, R. 1982. An example of health hazard: people killed by gas during a phreatic eruption, Dieng Plateau (Java, Indonesia) February 20th 1979. *Bulletin of Volcanology 45(2):* 153-156.

Le Maitre, R.W. 1989. *A Classification of Igneous Rocks and Glossary of Terms: recommendations of the International Union of Geological Sciences Subcommission on the Systematics of Igneous Rocks.* Blackwell Scientific publications, Great Britain. 190p.

Lowe, D.J. 1988. Stratigraphy, age, composition, and correlation of late Quaternary tephras interbedded with organic sediments in Waikato lakes, North Island, New Zealand. *New Zealand Journal of Geology and Geophysics 31:* 125-165.

Lowe, D.J.; Newnham, R.M. and Ward, C.M. 1999: Stratigraphy and chronology of a 15 cal yr sequence of multi-sourced silicic tephras in a montane peat bog, eastern North Island, New Zealand. *New Zealand Journal of Geology and Geophysics. 42*. 565-579.

MacCready, J.S. 1982. Some economic consequences of the eruptions (Washington State). *In* Keller, S.A.C. (*eds.*) *Mount St. Helens: one year later.* Eastern Washington University Press, Cheney. 215-224 p.

Manning, D.A. 1996: Middle – Late Pleistocene Tephrostratigraphy of the Eastern Bay of Plenty, New Zealand. *Quaternary International. 34/36.* 3-12.

Mighty River Power, 2002. www.mightyriverpower.co.nz

Nairn, I.A. 1980. Source, age, and eruptive mechanisms of Rotorua Ash. *New Zealand Journal of Geology and Geophysics 23:* 193-207.

Nairn, I.A. 1981. *Some studies of the geology, volcanic history and geothermal resources of the Okataina Volcanic Centre, Taupo Volcanic Zone, New Zealand.* Unpublished PhD. Thesis, Victoria University, Wellington.

Nairn, I.A. 1989. *Sheet V16AC Tarawera - Geological Map of New Zealand 1:50000*. New Zealand Department of Scientific and Industrial Research, Wellington.

Nairn, I.A. 1992. The Te Rere and Okareka eruptive episodes - Okataina Volcanic Centre, Taupo Volcanic Zone, New Zealand. *New Zealand Journal of Geology and Geophysics 35*: 93-108.

Nairn, I.A.; Self, S.; Cole, J.W.; Leonard, G.S.; Scutter, C. 2001. Distribution, stratigraphy, and history of proximal deposits from the c. AD 1305 Kaharoa eruptive episode at Tarawera volcano, New Zealand. *New Zealand Journal of Geology and Geophysics 44(3):* 467-484.

Newhall, C.G.; Melson, W.G. 1983. Explosive activity associated with the growth of volcanic domes. *Journal of Volcanology and Geothermal Research 17:* 111-131.

New Zealand Forestry Statistics. 2002. Online version **http://www.maf.govt.nz/statistics/primaryindustries/forestry/index.htm**

Pyle, D.M. 1989. The thickness, volume and grainsize of tephra fall deposits. *Bulletin of Volcanology 48:* 109-125.

Rojas-Ramos, M.; Villalba-Caloca, J.; Perez-Neria, J.; Catalan-Vazquez, M.; Martin-Del Pozzo, A.L.; Garcia-Ojeda, E. 2001. A seven months perspective study on the respiratory effects of exposure to ash from Popocatepetl volcano, Mexico. *Environmental Geochemistry and Health 23(4):* 383-396.

Rutherford, M.J.; Hill, R.M. 1993. Magma ascent rates from amphibole breakdown: an experimental study applied to the 1980-1986 Mount St. Helens eruptions. *Journal of Geophysical Research 98*(B11): 19,667-19,685

Rutherford, M.J.; Devine, J.D. 1988. The May 18, 1980 eruption of Mount St. Helens, stability and chemistry of amphibole in the magma chamber. *Journal of Geophysical Research 93*: 11949-11959.

Sandiford, A.; Alloway, B.; Shane, P. 2001. A 28000-6600 cal yr record of local and distal volcanism preserved in a paleolake, Auckland, New Zealand. *New Zealand Journal of Geology and Geophysics 44(2):* 323-336.

Shane, P. 1998. Correlation of rhyolitic pyroclastic eruptive units for the Taupo Volcanic Zone by Fe-Ti oxide compositional data. *Bulletin of Volcanology 60:* 224-238.

Sparks, R.S.J. 1986. The dimensions and dynamics of volcanic eruption columns. *Bulletin of Volcanology 48:* 3-15.

Sparks, R.S.J.; Bursik, M.I.; Carey, S.N.; Gilbert, J.S.; Glaze, L.S.; Sigurdsson, H.; Woods, A.W. 1997. *Volcanic Plumes.* John Wiley and Sons, England. 574p.

Speed, J. 2001. *The 11.9 ka Waiohau eruptive episode, Okataina Volcanic Centre, Taupo Volcanic Zone.* Unpublished MSc thesis, University of Auckland, New Zealand.

Stuiver, M. Reimer, P.J.; Bard, E.; Beck, J.W.; Burr, G.S.; Hughen, K.A.; Kromer, B. McCormac, G.; van der Plicht, J. and Spurk, M. 1998: INTCAL98 radiocarbon age calibration, 24,000 – 0 cal BP. *Radiocarbon. 40.* 1041-1083.

Sutton, A.N.; Blake, S.; Wilson, C.J.N. 1995. An outline geochemistry of rhyolitic eruptives from Taupo volcanic centre, New Zealand. *Journal of Volcanology and Geothermal Research 68:* 153-175.

Tait, S. Jaupart, C.; Thomas, R.; Gardner, J. 1998. Constraints on cooling rates and permeabilities of pumice in an explosive eruption jet from colour and magnetic mineralogy. *Journal of Volcanology and Geothermal Research 86(1-4):* 79-91.

Thomas, A.P.W. 1888. *Report on the eruption of Tarawera and Rotomahana, New Zealand.* Government Printer Wellington. 30p.

Thomas, N.; Jaupart, C.; Verginolle, S. 1994. On the vesicularity of pumice. *Journal of Geophysical Research 99(B8):* 15633-15644.

Topping, W.W.; Kohn, B.P. 1973. Rhyolitic tephra marker beds in the Tongariro area, North Island, New Zealand. *New Zealand Journal of Geology and Geophysics 16*: 375-395.

Vucetich, C.G.; Pullar, W.A. 1969. Stratigraphy and chronology of late Quaternary volcanic ash beds in the central North Island, New Zealand. *New Zealand Journal of Geology and Geophysics 12:* 784-837.

Vucetich, C.G,; Pullar, W.A. 1964: Stratigraphy and chronology of late Quaternary volcanic ash in Taupo, Rotorua, and Gisborne districts. Part 2. Stratigraphy of Holocene ash in the Rotorua and Gisborne districts. *New Zealand Geological Survey Bulletin 73*: 43-88.

Walker, G.P.L. 1971. Grainsize characteristics of pyroclastic deposits. *Geology 79:* 696-714.

Wilson, C.J.N.; Switsur, R.V.; Ward, A.P. 1988: A new ^{14}Cage for the Oruanui (Wairakei) eruption, New Zealand. *Geological magazine 125:* 297-300.

Wilson, C.J.N.; Houghton, B.F.; M^{c}Williams, M.; Lanphere, M.A.; Weaver, S.D.; Briggs, R.M.; Pringle, M.S. 1995. Chronology and dynamics of a large silicic magmatic system: central Taupo Volcanic Zone, New Zealand. *Geology 23:* 13-16.

Wilson, L.; Walker, G.P.L. 1987. Explosive volcanic eruptions - VI. Ejecta dispersal in plinian eruptions: the control of eruption conditions and atmospheric properties. *Geophysical Journal of the Royal Astronomical Society 89:* 657-679.

Wolfe, E.W.; Hoblitt, R.P. 1996. Overview of the eruptions. *In*: Newhall, C.G. and R.S. Punongbayan (*eds.*) *Fire and Mud: eruptions and lahars of Mount Pinatubo, Phillipines. Phillipine Institute of Volcanology and Seismology, Quezon City.* University of Washington Press, London. p 3-20.

Appendix I

Isopach and Isopleth Data

Isopach Data

SITE NUMBER	MAP NUMBER	NZMS 260	TOTAL (CM)	Am-6	Am-5	Am-4	Am-3	Am-2	Am-1	EASTINGS	NORTHINGS
1	U16	018 315	605	55	60	120	100	160	110	2801800	6331500
2	U15	994 323	579	79	100	70	60	160	110	2799400	6332300
3	U16	993 318	600	110	80	90	110	130	80	2799300	6331800
4	U16	943 329	169	40	0	32	23	53	27	2794300	6332900
5	U16	026 288	700							2802600	6328800
6	U16	979 263	154	38	0	28	83	15	0	2797900	6326300
7	U16	004 280	226	56	0	15	37	101	17	2800400	6328000
8	U16	003 291	243	30	0	14	33	140	26	2800300	6329100
9	U16	975 310	132	31	0	6	10	85	0	2797500	6331000
10	U16	972 239	80							2797200	6323900
11	U16	945 204	9							2794500	6320400
12	U16	954 222	35							2795400	6322200
13	U16	919196	16							2791900	6319600
14	U16	914 204	11							2791400	6320400
15	U16	918 234	12							2791800	6323400
16	U16	871 243	15						0	2787100	6324300
17	U16	009 229	45	25	5	10	5	5	0	2800900	6322900
18	U16	017 228	90	20	2	10	4	0	0	2801700	6322800
19	U16	043 193	11	2	0	2	5	2	0	2804300	6319300
20	U15	060 188	9							2806000	6318800
20a	U15	063 184	10							2806300	6318400
20b	U15	067 176	9							2806700	6317600
21	U16	903 355	180	45	0	25	30	55	25	2790300	6335500
22	U16	899 363	229	46	0	65	26	65	27	2789900	6336300
23	U16	888 366	180	57	0	12	30	56	25	2788800	6336600
24	U16	883 353	64	0	0	0	0	42	22	2788300	6335300
25	U16	883 359	110	20	0	0	0	70	20	2788300	6335900
26	U16	878 365	128	37	10	33	10	30	8	2787800	6336500
27a	U16	912 371	271	57	22	27	36	87	42	2791200	6337100
27b	U16	873 362	139	27	23	5	20	50	14	2787300	6336200
28	U16	854 363	134	13	0	8	20	65	28	2785400	6336300
29	U16	857 362	138	16	0	8	20	73	21	2785700	6336200
30	U16	860 363	92	11	0	2	6	59	14	2786000	6336300
31	U16	858 366	108	14	10	6	17	48	13	2785800	6336600
32	U16	859 379	143	33	10	9	29	44	18	2785900	6337900
33	U16	862 387	123	19	9	12	23	44	16	2786200	6338700
34	U15	896 406	171	31	19	10	32	40	39	2789600	6340600
62	U15	871 428	100	9	0	4	8	65	14	2787100	6342800
35	U15	881 432	114	16	0	0	0	78	20	2788100	6343200
36	U15	886 444	97	9	0	0	0	71	17	2788600	6344400
37	U15	897 444	106	0	0	0	0	78	28	2789700	6344400
38	U15	916 457	80	0	0	0	0	66	14	2791600	6345700
39	U15	898 484	80	0	0	0	0	70	10	2789800	6348400
40	U15	890 465	48	0	0	0	0	31	17	2789000	6346500
41	U15	863 475	76	23	11	0	0	27	15	2786300	6347500
42	U15	852 473	51	15	11	0	0	16	9	2785200	6347300
43	U15	814 471	53	8	0	0	0	34	11	2781400	6347100
44	U15	747 434	31	0	0	0	0	25	6	2774700	6343400
45	U15	771 423	56	0	0	0	0	50	6	2777100	6342300
46	U16	804 393	81	17	0	0	0	50	14	2780400	6339300
47	U16	802 365	31	0	0	0	0	25	6	2780200	6336500
48	U16	817 409	100	7	9	0	0	71	13	2781700	6340900
49	U16	833 408	84	15	0	0	0	58	11	2783300	6340800
50	U16	858 407	142	21	11	15	18	59	21	2785800	6340700

Isopach Data cont'd

SITE NUMBER	MAP_NUMBER	NZMS_260_	TOTAL (CM)	Am-6	Am-5	Am-4	Am-3	Am-2	Am-1	EASTINGS	NORTHINGS
51	U16	887 414	146	16	22	0	0	82	26	2788700	6341400
52	U15	998 464	28	8	0	0	0	16	4	2799800	6346400
53	U15	991 466	65	36	0	0	0	29	0	2799100	6346600
54	U15	970 470	40	13	0	0	0	9	18	2797000	6347000
55	U15	935 494	30	9	0	0	0	15	6	2793500	6349400
56	U15	923 507	24	0	0	0	0	24	0	2792300	6350700
57	U15	947 514	24	4	0	0	0	20	0	2794700	6351400
58	U15	006 545	34	14	5	0	0	15	0	2800600	6354500
59	U15	959 544	12	0	0	0	0	12	0	2795900	6354400
60	U15	001 566	17	7	0	0	0	10	0	2800100	6356600
61	U15	028 421	75							2802800	6342100
63	V16	109 147	7							2810900	6314700
64	U15	833 434	60	21	0	0	0	29	10	2783300	6343400
65	U15	060 513	54	19	0	0	0	20	15	2806000	6351300
66	U15	065 493	22	13	0	0	5	4	0	2806500	6349300
67	U15	083 496	22	0	0	0	0	15	7	2808300	6349600
68 Lk Okoroire	T15	555 612	10							2755500	6361200
69 Lk Rotoroa	S14	106 753	6							2710600	6375300
70	U16	046 247	36	9	0	0	0	17	10	2804600	6324700
74	V15	115514	70	0	0	0	0	55	15	2811500	6351400
75	V15	186 554	5							2818600	6355400
76	V15	231 523	15	6	0	0	0	4	5	2823100	6352300
77	U16	975 325	180	77	16	63	0	0	0	2797500	6332500
78	U16	967 323	301	41	48	72	36	52	52	2796700	6332300
79	U15	801 449	48	7	0	0	0	22	7	2780100	6344900
Lk Maratoto	S15	129 663	3							2712900	6366300
Lk Ngaroto	S15	115 583	2							2711500	6358300
Lk Mangakaware	S15	053 610	3							2705300	6361000
Lk Mangahia	S15	062 668	5							2706200	6366800
Lk Rotokauri	S14	036 802	5							2703600	6380200
Lk Kainui	S14	072 892	8							2707200	6389200
Lk Rotokaraka	S14	166 965	6							2716600	6396500
Lesson's Pond	S14	278 929	3							2727800	6392900
Lk Rotongata	T16	376 380	1							2737600	6338000
Lk Tunawhakapeka	S14	106 853	2							2710600	6385300
Lk Rotomanuka	S15	136 615	3							2713600	6361500
Kohuora Crater	R11	744 675	2							2674400	6467500
Pukaki Crater	R11	715 674	2							2671500	6467400
71	U16	027 262	210	0	0	0	0	0	0	2802700	6326200
72	U16	036 244	105	30	21		17	13	17	2803600	6324400
73	U15	916 409	148	31	8	14	38	42	15	2791600	6340900
80	U16	022 316	331	138	65	128				2802200	6331600
81	U16	054 296	600							2805400	6329600
82	U16	944 319	94				35	59		2794400	6331900
83	U15	765 473	43	13				12	18	2776500	6347300
84	U16	015 299	100							2801500	6329900
85	U16	048 273	160							2804800	6327300

Waikato Lake data (sites labelled Lk Maratoto to Lk Rotomanuka) are taken from Lowe (1988). Kohuroa and Pukaki Crater data are from Sandiford *et al.* (2001).

Isopleth Data

SITE NUMBER	Am-6 MP	Am-6 ML	Am-5 MP	Am-5 ML	Am-4 MP	Am-4 ML	Am-3 MP	Am-3 ML	Am-2 MP	Am-2 ML	Am-1 MP	Am-1 ML
1	48	13	0	0	37	0	0	0	85	27	0	0
2	41	12	0	0	68	22	0	0	107	48	0	0
3	23	9	0	0	54	42	0	0	108	67	0	0
4	12	3	0	0	28	7	12	3	58	15	2	1
5	0	0	0	0	0	0	0	0	0	0	0	0
6	8	4	0	0	13	3	8	1	35	9	0	0
7	43	12	0	0	58	18	9	3	68	28	5	1
8	47	15	0	0	63	21	7	2	62	26	6	1
9	24	10	0	0	47	13	11	5	72	33	0	0
10	0	0	0	0	0	0	0	0	0	0	0	0
11	0	0	0	0	0	0	0	0	0	0	0	0
12	0	0	0	0	0	0	0	0	0	0	0	0
13	0	0	0	0	0	0	0	0	0	0	0	0
14	0	0	0	0	0	0	0	0	0	0	0	0
15	0	0	0	0	0	0	0	0	0	0	0	0
16	0	0	0	0	0	0	0	0	0	0	0	0
17	0	0	0	0	0	0	0	0	0	0	0	0
18	0	0	0	0	0	0	0	0	0	0	0	0
19	0	0	0	0	0	0	0	0	0	0	0	0
20	0	0	0	0	0	0	0	0	0	0	0	0
20a	0	0	0	0	0	0	0	0	0	0	0	0
20b	0	0	0	0	0	0	0	0	0	0	0	0
21	2	1	0	0	22	9	9	4	29	13	1	0
22	5	1	6	1	26	8	10	2	24	6	5	1
23	5	1	0	0	13	4	9	2	35	7	4	2
24	6	1	0	0	11	3	8	2	31	5	5	1
25	5	2	5	1	12	6	9		28	6	2	2
26	8	2	0	0	21	8	6	1	35	9	5	1
27a	8	2	0	0	21	8	10	3	22	12	3	1
27b	4	2	0	0	23	5	7	2	33	8	4	1
28	3	1	0	0	8	3	5	1	28	6	1	1
29	4	2	0	0	8	3	8	1	24	6	2	1
30	7	4	0	0	9	4	3	1	23	7	2	1
31	2	1	0	0	6	1	4	2	24	5	1	1
32	4	1	0	0	6	2	5	2	23	7	2	1
33	4	1	0	0	4	1	4	1	21	6	2	0
34	15	2	22	3	30	5	20	5	35	11	15	5
62	2	1	0	0	0	0	0	0	0	0	0	0
35	4	0	0	0	0	0	0	0	0	0	0	0
36	1	1	0	0	0	0	0	0	0	0	0	0
37	1	0	0	0	0	0	0	0	0	0	0	0
38	1	0	0	0	0	0	0	0	0	0	0	0
39	0	0	0	0	0	0	0	0	0	0	0	0
40	0	0	0	0	0	0	0	0	0	0	0	0
41	0	0	0	0	0	0	0	0	0	0	0	0
42	0	0	0	0	0	0	0	0	0	0	0	0
43	0	0	0	0	0	0	0	0	0	0	0	0
44	0	0	0	0	0	0	0	0	0	0	0	0
45	0	0	0	0	0	0	0	0	0	0	0	0
46	1	0	0	0	0	0	0	0	0	0	0	0
47	1	0	0	0	0	0	0	0	0	0	0	0
48	1	0	0	0	0	0	0	0	0	0	0	0
49	1	0	0	0	0	0	0	0	0	0	0	0
50	2	1	0	0	8	4	3	0	17	7	4	1

Isopleth Data cont'd

SITE NUMBER	Am-6 MP	Am-6 ML	Am-5 MP	Am-5 ML	Am-4 MP	Am-4 ML	Am-3 MP	Am-3 ML	Am-2 MP	Am-2 ML	Am-1 MP	Am-1 ML
51	3	1	0	0	10	6	4	1	26	8	3	2
52	0	0	0	0	0	0	0	0	0	0	0	0
53	0	0	0	0	0	0	0	0	0	0	0	0
54	1	0	0	0	0	0	0	0	12	3	7	2
55	0	0	0	0	0	0	0	0	0	0	0	0
56	0	0	0	0	0	0	0	0	0	0	0	0
57	0	0	0	0	0	0	0	0	0	0	0	0
58	0	0	0	0	0	0	0	0	0	0	0	0
59	0	0	0	0	0	0	0	0	0	0	0	0
60	0	0	0	0	0	0	0	0	0	0	0	0
61	6	2	0	0	11	4	7	1	18	5	3	1
63	0	0	0	0	0	0	0	0	0	0	0	0
64	1	0	0	0	0	0	0	0	9	2	5	1
65	1	0	0	0	0	0	0	0	5	1	1	0
66	1	0	0	0	0	0	2	1	6	1	0	0
67	0	0	0	0	0	0	0	0	6	2	1	0
68 Lk Okoroire	0	0	0	0	0	0	0	0	0	0	0	0
69 Lk Rotoroa	0	0	0	0	0	0	0	0	0	0	0	0
70	0	0	0	0	0	0	0	0	0	0	0	0
74	0	0	0	0	0	0	0	0	0	0	0	0
75	0	0	0	0	0	0	0	0	0	0	0	0
76	0	0	0	0	0	0	0	0	3	1	1	0
77	37	14	3	1	47	17	0	0	0	0	0	0
78	25	9	14	5	50	28	18	7	87	46	21	6
79	1	0	0	0	0	0	0	0	3	1	2	1
Lk Maratoto	0	0	0	0	0	0	0	0	0	0	0	0
Lk Ngaroto	0	0	0	0	0	0	0	0	0	0	0	0
Lk Mangakaware	0	0	0	0	0	0	0	0	0	0	0	0
Lk Mangahia	0	0	0	0	0	0	0	0	0	0	0	0
Lk Rotokauri	0	0	0	0	0	0	0	0	0	0	0	0
Lk Kainui	0	0	0	0	0	0	0	0	0	0	0	0
Lk Rotokaraka	0	0	0	0	0	0	0	0	0	0	0	0
Lesson's Pond	0	0	0	0	0	0	0	0	0	0	0	0
Lk Rotongata	0	0	0	0	0	0	0	0	0	0	0	0
Lk Tunawhakapeka	0	0	0	0	0	0	0	0	0	0	0	0
Lk Rotomanuka	0	0	0	0	0	0	0	0	0	0	0	0
Kohuora Crater	0	0	0	0	0	0	0	0	0	0	0	0
Pukaki Crater	0	0	0	0	0	0	0	0	0	0	0	0
71	0	0	0	0	0	0	0	0	0	0	0	0
72	0	0	0	0	0	0	0	0	0	0	0	0
73	7	2	0	0	14	6	3	2	35	11	7	0
80	50	12	30	17	62	26	0	0	0	0	0	0
81	0	0	0	0	0	0	0	0	0	0	0	0
82	0	0	0	0	0	0	44	22	86	34	0	0
83	1	0	0	0	0	0	0	0	12	3	7	2
84	0	0	0	0	0	0	0	0	0	0	0	0
85	0	0	0	0	0	0	0	0	0	0	0	0

Appendix II

Grainsize Data

Grainsize samples were collected at five locations along the dispersal axis of the Rotorua A plinian eruption. Grainsize data are included below. 'Rt /' samples represent deposits taken from the Red Tank Road (# 2) proximal site of the Rotorua A pyroclastics. All samples have a site number prefix referring to sample sites in the text.

PARTICLE SIZE ANALYSIS

Earth Sciences - University of Waikato

Sample: rt c/1

Size distribution histogram

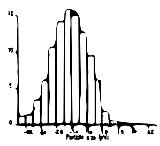

Results summary

Textural size classes
Gravel= 52.52% Sand= 46.89% Silt= 0.00% Clay= 0.00%
Gravel bearing detrital sediment
Sandy Gravel

Moment method parameters (phi)
Mean= -1.07 Sorting= 1.24 Skewness= 0.12 Kurtosis= 3.37

Graphical method parameters (phi)
Mean= -1.06 Sorting= 1.24 Skewness= 0.01 Kurtosis= 0.97
Median= -1.08 C= -4.06 D35= -1.56 D85= -0.58

Textural description:
Poorly sorted, Near symmetrical, Mesokurtic

Cumulative frequency

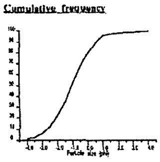

Raw data summary

Size (phi)	Size (mm)	Cumulative weight (g)	Interval frequency (%)	Cumulative frequency (%)
-4.00	16.0000	7.00	1.14	1.14
-3.50	11.3137	14.90	1.29	2.43
-3.00	8.0000	35.80	3.41	5.84
-2.50	5.6569	73.40	6.13	11.96
-2.00	4.0000	138.10	10.55	22.51
-1.50	2.8284	224.60	14.10	36.61
-1.00	2.0000	322.20	15.91	52.52
-0.50	1.4142	414.10	14.98	67.50
0.00	1.0000	491.50	12.62	80.11
0.50	0.7071	549.70	9.49	89.60
1.00	0.5000	538.40	6.31	95.91
1.50	0.3536	600.00	1.89	97.80
2.00	0.2500	603.60	0.59	98.39
2.50	0.1768	605.60	0.33	98.71
3.00	0.1250	607.40	0.29	99.01
3.50	0.0884	608.80	0.23	99.23
4.00	0.0625	609.90	0.18	99.41

Total weight = 613.50 g

Cumulative frequency

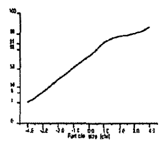

University of Waikato
Rapid Sediment Analyser
Operating System Version 7.1

PARTICLE SIZE ANALYSIS

Earth Sciences - University of Waikato

Sample: rt c/2

Size distribution histogram

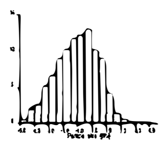

Results summary

Textural size classes
Gravel= 47.80% Sand= 51.56% Silt= 0.00% Clay= 0.00%
Gravel bearing detrital sediment
Sandy Gravel

Moment method parameters (phi)
Mean= -1.00 Sorting= 1.46 Skewness= -0.12 Kurtosis= 2.72

Graphical method parameters (phi)
Mean= -0.98 Sorting= 1.49 Skewness= -0.07 Kurtosis= 0.92
Median= -0.91 C= -4.34 D35= -1.55 D85= -0.31

Textural description:
Poorly sorted, Near symmetrical, Mesokurtic

Cumulative frequency

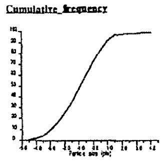

Raw data summary

Size (phi)	Size (mm)	Cumulative weight (g)	Interval frequency (%)	Cumulative frequency (%)
-4.50	22.6274	5.50	0.44	0.44
-4.00	16.0000	28.40	1.82	2.25
-3.50	11.3137	60.50	2.55	4.80
-3.00	8.0000	126.20	5.20	10.01
-2.50	5.6569	210.40	6.68	16.68
-2.00	4.0000	324.90	9.08	25.76
-1.50	2.8284	455.20	10.33	36.09
-1.00	2.0000	602.90	11.71	47.80
-0.50	1.4142	758.00	12.30	60.10
0.00	1.0000	923.60	13.13	73.23
0.50	0.7071	1053.70	10.32	[illegible].55
1.00	0.5000	1168.30	9.09	92.63
1.50	0.3536	1220.40	4.13	96.76
2.00	0.2500	1238.40	1.43	98.19
2.50	0.1768	1244.60	0.49	98.68
3.00	0.1250	1248.20	0.29	98.97
3.50	0.0884	1250.60	0.18	99.15
4.00	0.0625	1253.20	0.21	99.37

Total weight = 1261.20 g

Cumulative frequency

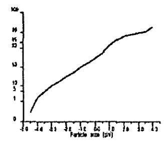

University of Waikato
Rapid Sediment Analyser
Operating System Version 7.1

PARTICLE SIZE ANALYSIS
Earth Sciences - University of Waikato

Sample: rt c/3

Size distribution histogram

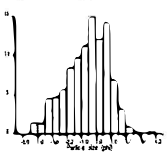

Cumulative frequency

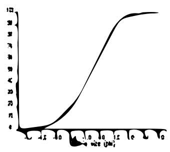

Cumulative frequency

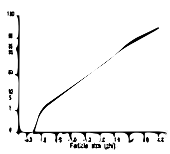

Results summary

Textural size classes
Gravel= 35.59% Sand= 63.93% Silt= 0.00% Clay= 0.00%
Gravel bearing detrital sediment
Sandy Gravel

Moment method parameters (phi)
Mean= -0.56 Sorting= 1.44 Skewness= -0.36 Kurtosis= 2.70

Graphical method parameters (phi)
Mean= -0.55 Sorting= 1.46 Skewness= -0.18 Kurtosis= 0.93
Median= -0.39 C= -4.13 D35= -1.03 D65= 0.14

Textural description:
Poorly sorted, Coarse skewed, Mesokurtic

Raw data summary

Size (phi)	Size (mm)	Cumulative weight (g)	Interval frequency (%)	Cumulative frequency (%)
-5.00	32.0000	0.00	0.00	0.00
-4.50	22.6274	0.00	0.00	0.00
-4.00	16.0000	7.90	1.34	1.34
-3.50	11.3137	15.10	1.22	2.56
-3.00	8.0000	41.50	4.48	7.05
-2.50	5.6569	69.20	4.70	11.75
-2.00	4.0000	102.70	5.69	17.44
-1.50	2.8284	152.50	8.46	25.90
-1.00	2.0000	209.60	9.70	35.59
-0.50	1.4142	275.70	11.22	46.82
0.00	1.0000	363.30	14.88	61.69
0.50	0.7071	434.50	12.09	73.78
1.00	0.5000	518.60	14.28	88.06
1.50	0.3536	559.00	6.86	94.92
2.00	0.2500	577.50	3.14	98.06
2.50	0.1768	582.30	0.82	98.88
3.00	0.1250	584.60	0.39	99.27
3.50	0.0884	585.30	0.12	99.39
4.00	0.0625	586.10	0.14	99.52

Total weight = 588.90 g

University of Waikato
Rapid Sediment Analyser
Operating System Version 7.1

PARTICLE SIZE ANALYSIS
Earth Sciences - University of Waikato

Sample: rt c/4

Size distribution histogram

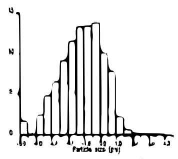

Cumulative frequency

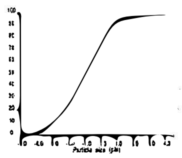

Cumulative frequency

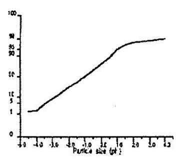

Results summary

Textural size classes
Gravel= 49.88% Sand= 49.14% Silt= 0.00% Clay= 0.00%
Gravel bearing detrital sediment
Sandy Gravel

Moment method parameters (phi)
Mean= -1.08 Sorting= 1.37 Skewness= -0.20 Kurtosis= 3.11

Graphical method parameters (phi)
Mean= -1.05 Sorting= 1.38 Skewness= -0.08 Kurtosis= 0.94
Median= -1.00 C= -4.70 D35= -1.57 D65= -0.44

Textural description:
Poorly sorted, Near symmetrical, Mesokurtic

Raw data summary

Size (phi)	Size (mm)	Cumulative weight (g)	Interval frequency (%)	Cumulative frequency (%)
-4.50	22.6274	17.20	1.67	1.87
-4.00	16.0000	18.90	0.17	1.83
-3.50	11.3137	44.70	2.50	4.34
-3.00	8.0000	94.80	4.86	9.20
-2.50	5.6569	163.30	6.65	15.85
-2.00	4.0000	257.50	9.14	25.00
-1.50	2.8284	376.30	11.53	36.53
-1.00	2.0000	513.90	13.36	49.88
-0.50	1.4142	652.10	13.41	63.30
0.00	1.0000	794.90	13.86	77.16
0.50	0.7071	899.10	10.11	87.27
1.00	0.5000	980.70	7.92	95.20
1.50	0.3536	1004.10	2.27	97.47
2.00	0.2500	1011.50	0.72	98.18
2.50	0.1768	1014.40	0.28	98.47
3.00	0.1250	1016.50	0.20	98.67
3.50	0.0884	1017.90	0.14	98.81
4.00	0.0625	1020.10	0.21	99.02

Total weight = 1030.20 g

University of Waikato
Rapid Sediment Analyser
Operating System Version 7.1

PARTICLE SIZE ANALYSIS
Earth Sciences - University of Waikato

Sample: rt c/5

Size distribution histogram

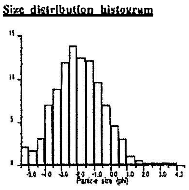

Cumulative frequency

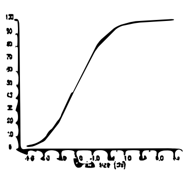

Cumulative frequency

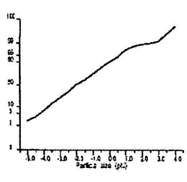

Results summary

Textural size classes
Gravel= 73.04% Sand= 26.63% Silt= 0.00% Clay= 0.00%
Gravel bearing detrital sediment
Sandy Gravel

Moment method parameters (phi)
Mean= -1.89 Sorting= 1.49 Skewness= 0.23 Kurtosis= 3.31

Graphical method parameters (phi)
Mean= -1.91 Sorting= 1.49 Skewness= 0.03 Kurtosis= 1.00
Median= -1.94 C= -5.28 D35= -2.49 D65= -1.33

Textural description:
Poorly sorted, Near symmetrical, Mesokurtic

Raw data summary

Size (phi)	Size (mm)	Cumulative weight (g)	Interval frequency (%)	Cumulative frequency (%)
-5.00	32.0000	55.50	2.09	2.09
-4.50	22.6274	99.60	1.66	3.75
-4.00	16.0000	184.10	3.18	6.94
-3.50	11.3137	371.80	7.07	14.01
-3.00	8.0000	606.60	8.85	22.86
-2.50	5.6569	922.40	11.90	34.76
-2.00	4.0000	1287.70	13.77	48.53
-1.50	2.8284	1617.80	12.43	60.97
-1.00	2.0000	1938.10	12.08	73.04
-0.50	1.4142	2193.80	9.64	82.68
0.00	1.0000	2381.30	7.07	89.75
0.50	0.7071	2502.40	4.56	94.31
1.00	0.5000	2581.50	2.98	97.29
1.50	0.3536	2608.80	1.03	98.32
2.00	0.2500	2621.90	0.49	98.82
2.50	0.1768	2627.90	0.23	99.04
3.00	0.1250	2632.40	0.17	99.21
3.50	0.0884	2638.40	0.23	99.44
4.00	0.0625	2644.80	0.24	99.68

Total weight = 2653.30 g

University of Waikato
Rapid Sediment Analyser
Operating System Version 7.1

PARTICLE SIZE ANALYSIS
Earth Sciences - University of Waikato

Sample: rt c/6

Size distribution histogram

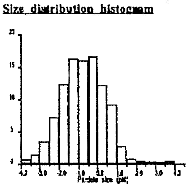

Cumulative frequency

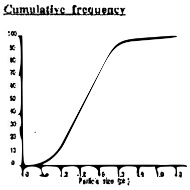

Cumulative frequency

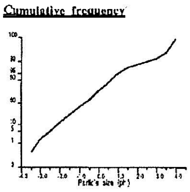

Results summary

Textural size classes
Gravel= 41.13% Sand= 58.75% Silt= 0.00% Clay= 0.00%
Gravel bearing detrital sediment
Sandy Gravel

Moment method parameters (phi)
Mean= -0.72 Sorting= 1.15 Skewness= 0.25 Kurtosis= 3.89

Graphical method parameters (phi)
Mean= -0.72 Sorting= 1.11 Skewness= -0.02 Kurtosis= 0.94
Median= -0.72 C= -3.34 D35= -1.19 D65= -0.26

Textural description:
Poorly sorted, Near symmetrical, Mesokurtic

Raw data summary

Size (phi)	Size (mm)	Cumulative weight (g)	Interval frequency (%)	Cumulative frequency (%)
-3.50	11.3137	2.40	0.58	0.58
-3.00	8.0000	7.90	1.33	1.91
-2.50	5.6569	22.10	3.43	5.33
-2.00	4.0000	52.30	7.29	12.62
-1.50	2.8284	103.30	12.31	24.93
-1.00	2.0000	170.40	16.20	41.13
-0.50	1.4142	238.70	16.00	57.13
0.00	1.0000	305.60	16.63	73.76
0.50	0.7071	356.30	12.24	88.00
1.00	0.5000	394.10	9.12	95.12
1.50	0.3536	405.20	2.68	97.80
2.00	0.2500	408.20	0.72	98.53
2.50	0.1768	410.30	0.51	99.03
3.00	0.1250	411.10	0.19	99.23
3.50	0.0884	411.90	0.19	99.42
4.00	0.0625	413.80	0.46	99.88

Total weight = 414.30 g

University of Waikato
Rapid Sediment Analyser
Operating System Version 7.1

PARTICLE SIZE ANALYSIS
Earth Sciences - University of Waikato

Sample: rt c/7

Size distribution histogram

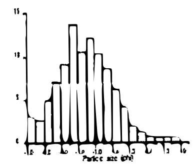

Cumulative frequency

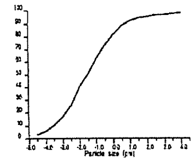

Cumulative frequency

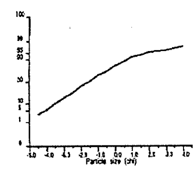

Results summary

Textural size classes
Gravel= 63.11% Sand= 34.90% Silt= 0.00% Clay= 0.00%
Gravel bearing detrital sediment
Sandy Gravel

Moment method parameters (phi)
Mean= -1.50 Sorting= 1.61 Skewness= 0.34 Kurtosis= 3.36

Graphical method parameters (phi)
Mean= -1.50 Sorting= 1.72 Skewness= 0.08 Kurtosis= 1.11
Median= -1.55 C= -4.84 D35= -2.20 D65= -0.91

Textural description:
Poorly sorted, Near symmetrical, Mesokurtic

Raw data summary

Size (phi)	Size (mm)	Cumulative weight (g)	Interval frequency (%)	Cumulative frequency (%)
-4.50	22.6274	59.10	3.11	3.11
-4.00	16.0000	108.70	2.61	5.73
-3.50	11.3137	200.40	4.83	10.56
-3.00	8.0000	334.90	7.09	17.65
-2.50	5.6569	507.70	9.10	26.75
-2.00	4.0000	768.10	13.72	40.47
-1.50	2.8284	967.70	10.52	50.99
-1.00	2.0000	1197.70	12.12	63.11
-0.50	1.4142	1394.10	10.35	73.45
0.00	1.0000	1556.40	8.55	82.01
0.50	0.7071	1673.20	6.15	88.16
1.00	0.5000	1753.80	4.24	92.40
1.50	0.3536	1790.40	1.94	94.34
2.00	0.2500	1813.10	1.20	95.53
2.50	0.1768	1826.00	0.68	96.21
3.00	0.1250	1835.80	0.52	96.73
3.50	0.0884	1846.80	0.58	97.31
4.00	0.0625	1860.00	0.70	98.00

Total weight = 1897.90 g

University of Waikato
Rapid Sediment Analyser
Operating System Version 7.1

PARTICLE SIZE ANALYSIS
Earth Sciences - University of Waikato

Sample: rt c/8

Size distribution histogram

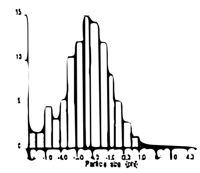

Cumulative frequency

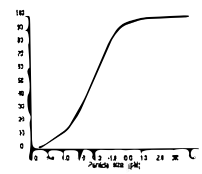

Cumulative frequency

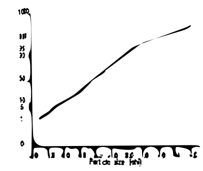

Results summary

Textural size classes
Gravel= 80.75% Sand= 18.79% Silt= 0.00% Clay= 0.00%
Gravel bearing detrital sediment
Gravel

Moment method parameters (phi)
Mean= -2.22 Sorting= 1.47 Skewness= -0.06 Kurtosis= 3.37

Graphical method parameters (phi)
Mean= -2.20 Sorting= 1.46 Skewness= -0.06 Kurtosis= 1.08
Median= -2.16 C= -5.73 D35= -2.70 D65= -1.64

Textural description:
Poorly sorted, Near symmetrical, Mesokurtic

Raw data summary

Size (phi)	Size (mm)	Cumulative weight (g)	Interval frequency (%)	Cumulative frequency (%)
-5.50	45.2548	53.90	1.88	1.88
-5.00	32.0000	106.70	1.84	3.73
-4.50	22.6274	242.20	4.73	8.46
-4.00	16.0000	340.30	3.43	11.89
-3.50	11.3137	500.00	5.58	17.46
-3.00	8.0000	795.50	10.32	27.79
-2.50	5.6569	1138.10	11.97	39.75
-2.00	4.0000	1565.80	14.93	54.68
-1.50	2.8284	1970.90	14.16	68.84
-1.00	2.0000	2311.90	11.91	80.75
-0.50	1.4142	2547.30	8.22	88.97
0.00	1.0000	2697.80	5.26	94.23
0.50	0.7071	2782.40	2.95	97.18
1.00	0.5000	2819.00	1.28	98.46
1.50	0.3536	2830.20	0.39	98.85
2.00	0.2500	2836.60	0.22	99.08
2.50	0.1768	2840.70	0.14	99.22
3.00	0.1250	2844.10	0.12	99.34
3.50	0.0884	2846.20	0.07	99.41
4.00	0.0625	2850.00	0.13	99.55

Total weight = 2863.00 g

University of Waikato
Rapid Sediment Analyser
Operating System Version 7.1

PARTICLE SIZE ANALYSIS
Earth Sciences - University of Waikato

Sample: rt b/1

Size distribution histogram

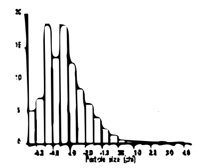

Cumulative frequency

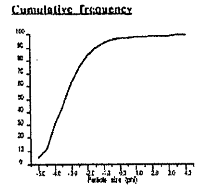

Cumulative frequency

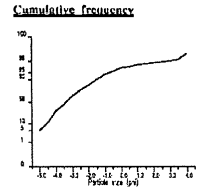

Results summary

Textural size classes
Gravel= 93.63% Sand= 6.83% Silt= 0.00% Clay= 0.00%
Gravel bearing detrital sediment
Gravel

Moment method parameters (phi)
Mean= -3.16 Sorting= 1.34 Skewness= 1.21 Kurtosis= 6.08

Graphical method parameters (phi)
Mean= -3.22 Sorting= 1.27 Skewness= 0.18 Kurtosis= 1.06
Median= -3.33 C= -5.00 D35= -3.83 D65= -2.89

Textural description:
Poorly sorted, Fine skewed, Mesokurtic

Raw data summary

Size (phi)	Size (mm)	Cumulative weight (g)	Interval frequency (%)	Cumulative frequency (%)
-5.00	32.0000	141.40	5.16	5.16
-4.50	22.6274	333.40	7.01	12.17
-4.00	16.0000	838.00	18.34	30.51
-3.50	11.3137	1202.10	13.36	43.87
-3.00	8.0000	1704.60	18.34	62.20
-2.50	5.6569	2045.90	12.45	74.66
-2.00	4.0000	2281.30	8.59	83.25
-1.50	2.8284	2452.40	6.24	89.49
-1.00	2.0000	2563.00	4.04	93.53
-0.50	1.4142	2626.10	2.30	95.83
0.00	1.0000	2662.50	1.33	97.16
0.50	0.7071	2679.70	0.63	97.79
1.00	0.5000	2691.00	0.41	98.20
1.50	0.3536	2697.40	0.23	98.43
2.00	0.2500	2702.80	0.20	98.63
2.50	0.1768	2707.80	0.18	98.81
3.00	0.1250	2712.80	0.19	99.00
3.50	0.0884	2716.80	0.14	99.14
4.00	0.0625	2722.80	0.23	99.36

Total weight = 2740.30 g

University of Waikato
Rapid Sediment Analyser
Operating System Version 7.1

PARTICLE SIZE ANALYSIS
Earth Sciences - University of Waikato

Sample: rt b/2

Size distribution histogram

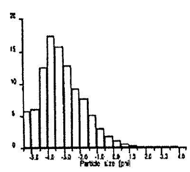

Cumulative frequency

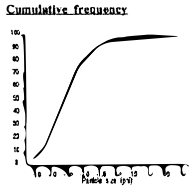

Cumulative frequency

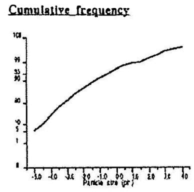

Results summary

Textural size classes
Gravel= 92.23% Sand= 7.40% Silt= 0.00% Clay= 0.00%
Gravel bearing detrital sediment
Gravel

Moment method parameters (phi)
Mean= -3.04 Sorting= 1.35 Skewness= 0.80 Kurtosis= 4.22

Graphical method parameters (phi)
Mean= -3.09 Sorting= 1.34 Skewness= 0.18 Kurtosis= 1.06
Median= -3.23 C= -5.41 D35= -3.69 D66= -2.70

Textural description:
Poorly sorted, Fine skewed, Mesokurtic

Raw data summary

Size (phi)	Size (mm)	Cumulative weight (g)	Interval frequency (%)	Cumulative frequency (%)
-5.00	32.0000	80.90	5.78	5.78
-4.50	22.6274	164.60	5.98	11.76
-4.00	16.0000	339.10	12.47	24.23
-3.50	11.3137	582.00	17.35	41.58
-3.00	8.0000	801.50	15.68	57.27
-2.50	5.6569	980.90	12.82	70.08
-2.00	4.0000	1110.10	9.23	79.32
-1.50	2.8284	1218.40	7.74	87.05
-1.00	2.0000	1290.80	5.17	92.23
-0.50	1.4142	1333.70	3.07	95.29
0.00	1.0000	1360.70	1.93	97.22
0.50	0.7071	1375.40	1.05	98.27
1.00	0.5000	1383.50	0.58	98.85
1.50	0.3536	1387.10	0.26	99.11
2.00	0.2500	1389.40	0.16	99.27
2.50	0.1768	1391.00	0.11	99.39
3.00	0.1250	1392.30	0.09	99.48
3.50	0.0884	1393.20	0.06	99.54
4.00	0.0625	1394.40	0.09	99.63

Total weight = 1399.60 g

University of Waikato
Rapid Sediment Analyser
Operating System Version 7.1

PARTICLE SIZE ANALYSIS
Earth Sciences - University of Waikato

Sample: rt b/3

Size distribution histogram

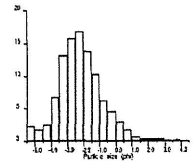

Cumulative frequency

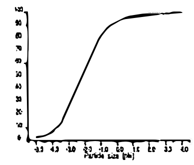

Cumulative frequency

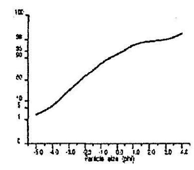

Results summary

Textural size classes
Gravel= 82.44% Sand= 16.88% Silt= 0.00% Clay= 0.00%
Gravel bearing detrital sediment
Gravel

Moment method parameters (phi)
Mean= -2.15 Sorting= 1.35 Skewness= 0.44 Kurtosis= 4.05

Graphical method parameters (phi)
Mean= -2.17 Sorting= 1.32 Skewness= 0.11 Kurtosis= 1.12
Median= -2.25 C= -5.28 D35= -2.72 D65= -1.76
Textural description:
Poorly sorted, Fine skewed, Leptokurtic

Raw data summary

Size (phi)	Size (mm)	Cumulative weight (g)	Interval frequency (%)	Cumulative frequency (%)
-6.00	32.0000	22.30	2.22	2.22
-4.50	22.6274	38.30	1.59	3.82
-4.00	18.0000	62.90	2.45	6.27
-3.50	11.3137	130.40	6.73	13.00
-3.00	8.0000	261.90	13.11	26.10
-2.50	5.6569	418.60	15.62	41.72
-2.00	4.0000	586.30	16.71	58.44
-1.50	2.8284	723.90	13.71	72.15
-1.00	2.0000	827.10	10.29	82.44
-0.50	1.4142	890.10	8.28	88.72
0.00	1.0000	935.30	4.51	93.22
0.50	0.7071	963.20	2.78	96.00
1.00	0.5000	979.80	1.65	97.66
1.50	0.3536	985.90	0.61	98.27
2.00	0.2500	989.70	0.38	98.64
2.50	0.1768	991.70	0.20	98.84
3.00	0.1250	993.90	0.22	99.06
3.50	0.0884	995.30	0.14	99.20
4.00	0.0625	996.50	0.12	99.32

Total weight = 1003.30 g

University of Waikato
Rapid Sediment Analyser
Operating System Version 7.1

PARTICLE SIZE ANALYSIS
Earth Sciences - University of Waikato

Sample: rt b/4

Size distribution histogram

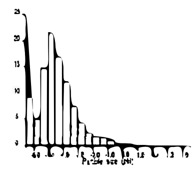

Cumulative frequency

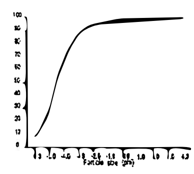

Cumulative frequency

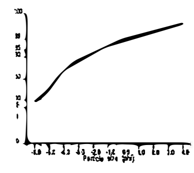

Results summary

Textural size classes
Gravel= 97.43% Sand= 2.21% Silt= 0.00% Clay= 0.00%
Gravel bearing detrital sediment
Gravel

Moment method parameters (phi)
Mean= -4.32 Sorting= 1.29 Skewness= 1.20 Kurtosis= 6.19

Graphical method parameters (phi)
Mean= -4.40 Sorting= 1.23 Skewness= 0.20 Kurtosis= 1.27
Median= -4.52 C= -6.45 D35= -4.88 D65= -4.08
Textural description:
Poorly sorted, Fine skewed, Leptokurtic

Raw data summary

Size (phi)	Size (mm)	Cumulative weight (g)	Interval frequency (%)	Cumulative frequency (%)
-6.00	64.0000	210.80	9.22	9.22
-5.50	45.2548	323.90	4.95	14.17
-5.00	32.0000	662.00	14.80	28.97
-4.50	22.6274	1159.90	21.79	50.76
-4.00	16.0000	1547.90	16.98	67.74
-3.50	11.3137	1826.20	12.18	79.91
-3.00	8.0000	1999.10	7.57	87.48
-2.50	5.6569	2095.20	4.21	91.69
-2.00	4.0000	2153.00	2.53	94.21
-1.50	2.8284	2194.30	1.81	96.02
-1.00	2.0000	2226.50	1.41	97.43
-0.50	1.4142	2247.40	0.91	98.35
0.00	1.0000	2258.20	0.47	98.82
0.50	0.7071	2263.80	0.25	99.06
1.00	0.5000	2268.30	0.20	99.26
1.50	0.3536	2270.60	0.11	99.37
2.00	0.2500	2272.40	0.07	99.44
2.50	0.1768	2273.70	0.06	99.50
3.00	0.1250	2275.10	0.06	99.56
3.50	0.0884	2276.00	0.04	99.60
4.00	0.0625	2276.90	0.04	99.64

Total weight = 2285.20 g

University of Waikato
Rapid Sediment Analyser
Operating System Version 7.1

PARTICLE SIZE ANALYSIS
Earth Sciences - University of Waikato

Sample: rt b/5

Size distribution histogram

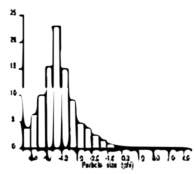

Cumulative frequency

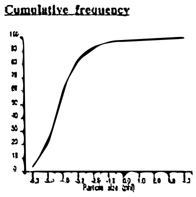

Cumulative frequency

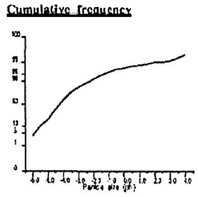

Results summary

Textural size classes
Gravel= 96.24% Sand= 3.15% Silt= 0.00% Clay= 0.00%
Gravel bearing detrital sediment
Gravel

Moment method parameters (phi)
Mean= -3.99 Sorting= 1.36 Skewness= 1.38 Kurtosis= 7.10

Graphical method parameters (phi)
Mean= -4.11 Sorting= 1.26 Skewness= 0.17 Kurtosis= 1.32
Median= -4.19 C= -6.38 D35= -4.52 D65= -3.80
Textural description:
Poorly sorted. Fine skewed, Leptokurtic

Raw data summary

Size (phi)	Size (mm)	Cumulative weight (g)	Interval frequency (%)	Cumulative frequency (%)
-6.00	64.0000	130.80	4.04	4.04
-5.50	45.2548	335.40	6.32	10.35
-5.00	32.0000	660.10	10.02	20.37
-4.50	22.6274	1156.20	15.37	35.75
-4.00	16.0000	1906.50	23.10	58.84
-3.50	11.3137	2395.00	15.08	73.92
-3.00	8.0000	2694.60	9.25	83.17
-2.50	5.6569	2852.90	4.89	88.06
-2.00	4.0000	2980.10	3.93	91.98
-1.50	2.8284	3065.20	2.63	94.61
-1.00	2.0000	3118.00	1.63	96.24
-0.50	1.4142	3148.00	0.93	97.16
0.00	1.0000	3167.40	0.60	97.76
0.50	0.7071	3180.40	0.40	98.16
1.00	0.5000	3191.70	0.35	98.51
1.50	0.3536	3198.70	0.22	98.73
2.00	0.2500	3204.50	0.18	98.91
2.50	0.1768	3209.10	0.14	99.05
3.00	0.1250	3213.60	0.14	99.19
3.50	0.0884	3216.40	0.09	99.27
4.00	0.0625	3220.10	0.11	99.39

Total weight = 3239.90 g

University of Waikato
Rapid Sediment Analyser
Operating System Version 7.1

PARTICLE SIZE ANALYSIS
Earth Sciences - University of Waikato

Sample: rt b/6

Size distribution histogram

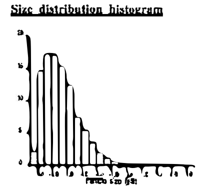

Cumulative frequency

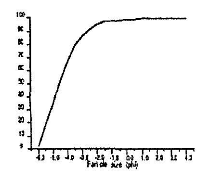

Cumulative frequency

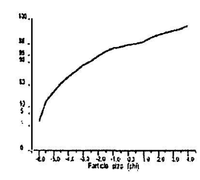

Results summary

Textural size classes
Gravel= 97.89% Sand= 1.80% Silt= 0.00% Clay= 0.00%
Gravel bearing detrital sediment
Gravel

Moment method parameters (phi)
Mean= -4.30 Sorting= 1.28 Skewness= 1.39 Kurtosis= 6.86

Graphical method parameters (phi)
Mean= -4.40 Sorting= 1.20 Skewness= 0.24 Kurtosis= 1.00
Median= -4.53 C= -6.26 D35= -4.97 D65= -4.04
Textural description:
Poorly sorted, Fine skewed, Mesokurtic

Raw data summary

Size (phi)	Size (mm)	Cumulative weight (g)	Interval frequency (%)	Cumulative frequency (%)
-6.00	64.0000	64.60	2.10	2.10
-5.50	45.2548	516.40	14.69	16.79
-5.00	32.0000	1045.20	17.20	33.99
-4.50	22.6274	1568.50	17.02	51.00
-4.00	16.0000	2035.50	15.19	66.19
-3.50	11.3137	2415.80	12.37	78.56
-3.00	8.0000	2642.80	7.38	85.94
-2.50	5.6569	2810.50	5.45	91.39
-2.00	4.0000	2917.00	3.46	94.86
-1.50	2.8284	2978.70	1.94	96.80
-1.00	2.0000	3010.40	1.10	97.89
-0.50	1.4142	3027.90	0.57	98.46
0.00	1.0000	3038.60	0.35	98.81
0.50	0.7071	3045.30	0.22	99.03
1.00	0.5000	3051.00	0.19	99.21
1.50	0.3536	3054.80	0.12	99.34
2.00	0.2500	3057.40	0.08	99.42
2.50	0.1768	3059.60	0.07	99.49
3.00	0.1250	3061.40	0.06	99.55
3.50	0.0884	3063.50	0.07	99.62
4.00	0.0625	3065.90	0.08	99.70

Total weight = 3075.20 g

University of Waikato
Rapid Sediment Analyser
Operating System Version 7.1

PARTICLE SIZE ANALYSIS

Earth Sciences - University of Waikato

Sample: rt b/7

Size distribution histogram

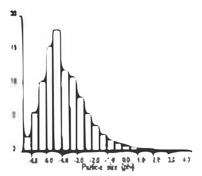

Cumulative frequency

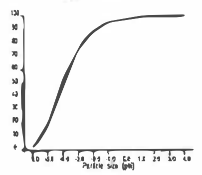

Cumulative frequency

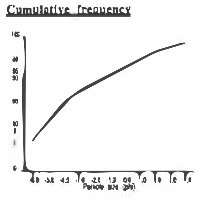

Results summary

Textural size classes

Gravel= 94.78% Sand= 4.98% Silt= 0.00% Clay= 0.00%

Gravel bearing detrital sediment

Gravel

Moment method parameters (phi)

Mean= -3.76 Sorting= 1.47 Skewness= 1.07 Kurtosis= 4.82

Graphical method parameters (phi)

Mean= -3.66 Sorting= 1.41 Skewness= 0.26 Kurtosis= 1.11

Median= -4.05 C= -6.27 D35= -4.47 D65= -3.45

Textural description:

Poorly sorted, Fine skewed, Mesokurtic

Raw data summary

Size (phi)	Size (mm)	Cumulative weight (g)	Interval frequency (%)	Cumulative frequency (%)
-6.00	64.0000	50.80	2.17	2.17
-5.50	45.2548	184.60	5.72	7.89
-5.00	32.0000	429.10	10.45	18.33
-4.50	22.6274	792.60	15.53	33.87
-4.00	16.0000	1215.10	18.05	51.92
-3.50	11.3137	1495.90	12.00	63.92
-3.00	8.0000	1755.80	11.10	75.02
-2.50	5.6569	1942.50	7.98	83.00
-2.00	4.0000	2071.30	5.50	88.50
-1.50	2.8284	2159.50	3.77	92.27
-1.00	2.0000	2218.30	2.51	94.78
-0.50	1.4142	2256.30	1.62	96.41
0.00	1.0000	2282.70	1.13	97.53
0.50	0.7071	2301.20	0.79	98.33
1.00	0.5000	2315.50	0.61	98.94
1.50	0.3536	2322.90	0.32	99.25
2.00	0.2500	2327.40	0.19	99.44
2.50	0.1768	2330.40	0.13	99.57
3.00	0.1250	2331.90	0.06	99.64
3.50	0.0884	2333.10	0.05	99.69
4.00	0.0625	2334.90	0.08	99.76

Total weight = 2340.40 g

University of Waikato
Rapid Sediment Analyser
Operating System Version 7.1

PARTICLE SIZE ANALYSIS

Earth Sciences - University of Waikato

Sample: rt b/8

Size distribution histogram

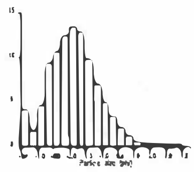

Cumulative frequency

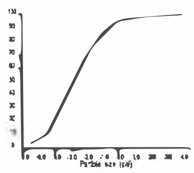

Cumulative frequency

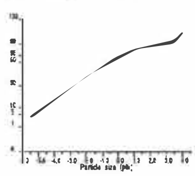

Results summary

Textural size classes

Gravel= 86.18% Sand= 13.30% Silt= 0.00% Clay= 0.00%

Gravel bearing detrital sediment

Gravel

Moment method parameters (phi)

Mean= -2.67 Sorting= 1.58 Skewness= 0.48 Kurtosis= 3.87

Graphical method parameters (phi)

Mean= -2.70 Sorting= 1.58 Skewness= 0.05 Kurtosis= 1.08

Median= -2.74 C= -5.88 D35= -3.32 D65= -2.16

Textural description:

Poorly sorted, Near symmetrical, Mesokurtic

Raw data summary

Size (phi)	Size (mm)	Cumulative weight (g)	Interval frequency (%)	Cumulative frequency (%)
-5.50	45.2548	89.20	4.24	4.24
-5.00	32.0000	127.20	1.80	6.04
-4.50	22.6274	223.80	4.59	10.63
-4.00	16.0000	420.10	9.32	19.95
-3.50	11.3137	643.30	10.60	30.55
-3.00	8.0000	904.80	12.42	42.98
-2.50	5.6569	1187.10	13.40	56.37
-2.00	4.0000	1458.40	12.88	69.25
-1.50	2.8284	1665.90	9.85	79.10
-1.00	2.0000	1815.00	7.08	86.18
-0.50	1.4142	1920.40	5.00	91.19
0.00	1.0000	1990.20	3.31	94.50
0.50	0.7071	2034.10	2.08	96.59
1.00	0.5000	2060.40	1.25	97.83
1.50	0.3536	2070.80	0.49	98.33
2.00	0.2500	2077.10	0.30	98.63
2.50	0.1768	2081.20	0.19	98.82
3.00	0.1250	2084.90	0.18	99.00
3.50	0.0884	2087.80	0.14	99.14
4.00	0.0625	2095.00	0.34	99.48

Total weight = 2106.00 g

University of Waikato
Rapid Sediment Analyser
Operating System Version 7.1

PARTICLE SIZE ANALYSIS

Earth Sciences - University of Waikato

Sample: 4/a

Size distribution histogram

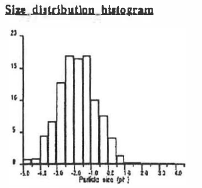

Cumulative frequency

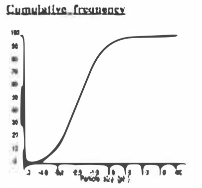

Cumulative frequency

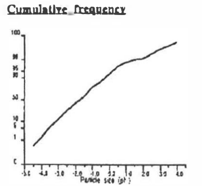

Results summary

Textural size classes

Gravel= 75.63% Sand= 24.08% Silt= 0.00% Clay= 0.00%

Gravel bearing detrital sediment

Sandy Gravel

Moment method parameters (phi)

Mean= -1.73 Sorting= 1.16 Skewness= 0.35 Kurtosis= 3.91

Graphical method parameters (phi)

Mean= -1.74 Sorting= 1.16 Skewness= 0.04 Kurtosis= 1.06

Median= -1.77 C= -4.35 D35= -2.22 D65= -1.32

Textural description:

Poorly sorted, Near symmetrical, Mesokurtic

Raw data summary

Size (phi)	Size (mm)	Cumulative weight (g)	Interval frequency (%)	Cumulative frequency (%)
-4.50	22.6274	6.80	0.71	0.71
-4.00	16.0000	15.90	0.95	1.66
-3.50	11.3137	57.80	4.38	6.03
-3.00	8.0000	121.80	6.68	12.69
-2.50	5.6569	243.80	12.71	25.40
-2.00	4.0000	406.10	16.91	42.31
-1.50	2.8284	564.40	16.49	58.80
-1.00	2.0000	726.00	16.84	75.63
-0.50	1.4142	822.40	10.04	85.68
0.00	1.0000	895.20	7.58	93.26
0.50	0.7071	933.40	3.98	97.24
1.00	0.5000	946.20	1.33	98.57
1.50	0.3536	949.70	0.36	98.94
2.00	0.2500	951.90	0.23	99.17
2.50	0.1768	953.50	0.17	99.33
3.00	0.1250	954.90	0.15	99.48
3.50	0.0884	956.00	0.11	99.59
4.00	0.0625	957.10	0.11	99.71

Total weight = 959.90 g

University of Waikato
Rapid Sediment Analyser
Operating System Version 7.1

PARTICLE SIZE ANALYSIS

Earth Sciences - University of Waikato

Sample: 4/b

Size distribution histogram

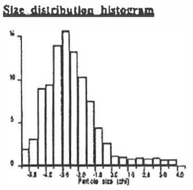

Cumulative frequency

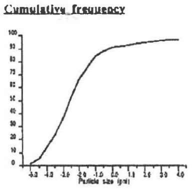

Cumulative frequency

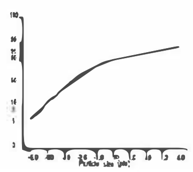

Results summary

Textural size classes

Gravel= 83.99% Sand= 13.88% Silt= 0.00% Clay= 0.00%

Gravel bearing detrital sediment

Gravel

Moment method parameters (phi)

Mean= -2.35 Sorting= 1.62 Skewness= 1.13 Kurtosis= 5.19

Graphical method parameters (phi)

Mean= -2.50 Sorting= 1.73 Skewness= 0.26 Kurtosis= 1.45

Median= -2.60 C= -6.00 D35= -3.08 D65= -2.04

Textural description:

Poorly sorted, Fine skewed, Leptokurtic

Raw data summary

Size (phi)	Size (mm)	Cumulative weight (g)	Interval frequency (%)	Cumulative frequency (%)
-5.00	32.0000	28.00	1.94	1.94
-4.50	22.6274	72.90	3.11	5.05
-4.00	16.0000	201.90	8.93	13.97
-3.50	11.3137	338.50	9.45	23.43
-3.00	8.0000	539.50	13.91	37.34
-2.50	5.6569	765.50	15.64	52.98
-2.00	4.0000	956.20	13.20	66.18
-1.50	2.8284	1105.90	10.36	76.54
-1.00	2.0000	1213.60	7.45	83.99
-0.50	1.4142	1277.60	4.43	88.42
0.00	1.0000	1315.70	2.64	91.06
0.50	0.7071	1332.10	1.14	92.19
1.00	0.5000	1346.20	0.98	93.17
1.50	0.3536	1358.00	0.82	93.99
2.00	0.2500	1370.20	0.84	94.83
2.50	0.1768	1381.70	0.80	95.63
3.00	0.1250	1394.40	0.88	96.50
3.50	0.0884	1404.20	0.68	97.18
4.00	0.0625	1414.10	0.69	97.87

Total weight = 1444.90 g

University of Waikato
Rapid Sediment Analyser
Operating System Version 7.1

PARTICLE SIZE ANALYSIS

Earth Sciences - University of Waikato

Sample: 4/c

Size distribution histogram

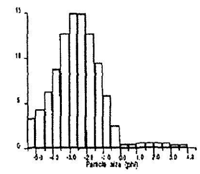

Results summary

Textural size classes
Gravel= 86.97% Sand= 12.22% Silt= 0.00% Clay= 0.00%
Gravel bearing detrital sediment
Gravel

Moment method parameters (phi)
Mean= -2.43 Sorting= 1.49 Skewness= 0.81 Kurtosis= 5.06

Graphical method parameters (phi)
Mean= -2.51 Sorting= 1.40 Skewness= 0.01 Kurtosis= 1.08
Median= -2.50 C= -5.00 D35= -3.00 D65= -2.00

Textural description:
Poorly sorted, Near symmetrical, Mesokurtic

Cumulative frequency

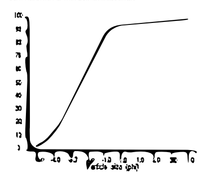

Cumulative frequency

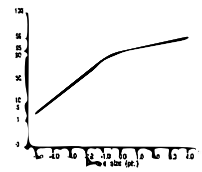

Raw data summary

Size (phi)	Size (mm)	Cumulative weight (g)	Interval frequency (%)	Cumulative frequency (%)
-5.00	32.0000	28.90	3.25	3.26
-4.50	22.6274	63.00	4.36	7.61
-4.00	16.0000	114.00	6.16	13.77
-3.50	11.3137	186.10	8.71	22.49
-3.00	8.0000	290.40	12.60	35.09
-2.50	5.6569	413.50	14.87	49.96
-2.00	4.0000	536.90	14.91	64.87
-1.50	2.8284	641.60	12.84	77.51
-1.00	2.0000	719.80	9.46	86.97
-0.50	1.4142	767.30	5.74	92.71
0.00	1.0000	788.00	2.50	95.22
0.50	0.7071	791.40	0.41	95.63
1.00	0.5000	795.40	0.46	96.11
1.50	0.3536	800.40	0.60	96.71
2.00	0.2500	805.40	0.60	97.32
2.50	0.1768	810.40	0.60	97.92
3.00	0.1250	815.10	0.57	98.49
3.50	0.0884	818.00	0.35	98.84
4.00	0.0625	820.90	0.35	99.19

Total weight = 827.60 g

University of Waikato
Rapid Sediment Analyser
Operating System Version 7.1

PARTICLE SIZE ANALYSIS

Earth Sciences - University of Waikato

Sample: 4/d

Size distribution histogram

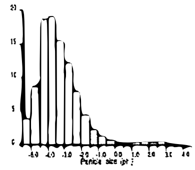

Results summary

Textural size classes
Gravel= 93.08% Sand= 5.74% Silt= 0.00% Clay= 0.00%
Gravel bearing detrital sediment
Gravel

Moment method parameters (phi)
Mean= -3.20 Sorting= 1.45 Skewness= 1.87 Kurtosis= 8.36

Graphical method parameters (phi)
Mean= -3.35 Sorting= 1.30 Skewness= 0.31 Kurtosis= 1.29
Median= -3.51 C= -5.00 D35= -3.90 D65= -3.03

Textural description:
Poorly sorted, Strongly fine skewed, Leptokurtic

Cumulative frequency

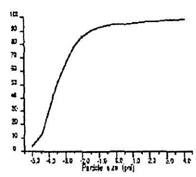

Cumulative frequency

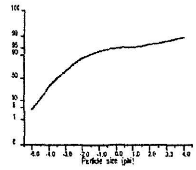

Raw data summary

Size (phi)	Size (mm)	Cumulative weight (g)	Interval frequency (%)	Cumulative frequency (%)
-5.00	32.0000	40.00	3.90	3.90
-4.50	22.6274	126.50	8.63	12.53
-4.00	16.0000	319.90	18.67	31.20
-3.50	11.3137	517.00	19.22	50.42
-3.00	8.0000	675.80	15.49	65.91
-2.50	5.6569	801.60	12.27	78.17
-2.00	4.0000	883.30	7.97	86.14
-1.50	2.8284	929.20	4.48	90.62
-1.00	2.0000	954.40	2.46	93.08
-0.50	1.4142	966.00	1.33	94.40
0.00	1.0000	976.00	0.78	95.18
0.50	0.7071	979.00	0.29	95.47
1.00	0.5000	983.20	0.41	95.88
1.50	0.3536	988.60	0.53	96.41
2.00	0.2500	994.50	0.58	96.99
2.50	0.1768	999.70	0.51	97.49
3.00	0.1250	1005.30	0.55	98.04
3.50	0.0884	1009.40	0.40	98.44
4.00	0.0625	1013.30	0.38	98.82

Total weight = 1025.40 g

University of Waikato
Rapid Sediment Analyser
Operating System Version 7.1

PARTICLE SIZE ANALYSIS

Earth Sciences - University of Waikato

Sample: 4/c

Size distribution histogram

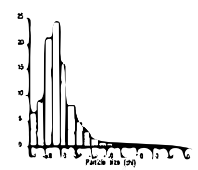

Results summary

Textural size classes
Gravel= 96.42% Sand= 3.18% Silt= 0.00% Clay= 0.00%
Gravel bearing detrital sediment
Gravel

Moment method parameters (phi)
Mean= -4.00 Sorting= 1.28 Skewness= 2.10 Kurtosis= 10.37

Graphical method parameters (phi)
Mean= -4.11 Sorting= 1.05 Skewness= 0.27 Kurtosis= 1.33
Median= -4.23 C= -5.50 D35= -4.54 D65= -3.89

Textural description:
Poorly sorted, Fine skewed, Leptokurtic

Cumulative frequency

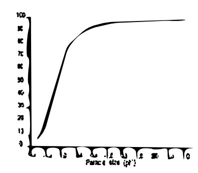

Cumulative frequency

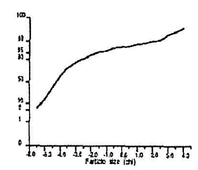

Raw data summary

Size (phi)	Size (mm)	Cumulative weight (g)	Interval frequency (%)	Cumulative frequency (%)
-5.50	45.2548	45.80	6.55	6.55
-5.00	32.0000	107.40	8.81	15.37
-4.50	22.6274	256.90	21.39	36.76
-4.00	16.0000	428.90	24.61	61.37
-3.50	11.3137	543.40	16.38	77.75
-3.00	8.0000	599.90	8.08	85.83
-2.50	5.6569	634.00	4.88	90.71
-2.00	4.0000	655.60	3.09	93.80
-1.50	2.8284	667.30	1.67	95.48
-1.00	2.0000	673.90	0.94	96.42
-0.50	1.4142	678.60	0.67	97.10
0.00	1.0000	682.40	0.54	97.64
0.50	0.7071	684.20	0.26	97.90
1.00	0.5000	687.00	0.40	98.30
1.50	0.3536	689.60	0.37	98.67
2.00	0.2500	691.30	0.24	98.91
2.50	0.1768	692.80	0.21	99.13
3.00	0.1250	694.30	0.21	99.34
3.50	0.0884	695.10	0.11	99.46
4.00	0.0625	696.00	0.13	99.59

Total weight = 698.90 g

University of Waikato
Rapid Sediment Analyser
Operating System Version 7.1

PARTICLE SIZE ANALYSIS

Earth Sciences - University of Waikato

Sample: 4/f

Size distribution histogram

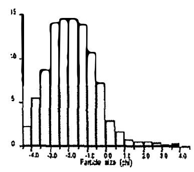

Results summary

Textural size classes
Gravel= 73.80% Sand= 25.57% Silt= 0.00% Clay= 0.00%
Gravel bearing detrital sediment
Sandy Gravel

Moment method parameters (phi)
Mean= -1.75 Sorting= 1.32 Skewness= 0.74 Kurtosis= 4.40

Graphical method parameters (phi)
Mean= -1.80 Sorting= 1.28 Skewness= 0.08 Kurtosis= 1.01
Median= -1.84 C= -4.00 D35= -2.35 D65= -1.32

Textural description:
Poorly sorted, Near symmetrical, Mesokurtic

Cumulative frequency

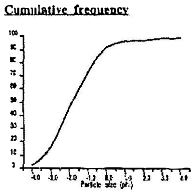

Cumulative frequency

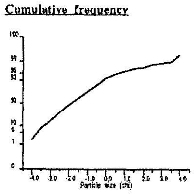

Raw data summary

Size (phi)	Size (mm)	Cumulative weight (g)	Interval frequency (%)	Cumulative frequency (%)
-4.00	16.0000	13.30	2.27	2.27
-3.50	11.3137	45.20	5.44	7.71
-3.00	8.0000	96.60	8.77	16.48
-2.50	5.6569	179.30	14.11	30.58
-2.00	4.0000	265.40	14.69	45.27
-1.50	2.8284	350.80	14.57	59.83
-1.00	2.0000	432.70	13.97	73.80
-0.50	1.4142	495.90	10.78	84.58
0.00	1.0000	538.20	7.21	91.80
0.50	0.7071	555.50	2.95	94.75
1.00	0.5000	565.40	1.69	96.44
1.50	0.3536	569.90	0.77	97.20
2.00	0.2500	573.20	0.56	97.77
2.50	0.1768	576.20	0.51	98.28
3.00	0.1250	578.90	0.46	98.74
3.50	0.0884	580.70	0.31	99.04
4.00	0.0625	582.60	0.32	99.37

Total weight = 586.30 g

University of Waikato
Rapid Sediment Analyser
Operating System Version 7.1

PARTICLE SIZE ANALYSIS
Earth Sciences - University of Waikato

Sample: # 22/a

Size distribution histogram

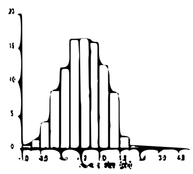

Cumulative frequency

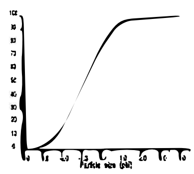

Cumulative frequency

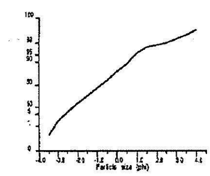

Results summary

Textural size classes
Gravel= 43.09% Sand= 56.48% Silt= 0.00% Clay= 0.00%
Gravel bearing detrital sediment
Sandy Gravel

Moment method parameters (phi)
Mean= -0.80 Sorting= 1.11 Skewness= 0.09 Kurtosis= 3.26

Graphical method parameters (phi)
Mean= -0.80 Sorting= 1.11 Skewness= -0.03 Kurtosis= 0.93
Median= -0.79 C= -3.37 D35= -1.25 D65= -0.33

Textural description:
Poorly sorted, Near symmetrical, Mesokurtic

Raw data summary

Size (phi)	Size (mm)	Cumulative weight (g)	Interval frequency (%)	Cumulative frequency (%)
-3.50	11.3137	3.90	0.58	0.58
-3.00	8.0000	14.50	1.58	2.17
-2.50	5.6569	41.30	4.00	6.17
-2.00	4.0000	99.60	8.71	14.88
-1.50	2.8284	180.10	12.03	26.91
-1.00	2.0000	288.40	16.18	43.09
-0.50	1.4142	398.40	16.44	59.52
0.00	1.0000	504.80	15.87	75.39
0.50	0.7071	588.50	12.54	87.93
1.00	0.5000	645.00	8.44	96.37
1.50	0.3536	657.60	1.88	98.25
2.00	0.2500	660.90	0.49	98.74
2.50	0.1768	662.70	0.27	99.01
3.00	0.1250	664.40	0.25	99.27
3.50	0.0884	665.30	0.13	99.40
4.00	0.0625	666.40	0.16	99.57

Total weight = 669.30 g

University of Waikato
Rapid Sediment Analyser
Operating System Version 7.1

PARTICLE SIZE ANALYSIS
Earth Sciences - University of Waikato

Sample: # 22/b

Size distribution histogram

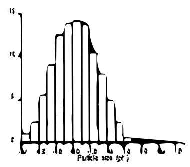

Cumulative frequency

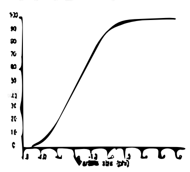

Cumulative frequency

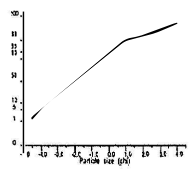

Results summary

Textural size classes
Gravel= 72.43% Sand= 27.18% Silt= 0.00% Clay= 0.00%
Gravel bearing detrital sediment
Sandy Gravel

Moment method parameters (phi)
Mean= -1.77 Sorting= 1.30 Skewness= 0.25 Kurtosis= 3.15

Graphical method parameters (phi)
Mean= -1.78 Sorting= 1.31 Skewness= 0.03 Kurtosis= 0.95
Median= -1.80 C= -4.49 D35= -2.34 D65= -1.27

Textural description:
Poorly sorted, Near symmetrical, Mesokurtic

Raw data summary

Size (phi)	Size (mm)	Cumulative weight (g)	Interval frequency (%)	Cumulative frequency (%)
-4.50	22.6274	6.10	0.96	0.96
-4.00	18.0000	21.10	2.36	3.32
-3.50	11.3137	56.60	5.58	8.90
-3.00	8.0000	114.30	9.07	17.97
-2.50	5.6569	193.80	12.50	30.47
-2.00	4.0000	282.70	13.98	44.44
-1.50	2.8284	373.10	14.21	68.65
-1.00	2.0000	460.70	13.77	72.43
-0.50	1.4142	527.60	10.52	82.94
0.00	1.0000	578.70	8.03	90.98
0.50	0.7071	610.20	4.95	95.93
1.00	0.5000	625.60	2.42	98.35
1.50	0.3536	628.80	0.50	98.85
2.00	0.2500	630.00	0.19	99.04
2.50	0.1768	831.10	0.17	99.21
3.00	0.1250	632.30	0.19	99.40
3.50	0.0884	833.10	0.13	99.53
4.00	0.0625	633.60	0.08	99.61

Total weight = 636.10 g

University of Waikato
Rapid Sediment Analyser
Operating System Version 7.1

PARTICLE SIZE ANALYSIS
Earth Sciences - University of Waikato

Sample: # 22/c

Size distribution histogram

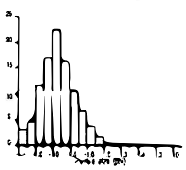

Cumulative frequency

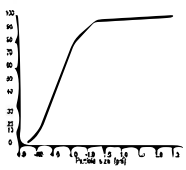

Cumulative frequency

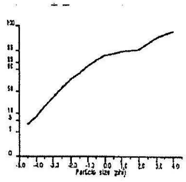

Results summary

Textural size classes
Gravel= 92.46% Sand= 7.30% Silt= 0.00% Clay= 0.00%
Gravel bearing detrital sediment
Gravel

Moment method parameters (phi)
Mean= -2.69 Sorting= 1.12 Skewness= 1.01 Kurtosis= 6.15

Graphical method parameters (phi)
Mean= -2.64 Sorting= 1.07 Skewness= 0.10 Kurtosis= 1.11
Median= -2.69 C= -4.84 D35= -3.04 D65= -2.31

Textural description:
Poorly sorted, Fine skewed, Leptokurtic

Raw data summary

Size (phi)	Size (mm)	Cumulative weight (g)	Interval frequency (%)	Cumulative frequency (%)
-4.50	22.6274	24.80	3.08	3.08
-4.00	16.0000	61.10	4.51	7.59
-3.50	11.3137	156.40	11.84	19.42
-3.00	8.0000	292.50	16.90	36.33
-2.50	5.6569	472.70	22.38	58.71
-2.00	4.0000	604.50	16.37	75.07
-1.50	2.8284	689.50	10.56	85.83
-1.00	2.0000	744.50	6.83	92.46
-0.50	1.4142	774.80	3.76	96.22
0.00	1.0000	788.60	1.71	97.94
0.50	0.7071	792.80	0.52	98.46
1.00	0.5000	795.40	0.32	98.78
1.50	0.3536	797.00	0.20	98.98
2.00	0.2500	796.50	0.19	99.17
2.50	0.1768	800.10	0.20	99.37
3.00	0.1250	801.60	0.19	99.55
3.50	0.0884	802.50	0.11	99.66
4.00	0.0625	803.30	0.10	99.76

Total weight = 805.20 g

University of Waikato
Rapid Sediment Analyser
Operating System Version 7.1

PARTICLE SIZE ANALYSIS
Earth Sciences - University of Waikato

Sample: # 22/d

Size distribution histogram

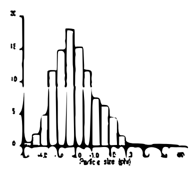

Cumulative frequency

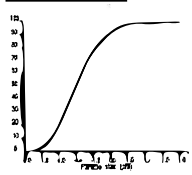

Cumulative frequency

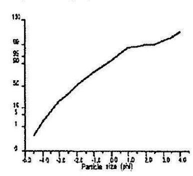

Results summary

Textural size classes
Gravel= 78.36% Sand= 21.18% Silt= 0.00% Clay= 0.00%
Gravel bearing detrital sediment
Sandy Gravel

Moment method parameters (phi)
Mean= -1.90 Sorting= 1.23 Skewness= 0.61 Kurtosis= 3.93

Graphical method parameters (phi)
Mean= -1.93 Sorting= 1.24 Skewness= 0.15 Kurtosis= 1.01
Median= -2.04 C= -4.38 D35= -2.45 D65= -1.56

Textural description:
Poorly sorted, Fine skewed, Mesokurtic

Raw data summary

Size (phi)	Size (mm)	Cumulative weight (g)	Interval frequency (%)	Cumulative frequency (%)
-4.50	22.6274	4.70	0.56	0.56
-4.00	16.0000	19.90	1.82	2.38
-3.50	11.3137	60.40	4.84	7.21
-3.00	8.0000	157.90	11.64	18.88
-2.50	5.8589	281.60	14.77	33.63
-2.00	4.0000	431.60	17.91	51.54
-1.50	2.8284	658.60	15.17	66.71
-1.00	2.0000	656.20	11.66	78.38
-0.50	1.4142	719.00	7.50	85.86
0.00	1.0000	772.20	6.35	92.21
0.50	0.7071	809.30	4.43	96.64
1.00	0.5000	823.30	1.67	98.32
1.50	0.3536	826.20	0.35	98.68
2.00	0.2500	828.30	0.25	98.91
2.50	0.1768	829.70	0.17	99.08
3.00	0.1250	831.20	0.18	99.26
3.50	0.0884	832.10	0.11	99.37
4.00	0.0625	833.60	0.18	99.55

Total weight = 837.40 g

University of Waikato
Rapid Sediment Analyser
Operating System Version 7.1

PARTICLE SIZE ANALYSIS

Earth Sciences - University of Waikato

Sample: # 22/c

Size distribution histogram

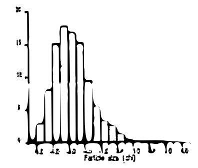

Cumulative frequency

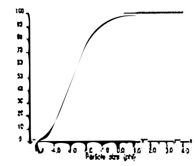

Cumulative frequency

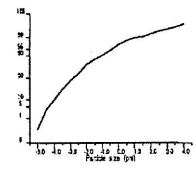

Results summary

Textural size classes
Gravel= 91.37% Sand= 8.21% Silt= 0.00% Clay= 0.00%
Gravel bearing detrital sediment
Gravel

Moment method parameters (phi)
Mean= -2.70 Sorting= 1.18 Skewness= 0.82 Kurtosis= 4.62

Graphical method parameters (phi)
Mean= -2.76 Sorting= 1.16 Skewness= 0.15 Kurtosis= 1.09
Median= -2.83 C= -4.92 D35= -3.26 D65= -2.37
Textural description:
Poorly sorted, Fine skewed, Mesokurtic

Raw data summary

Size (phi)	Size (mm)	Cumulative weight (g)	Interval frequency (%)	Cumulative frequency (%)
-5.00	32.0000	7.50	0.53	0.53
-4.50	22.6274	47.50	2.80	3.33
-4.00	16.0000	161.20	7.97	11.30
-3.50	11.3137	375.90	15.05	26.34
-3.00	8.0000	629.50	17.77	44.12
-2.50	5.6569	872.00	16.99	61.11
-2.00	4.0000	1090.70	15.33	76.44
-1.50	2.8284	1224.70	9.39	85.83
-1.00	2.0000	1303.60	5.54	91.37
-0.50	1.4142	1350.20	3.25	94.62
0.00	1.0000	1386.40	2.54	97.16
0.50	0.7071	1406.20	1.39	98.55
1.00	0.5000	1413.10	0.48	99.03
1.50	0.3536	1415.10	0.14	99.17
2.00	0.2500	1416.40	0.09	99.26
2.50	0.1768	1417.60	0.08	99.35
3.00	0.1250	1418.90	0.09	99.44
3.50	0.0884	1419.80	0.06	99.50
4.00	0.0625	1420.90	0.08	99.58

Total weight = 1426.90 g

University of Waikato
Rapid Sediment Analyser
Operating System Version 7.1

PARTICLE SIZE ANALYSIS

Earth Sciences - University of Waikato

Sample: # 22/f

Size distribution histogram

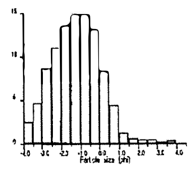

Cumulative frequency

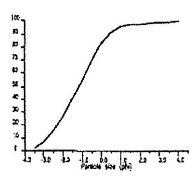

Cumulative frequency

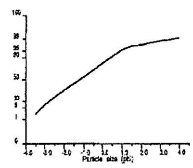

Results summary

Textural size classes
Gravel= 55.18% Sand= 44.01% Silt= 0.00% Clay= 0.00%
Gravel bearing detrital sediment
Sandy Gravel

Moment method parameters (phi)
Mean= -1.17 Sorting= 1.26 Skewness= 0.35 Kurtosis= 3.58

Graphical method parameters (phi)
Mean= -1.20 Sorting= 1.26 Skewness= -0.01 Kurtosis= 0.96
Median= -1.17 C= -3.80 D35= -1.89 D65= -0.67
Textural description:
Poorly sorted, Near symmetrical, Mesokurtic

Raw data summary

Size (phi)	Size (mm)	Cumulative weight (g)	Interval frequency (%)	Cumulative frequency (%)
-3.50	11.3137	10.10	2.48	2.48
-3.00	8.0000	29.00	4.65	7.13
-2.50	5.6569	63.60	8.56	15.69
-2.00	4.0000	108.50	10.99	26.68
-1.50	2.8284	163.90	13.62	40.30
-1.00	2.0000	224.40	14.88	55.18
-0.50	1.4142	284.90	14.88	70.05
0.00	1.0000	338.40	13.15	83.21
0.50	0.7071	371.90	8.24	91.44
1.00	0.5000	389.80	4.40	95.84
1.50	0.3536	394.90	1.25	97.10
2.00	0.2500	397.50	0.64	97.74
2.50	0.1768	399.30	0.44	98.18
3.00	0.1250	401.10	0.44	98.62
3.50	0.0884	402.00	0.22	98.84
4.00	0.0625	403.40	0.34	99.19

Total weight = 406.70 g

University of Waikato
Rapid Sediment Analyser
Operating System Version 7.1

PARTICLE SIZE ANALYSIS

Earth Sciences - University of Waikato

Sample: 34a/a

Size distribution histogram

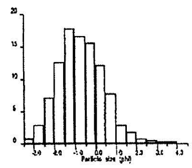

Cumulative frequency

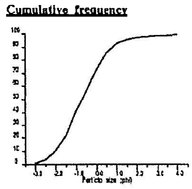

Cumulative frequency

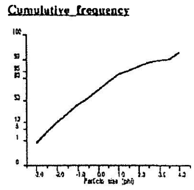

Results summary

Textural size classes
Gravel= 40.95% Sand= 58.42% Silt= 0.00% Clay= 0.00%
Gravel bearing detrital sediment
Sandy Gravel

Moment method parameters (phi)
Mean= -0.68 Sorting= 1.13 Skewness= 0.48 Kurtosis= 3.57

Graphical method parameters (phi)
Mean= -0.69 Sorting= 1.13 Skewness= 0.08 Kurtosis= 1.01
Median= -0.73 C= -2.97 D35= -1.17 D66= -0.26
Textural description:
Poorly sorted, Near symmetrical, Mesokurtic

Raw data summary

Size (phi)	Size (mm)	Cumulative weight (g)	Interval frequency (%)	Cumulative frequency (%)
-3.00	8.0000	3.30	0.83	0.83
-2.50	5.6568	14.80	2.88	3.71
-2.00	4.0000	42.80	7.01	10.72
-1.50	2.8284	92.70	12.50	23.22
-1.00	2.0000	163.50	17.74	40.96
-0.50	1.4142	229.60	16.56	57.52
0.00	1.0000	291.40	15.48	73.00
0.50	0.7071	339.70	12.10	85.10
1.00	0.5000	370.80	7.79	92.89
1.50	0.3536	382.30	2.88	95.77
2.00	0.2500	389.60	1.83	97.60
2.50	0.1768	392.50	0.73	98.32
3.00	0.1250	394.60	0.53	98.85
3.50	0.0884	395.60	0.25	99.10
4.00	0.0625	396.70	0.28	99.37

Total weight = 399.20 g

University of Waikato
Rapid Sediment Analyser
Operating System Version 7.1

PARTICLE SIZE ANALYSIS

Earth Sciences - University of Waikato

Sample: 34a/b

Size distribution histogram

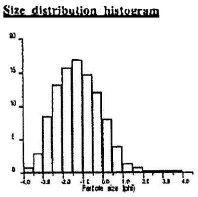

Cumulative frequency

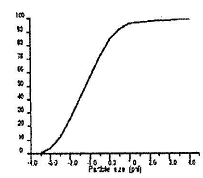

Cumulative frequency

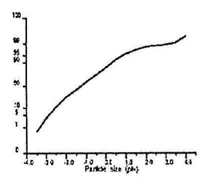

Results summary

Textural size classes
Gravel= 67.91% Sand= 41.47% Silt= 0.00% Clay= 0.00%
Gravel bearing detrital sediment
Sandy Gravel

Moment method parameters (phi)
Mean= -1.17 Sorting= 1.16 Skewness= 0.52 Kurtosis= 3.81

Graphical method parameters (phi)
Mean= -1.20 Sorting= 1.15 Skewness= 0.07 Kurtosis= 0.95
Median= -1.23 C= -3.46 D35= -1.69 D65= -0.76
Textural description:
Poorly sorted, Near symmetrical, Mesokurtic

Raw data summary

Size (phi)	Size (mm)	Cumulative weight (g)	Interval frequency (%)	Cumulative frequency (%)
-3.50	11.3137	3.60	0.75	0.75
-3.00	8.0000	17.60	2.96	3.71
-2.50	5.6569	58.30	8.43	12.14
-2.00	4.0000	121.40	13.13	25.27
-1.50	2.8284	196.70	15.67	40.95
-1.00	2.0000	278.20	16.97	57.91
-0.50	1.4142	348.60	14.66	72.56
0.00	1.0000	406.10	11.97	84.53
0.50	0.7071	444.30	7.95	92.49
1.00	0.5000	463.00	3.69	96.38
1.50	0.3536	469.30	1.31	97.69
2.00	0.2500	472.80	0.69	98.38
2.50	0.1768	474.00	0.29	98.67
3.00	0.1250	475.00	0.21	98.88
3.50	0.0884	476.20	0.25	99.13
4.00	0.0625	477.40	0.25	99.38

Total weight = 480.40 g

University of Waikato
Rapid Sediment Analyser
Operating System Version 7.1

PARTICLE SIZE ANALYSIS

Earth Sciences - University of Waikato

Sample: 34a/c

Size distribution histogram

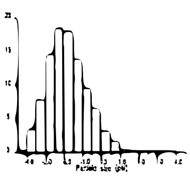

Cumulative frequency

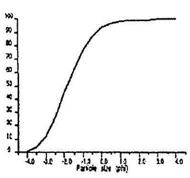

Cumulative frequency

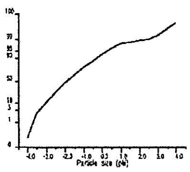

Results summary

Textural size classes
Gravel= 77.08% Sand= 22.58% Silt= 0.00% Clay= 0.00%
Gravel bearing detrital sediment
Sandy Gravel

Moment method parameters (phi)
Mean= -1.75 Sorting= 1.14 Skewness= 0.83 Kurtosis= 4.80

Graphical method parameters (phi)
Mean= -1.79 Sorting= 1.11 Skewness= 0.13 Kurtosis= 1.03
Median= -1.86 C= -3.91 D35= -2.27 D65= -1.44

Textural description:
Poorly sorted, Fine skewed, Mesokurtic

Raw data summary

Size (phi)	Size (mm)	Cumulative weight (g)	Interval frequency (%)	Cumulative frequency (%)
-4.00	16.0000	2.30	0.41	0.41
-3.50	11.3137	22.00	3.48	3.88
-3.00	8.0000	66.90	7.93	11.81
-2.50	5.6568	150.10	14.69	26.50
-2.00	4.0000	255.40	18.59	45.09
-1.50	2.8284	358.30	18.17	63.26
-1.00	2.0000	436.60	13.82	77.08
-0.50	1.4142	490.60	9.53	86.62
0.00	1.0000	528.60	6.71	93.33
0.50	0.7071	546.50	3.16	96.49
1.00	0.5000	555.60	1.61	98.09
1.50	0.3536	558.30	0.48	98.57
2.00	0.2500	559.70	0.25	98.82
2.50	0.1768	560.70	0.18	98.99
3.00	0.1250	562.10	0.25	99.24
3.50	0.0884	563.50	0.25	99.49
4.00	0.0525	564.50	0.18	99.66

Total weight = 566.40 g

University of Waikato
Rapid Sediment Analyser
Operating System Version 7.1

PARTICLE SIZE ANALYSIS

Earth Sciences - University of Waikato

Sample: 34a/d

Size distribution histogram

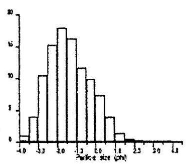

Cumulative frequency

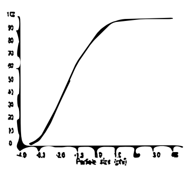

Cumulative frequency

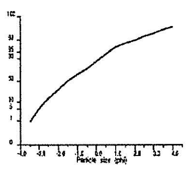

Results summary

Textural size classes
Gravel= 64.70% Sand= 34.88% Silt= 0.00% Clay= 0.00%
Gravel bearing detrital sediment
Sandy Gravel

Moment method parameters (phi)
Mean= -1.33 Sorting= 1.14 Skewness= 0.49 Kurtosis= 3.27

Graphical method parameters (phi)
Mean= -1.34 Sorting= 1.15 Skewness= 0.15 Kurtosis= 0.94
Median= -1.45 C= -3.50 D35= -1.87 D65= -0.99

Textural description:
Poorly sorted, Fine skewed, Mesokurtic

Raw data summary

Size (phi)	Size (mm)	Cumulative weight (g)	Interval frequency (%)	Cumulative frequency (%)
-3.50	11.3137	5.60	0.99	0.99
-3.00	8.0000	27.40	3.85	4.83
-2.50	5.6569	85.90	10.32	15.16
-2.00	4.0000	172.10	15.21	30.36
-1.50	2.8284	274.30	18.03	48.39
-1.00	2.0000	366.70	16.30	64.70
-0.50	1.4142	432.60	11.63	76.32
0.00	1.0000	488.00	9.77	86.10
0.50	0.7071	529.40	7.30	93.40
1.00	0.5000	551.10	3.83	97.23
1.50	0.3536	558.60	1.32	98.55
2.00	0.2500	561.30	0.48	99.03
2.50	0.1768	562.60	0.23	99.26
3.00	0.1250	563.30	0.12	99.38
3.50	0.0884	563.90	0.11	99.49
4.00	0.0625	564.40	0.09	99.58

Total weight = 566.80 g

University of Waikato
Rapid Sediment Analyser
Operating System Version 7.1

PARTICLE SIZE ANALYSIS

Earth Sciences - University of Waikato

Sample: 34a/e

Size distribution histogram

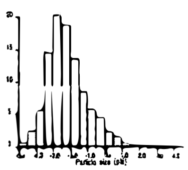

Cumulative frequency

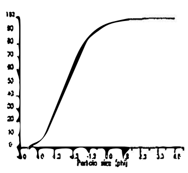

Cumulative frequency

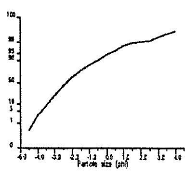

Results summary

Textural size classes
Gravel= 84.22% Sand= 15.27% Silt= 0.00% Clay= 0.00%
Gravel bearing detrital sediment
Gravel

Moment method parameters (phi)
Mean= -2.15 Sorting= 1.18 Skewness= 0.86 Kurtosis= 4.48

Graphical method parameters (phi)
Mean= -2.20 Sorting= 1.16 Skewness= 0.21 Kurtosis= 1.14
Median= -2.33 C= -4.43 D35= -2.71 D65= -1.90

Textural description:
Poorly sorted, Fine skewed, Leptokurtic

Raw data summary

Size (phi)	Size (mm)	Cumulative weight (g)	Interval frequency (%)	Cumulative frequency (%)
-4.50	22.6274	5.30	0.64	0.64
-4.00	16.0000	25.70	2.48	3.12
-3.50	11.3137	71.90	5.61	8.73
-3.00	8.0000	190.60	14.41	23.14
-2.50	5.6569	357.90	20.31	43.46
-2.00	4.0000	512.50	18.77	62.23
-1.50	2.8284	624.10	13.55	75.78
-1.00	2.0000	693.60	8.44	84.22
-0.50	1.4142	741.00	5.76	89.97
0.00	1.0000	777.60	4.44	94.41
0.50	0.7071	796.40	2.28	96.70
1.00	0.5000	809.00	1.53	98.23
1.50	0.3536	813.60	0.56	98.79
2.00	0.2500	815.40	0.22	99.00
2.50	0.1768	816.70	0.16	99.16
3.00	0.1250	817.90	0.15	99.31
3.50	0.0884	818.60	0.08	99.39
4.00	0.0625	819.40	0.10	99.49

Total weight = 823.60 g

University of Waikato
Rapid Sediment Analyser
Operating System Version 7.1

PARTICLE SIZE ANALYSIS

Earth Sciences - University of Waikato

Sample: 34a/f

Size distribution histogram

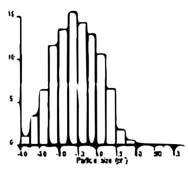

Cumulative frequency

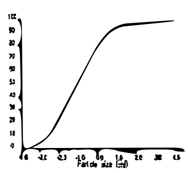

Cumulative frequency

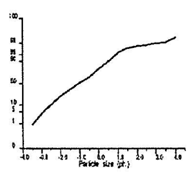

Results summary

Textural size classes
Gravel= 51.58% Sand= 47.76% Silt= 0.00% Clay= 0.00%
Gravel bearing detrital sediment
Sandy Gravel

Moment method parameters (phi)
Mean= -1.02 Sorting= 1.19 Skewness= 0.22 Kurtosis= 3.14

Graphical method parameters (phi)
Mean= -1.03 Sorting= 1.21 Skewness= 0.02 Kurtosis= 0.90
Median= -1.05 C= -3.49 D35= -1.53 D65= -0.53

Textural description:
Poorly sorted, Near symmetrical, Mesokurtic

Raw data summary

Size (phi)	Size (mm)	Cumulative weight (g)	Interval frequency (%)	Cumulative frequency (%)
-3.50	11.3137	5.30	0.93	0.93
-3.00	8.0000	24.20	3.33	4.26
-2.50	5.6569	60.70	6.42	10.68
-2.00	4.0000	126.90	11.65	22.34
-1.50	2.8284	204.20	13.61	35.94
-1.00	2.0000	293.00	15.63	51.58
-0.50	1.4142	374.90	14.42	65.99
0.00	1.0000	448.70	12.99	78.98
0.50	0.7071	509.20	10.65	89.63
1.00	0.5000	548.30	6.53	96.16
1.50	0.3536	556.20	1.74	97.91
2.00	0.2500	559.40	0.56	98.47
2.50	0.1768	560.80	0.25	98.72
3.00	0.1250	562.20	0.25	98.96
3.50	0.0884	563.30	0.19	99.16
4.00	0.0625	564.30	0.18	99.33

Total weight = 568.10 g

University of Waikato
Rapid Sediment Analyser
Operating System Version 7.1

PARTICLE SIZE ANALYSIS

Earth Sciences - University of Waikato

Sample: # 43/a

Size distribution histogram

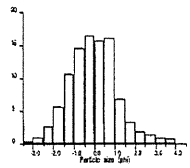

Cumulative frequency

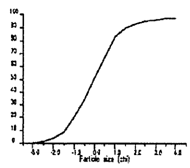

Cumulative frequency

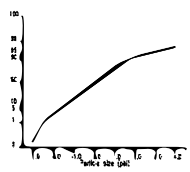

Results summary

Textural size classes

Gravel= 20.08% Sand= 77.79% Silt= 0.00% Clay= 0.00%

Gravel bearing detrital sediment

Gravelly Sand

Moment method parameters (phi)

Mean= -0.03 Sorting= 1.17 Skewness= 0.37 Kurtosis= 3.60

Graphical method parameters (phi)

Mean= -0.05 Sorting= 1.25 Skewness= 0.08 Kurtosis= 1.16

Median= -0.03 C= -2.61 D35= -0.49 D65= 0.45

Textural description:

Poorly sorted, Near symmetrical, Leptokurtic

Raw data summary

Size (phi)	Size (mm)	Cumulative weight (g)	Interval frequency (%)	Cumulative frequency (%)
-3.00	8.0000	0.90	0.27	0.27
-2.50	5.6569	4.00	0.93	1.20
-2.00	4.0000	12.80	2.63	3.83
-1.50	2.8284	31.80	5.68	9.50
-1.00	2.0000	67.20	10.58	20.08
-0.50	1.4142	115.80	14.52	34.61
0.00	1.0000	170.90	16.47	51.08
0.50	0.7071	223.20	15.63	66.71
1.00	0.5000	277.00	16.08	82.79
1.50	0.3536	300.00	6.87	89.66
2.00	0.2500	310.90	3.26	92.92
2.50	0.1768	317.00	1.82	94.74
3.00	0.1250	321.60	1.37	96.11
3.50	0.0884	324.80	0.96	97.07
4.00	0.0625	327.50	0.81	97.88

Total weight = 334.60 g

University of Waikato
Rapid Sediment Analyser
Operating System Version 7.1

PARTICLE SIZE ANALYSIS

Earth Sciences - University of Waikato

Sample: # 43/b

Size distribution histogram

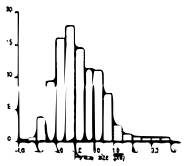

Cumulative frequency

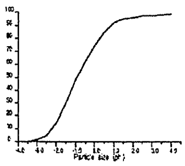

Cumulative frequency

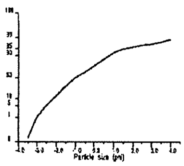

Results summary

Textural size classes

Gravel= 46.15% Sand= 50.49% Silt= 0.00% Clay= 0.00%

Gravel bearing detrital sediment

Sandy Gravel

Moment method parameters (phi)

Mean= -0.78 Sorting= 1.21 Skewness= 0.71 Kurtosis= 3.98

Graphical method parameters (phi)

Mean= -0.81 Sorting= 1.21 Skewness= 0.19 Kurtosis= 0.96

Median= -0.94 C= -3.02 D35= -1.37 D65= -0.39

Textural description:

Poorly sorted, Fine skewed, Mesokurtic

Raw data summary

Size (phi)	Size (mm)	Cumulative weight (g)	Interval frequency (%)	Cumulative frequency (%)
-3.50	11.3137	0.80	0.20	0.20
-3.00	8.0000	4.20	0.84	1.04
-2.50	5.6569	19.60	3.60	4.64
-2.00	4.0000	57.90	9.46	14.30
-1.50	2.8284	122.60	15.98	30.27
-1.00	2.0000	195.00	17.88	48.15
-0.50	1.4142	253.40	14.42	62.57
0.00	1.0000	299.00	11.26	73.83
0.50	0.7071	343.90	11.09	84.91
1.00	0.5000	374.00	7.43	92.35
1.50	0.3536	384.50	2.59	94.94
2.00	0.2500	389.40	1.21	96.15
2.50	0.1768	392.40	0.74	96.89
3.00	0.1250	394.80	0.59	97.48
3.50	0.0884	397.10	0.57	98.05
4.00	0.0625	399.50	0.59	98.64

Total weight = 405.00 g

University of Waikato
Rapid Sediment Analyser
Operating System Version 7.1

PARTICLE SIZE ANALYSIS

Earth Sciences - University of Waikato

Sample: # 43/c

Size distribution histogram

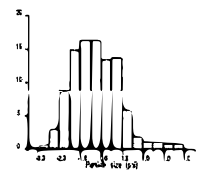

Cumulative frequency

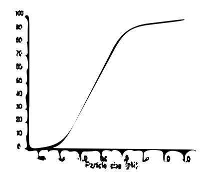

Cumulative frequency

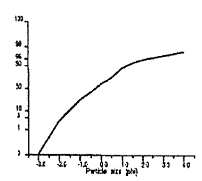

Results summary

Textural size classes

Gravel= 27.01% Sand= 70.94% Silt= 0.00% Clay= 0.00%

Gravel bearing detrital sediment

Gravelly Sand

Moment method parameters (phi)

Mean= -0.24 Sorting= 1.13 Skewness= 0.59 Kurtosis= 3.79

Graphical method parameters (phi)

Mean= -0.28 Sorting= 1.20 Skewness= 0.14 Kurtosis= 1.04

Median= -0.30 C= -2.44 D35= -0.76 D65= 0.20

Textural description:

Poorly sorted, Fine skewed, Mesokurtic

Raw data summary

Size (phi)	Size (mm)	Cumulative weight (g)	Interval frequency (%)	Cumulative frequency (%)
-3.00	8.0000	0.20	0.09	0.09
-2.50	5.6569	1.40	0.56	0.65
-2.00	4.0000	7.40	2.79	3.46
-1.50	2.8284	28.10	8.71	12.16
-1.00	2.0000	58.00	14.86	27.01
-0.50	1.4142	93.10	16.35	43.36
0.00	1.0000	128.30	16.39	59.76
0.50	0.7071	157.10	13.41	73.17
1.00	0.5000	186.30	13.60	86.77
1.50	0.3536	198.90	5.87	92.64
2.00	0.2500	202.90	1.86	94.50
2.50	0.1768	205.10	1.02	95.53
3.00	0.1250	207.30	1.02	96.55
3.50	0.0884	208.80	0.70	97.25
4.00	0.0625	210.30	0.70	97.95

Total weight = 214.70 g

University of Waikato
Rapid Sediment Analyser
Operating System Version 7.1